DEVELOPMENT OF HYBRID POLYMER MATRIX NANOCOMPOSITE WITH IMPROVED MECHANICAL AND THERMAL PROPERTIES

A thesis submitted to the

UPES

For the award of

Doctor of philosophy

in

Engineering

By

Avani Kumar Upadhyay

Jan 2024

SUPERVISOR

Dr. Manjeet Singh Goyat

CO-SUPERVISOR

Dr. Ajay Kumar

UPES
UNIVERSITY OF TOMORROW

School of Advanced Engineering (SoAE)

UPES

Dehradun, Uttarakhand - 248007

DEVELOPMENT OF HYBRID POLYMER MATRIX NANOCOMPOSITE WITH IMPROVED MECHANICAL AND THERMAL PROPERTIES

A thesis submitted to the

UPES

For the award of

Doctor of Philosophy

In

Engineering

By

Avani Kumar Upadhyay

SAP ID- 500051425

Supervisor

Dr. Manjeet Singh Goyat

Sr. Associate Professor

School of advanced Engineering, UPES

Co-Supervisor

Dr. Ajay Kumar

Professor

School of advanced Engineering, UPES

School of Advanced Engineering (SoAE)

UPES

Dehradun, Uttarakhand - 248007

DECLARATION

I declare that the thesis entitled "**Development of hybrid polymer matrix nanocomposite with improved mechanical and thermal properties**" has been prepared by me under the guidance of Dr. Manjeent Singh Goyat, Sr. Associate Professor, Department of Applied Science and Dr. Ajay Kumar, Professor, Department of Mechanical Engineering, UPES. No part of this thesis has formed the basis for the award of any degree or fellowship previously.

Avani Kumar Upadhyay

School of Advanced Engineering [SoAE],

UPES, Dehradun-248007, Uttarakhand

CERTIFICATE

I certify that **Avani Kumar Upadhyay** has prepared his thesis entitled **"Development of hybrid polymer matrix nanocomposite with improved mechanical and thermal properties"**, for the award of PhD degree of the University of Petroleum & Energy Studies, under my guidance. He has carried out the work at the School of Advanced Engineering, UPES, Dehradun.

Dr. Manjeent Singh Goyat
SoAE, UPES Dehradun -248007, Uttarakhand
Date: 10-01-2024

Dr. Ajay Kumar
SoAE, UPES Dehradun -248007, Uttarakhand
Date:

ii

ABSTRACT

The remarkable characteristics of multi-walled carbon nanotubes (MWCNTs) have captivated scientists globally over the past decade. However, preserving these properties is essential. Despite various methods available for synthesizing hybrid MWCNTs, many involve chemicals like hydrazine, which can harm the environment. The objective of this thesis is to develop multi-scale composites by integrating nanoscale reinforcement into an epoxy (EP) matrix using simple, cost-effective, environmentally friendly, and controlled methods. This research examines the mechanical properties of hybrid nanocomposites created through an ultrasonic dual mixing technique.

Hybrid epoxy nanocomposite (HENC) samples were prepared with varying particle concentrations and curing cycles to determine the optimal parameters (MWCNT wt%, SiO2 wt%, and curing cycle). Taguchi-based grey relation analysis was employed to identify the most favorable set of control variables that maximize tensile strength and fracture toughness (KIC). Confirmation tests were conducted to verify the properties of the composites. Particle sizes were confirmed using X-ray diffraction (XRD) and a particle size analyzer. The resulting HENCs were characterized by XRD, thermogravimetric analysis (TGA), differential scanning calorimetry (DSC), and field emission scanning electron microscopy (FESEM).

The characterization results indicated that the HENCs possess superior properties compared to neat epoxy and single particle nano/micro composites. HENCs were successfully developed using pre-optimized ultrasonic dual mixing parameters at varying particle concentrations. The mechanical properties of the HENCs showed significant improvement with an ideal concentration of 1% MWCNT and 10% SiO2, along with curing cycle-2. Specifically, the tensile strength (TS), tensile modulus (TM), strain to break percentage (STBP), hardness, and fracture toughness (KIC) of HENCs improved by 13%, 200%, 18%, 17%, and 65%, respectively.

Moreover, the thermal properties of HENCs surpassed those of pure epoxy composites, with the glass transition temperature approximately 37% higher. The homogeneous dispersion of MWCNTs and SiO2 nanoparticles and their threshold limits likely contributed to the enhanced mechanical characteristics of HENCs. The optimal parameters for maximizing tensile strength were found to be 1 wt.% MWCNT, 10 wt.% SiO2, and curing cycle-2. For maximum fracture toughness, the optimal parameters were 0.3 wt.% MWCNT, 10 wt.% SiO2, and curing cycle-5.

FESEM analysis revealed the toughening mechanisms in HENCs, including crack bridging, crack pinning, crack deflection, crack twisting, crack blunting, fiber pullout, and particle debonding. Compared to other reports, these findings were remarkably efficient and rapid.

ACKNOWLEDGMENT

I would first like to thank my Ph.D. advisor, **Dr. Manjeet Singh Goyat** (Sr. Associate Professor) and **Dr. Ajay Kumar** (Professor), for the past five years of great support at UPES. Their passion and persistence in science have always encouraged me during PhD study. In the first year, they spent enormous efforts guiding research and never lost their patience when the experiment was not going well. They would seek every chance to train paper writing and presenting skills that help build confidence and become a qualified researcher. Without their constant support, I would never be able to accomplish a PhD study. All the knowledge and merit that they passed on, has made me today and will continue benefiting my future life.

I am grateful to the R&D team at UPES for their seed support in every manner and further acknowledge the continuous encouragement received from Dr. D.K Awasthi for supporting this work in all its stages. I especially want to thank Mr. Mange Ram, Mr. Naveneet Kumar, Mr. Ranjit and other mechanical workshop lab technician for helping consistently during my experimentation. I am also grateful to all the lab staff and their support at our Institute (UPES).

I would like to thank my parents for their constant support and love at every stage of my life. Completing this degree would never be possible without their love and encouragement. My special gratitude to my friend and colleague Dr. Ram Kunwar for helping and encouraging me truly in this Ph.D. work. Finally, a gratitude to all dear colleagues Dr. Prashant Shukla, and Dr. Sachin Sharma, Dr. Swapnil Bhurat and Dr. Jitendra yadav for their continuous help and support.

I would like to thank my wife for consistently, patiently helping and supporting throughout this journey. Her help in my difficult time was always boosted me to complete this work on time. My daughter, my stress reliever, is the important contributor to the accomplishment of this thesis work. She took and understand her by default duty of keeping me happy and stress-free during this journey.

TABLE OF CONTENTS

LIST OF FIGURES

LIST OF TABLES

LIST OF ABBREVIATIONS

ABBREVIATION	DEFINITIONS
AFM	Atomic Force Microscopy
CNT	Carbon nanotube
CVD	Chemical vapour deposition
DGEBA	Diglycidyl ether of bisphenol-A
DNA	Deoxyribonucleic Acid
DOE	Design of experiment
DSC	Differential scanning calorimeter
DWCNT	Double wall carbon nanotube
EP	Epoxy
FESEM	Field emission scanning electron microscopy
FM	Flexural modulus
FS	Flexural strength
FT	Fracture toughness
FTIR	Fourier Transform Infrared Spectroscopy
GC	Gray coefficient
GI	Gray Index
GRA	Gray relation analysis
HENC	Hybrid epoxy nanocomposite
HPNC	Hybrid polymer nanocomposite
HS	Hybrid sample
MEK	Methyl ethyl ketone
MWCNT	Multi wall carbon nanotube
NSNR	Normalized signal to noise ratio
ONP	Oxide nanoparticles
PNC	Polymer matrix nanocomposites
PTS	Predicted tensile strength
ROM	Rule of mixture

SEM	Scanning electron microscopy
SENB	Single-Edge Notched Bending
SNRA	Signal to noise ration
STBP	Strain to break percentage
SWCNT	Single wall carbon nanotube
TEM	Transmission electron microscopy
TGA	Thermal gravimetric analysis
TM	Tensile modulus
TS	Tensile strength
UDM	Ultrasonic dual mixing
XRD	X-ray diffraction

CHAPTER 1

INTRODUCTION

The incorporation of foreign elements into the polymer structure has become pervasive in the present scenario. The manufacturing of polymer composites fulfils the demand for lightweight materials in various industries, such as automotive, sports, aviation, etc. (A. Kumar & Shukla, 2014). Researchers have recently started focusing on adding nanostructure to the polymer matrix to enhance its properties without increasing its weight. This gives rise to the polymer matrix nanocomposites (PNC) field, in which the solute has at least one dimension in the nanometres (Thostenson et al., 2005). Furthermore, by altering the form, size, type, and concentration of nanofillers, various characteristics may be created. In 1990, Toyota's central research laboratory (Japan) experimented on a nylon-6 nanocomposite. They discovered that adding a small quantity of nanofillers significantly improved the composite's mechanical characteristics (Usuki et al., 1993). The shape and qualities of the filler-matrix interface also impact PNC's properties (Idumah & Obele, 2021). Replacing microfillers with nanofillers improves mechanical properties and provides better interfacial strength (Huang et al., 2017). Researchers have tried to mix various dimensions of nanofillers like carbon dots (zero dimension), nanowires/nanotubes/ nanoparticles (1D), Graphene nanosheets (2D), and nanocones (3D) in polymers. Mixing nanofillers provides a larger interfacial area for a given volume, resulting in better filler matrix interaction. Figure 1-1 shows the surface area to volume ratio for the typical shapes of the nanofillers. Additionally, Figure 1-1 shows that decreasing the diameter of the nanotubes and nanoparticles provides more surface area to volume ratio. Thus, nanofillers impart high reinforcing efficiency due to their higher aspect ratio (Voon et al., 2018). Further, the degree of mixing of nanofillers is also one of the challenging parameters that govern properties of nanocomposites. Uniformly dispersed nanofiller gives a homogeneous microstructure, resulting in better physical properties of the composites. Dispersion quality largely depends on the nanocomposite manufacturing technique (Baig et al., 2018). Figure 1-2

describes the result of dispersion on the characteristics of the composite. Carbon nanotubes (1-D) and oxide nanoparticles (ONP) (0-D) have proven to be one of the best nanofillers for polymer nanocomposites (Y. Li et al., 2019). These particles have excellent physical and chemical properties (Wöll, 2020; Yakobson & Avouris, 2007). Moreover, the fabrication of nanocomposites containing CNTs and oxide particles is challenging due to various issues like particle segregation, parameters optimization, and filler orientation (A. Kumar et al., 2021). Researchers have tried to modify the CNTs and oxide particles to overcome the mentioned problems. Different modification methods are proposed, out of which functionalization of CNTs by other chemical groups is proven to be appropriate (Yuan et al., 2014). Some chemical modifiers weaken the interfacial bonding between particles and the polymer base because of adverse effects like weakening filler surfaces.
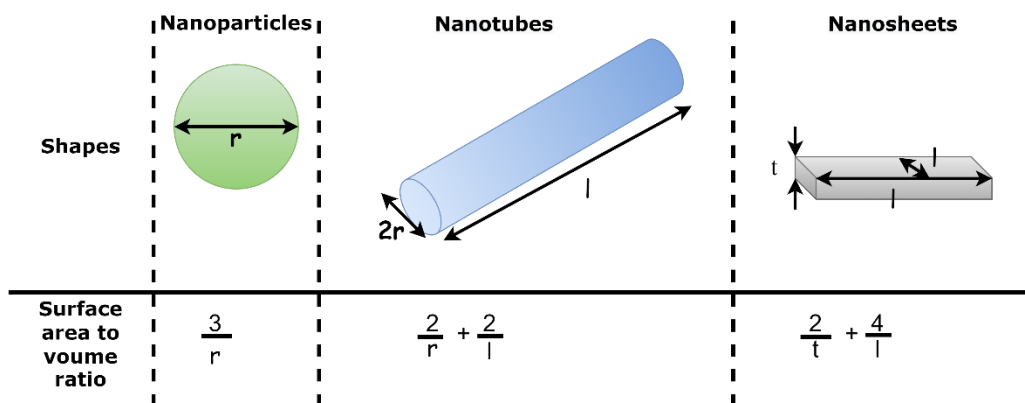
Figure 1-1: Schematic of surface area (A_s) / Volume (V) for diverse nanofiller dimensions.
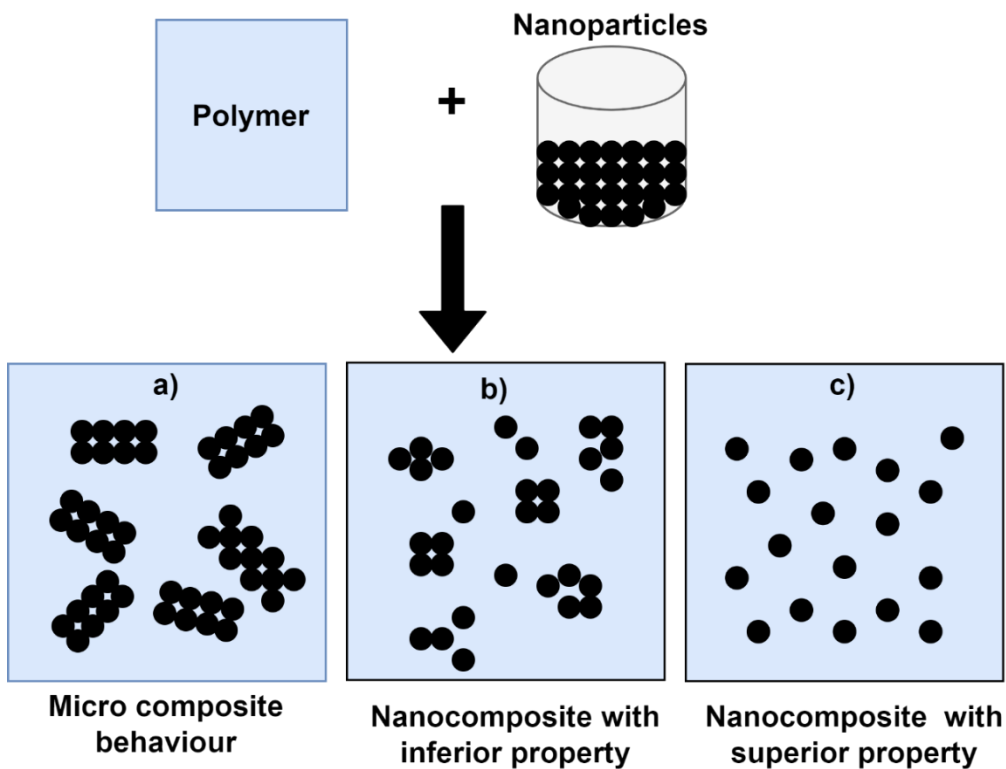
Figure 1-2: The impact of particle size distribution on composite performance a) macro clustering (phase separation) b) micro agglomeration c) homogeneous distribution.

CNTs/ONP-based polymer nanocomposites are multifunctional composites having ever-increasing demand in various industries like aviation, railways, automobile, sports, and energy (Gibson, 2010). Mechanical and thermal properties are two important sets of properties demanded in the sectors mentioned earlier. Further, creating a solid network of nanofillers, selecting a proper set of particle and matrix combinations, and forming strong particle and matrix interfaces are three critical factors affecting high-performance nanocomposites' mechanical and thermal properties. Figure 1-3 depicts the common consideration for high-performance polymer nanocomposites.
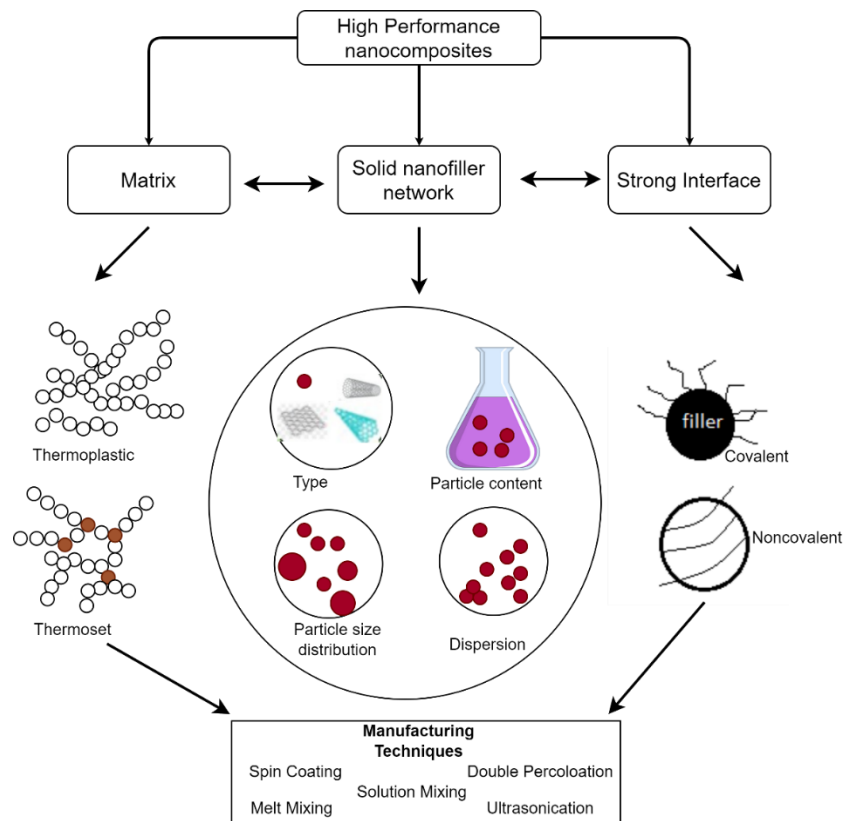
Figure 1-3: Factors considered for the development of high-performance PNCs .

The remarkable mechanical capabilities, widespread accessibility, and high engineering demand for epoxy-based composites have captivated scientists for the last twenty years (Cha et al., 2017). Neat epoxy composite nonetheless exhibits excellent young's modulus, strength, chemical inertness, and adhesion. Because of its high crosslinking density after curing, epoxy composites exhibits low fracture strength and ductility (Gómez-Del Río et al., 2016). Several efforts have addressed these constraints by including different nanofillers in the epoxy composites (Ghosh et al., 2013; Goyat et al., 2018; Zunjarrao & Singh, 2006). MWCNTs' high low weight, high aspect ratio and exceptional strength make them a promising material for reinforcing epoxy matrices (Goyat et al., 2015). Although CNT provides good thermal and mechanical characteristics to the epoxy composite, it suffers from some significant challenges like limited solubility, poor dispersion, weak interface formation, high cost of functionalization, and loss of transparency. Hence,

scientists have started reinforcing the epoxy with hard, non-toxic, and transparent ONPs like SiO_2, Al_2O_3, and TiO_2 (Goyat et al., 2021). Dispersion of ONPs is also a critical issue due to its large A_s/V. Large loading of ONPs leads to particle agglomeration, which reduces PNC's thermal and mechanical strength (polymer nanocomposite) (Bazrgari et al., 2018).

Mixing both ONPs (0-D) and CNTs (1-D) into the epoxy matrix is a comparatively new concept known as hybrid polymer matrix nanocomposite (HPNCs). HPNCs have shown better mechanical properties due to the amalgamation of advantages obtained by both particles. To achieve the optimal mechanical and thermal characteristics of HPNCs, a number of factors must be managed. In order to create HPNCs, Xiao et al. (Xiao et al., 2018) mixed MWCNT and SiO_2 into an epoxy base in a 1:6 ratio. They concluded that SiO_2 particles might form strong bonds with MWCNT and alleviate some of the Van der Waals forces between the MWCNT nanoparticles, resulting in less particle agglomeration. Monfared et al. (Moghimi Monfared et al., 2018) used the ultra-sonication method to develop SiO_2-MWCNT-Epoxy nanocomposite. The authors have reported an enhancement of 31% in the TS by mixing SiO_2 with MWCNT in a ratio of 9:1. Rathi and Khandelwal (Rathi & Kundalwal, 2020) used ZrO_2 in the MWCNT-epoxy nanocomposite. The authors concluded that ZrO_2 makes a strong bond with MWCNT, which increases the tensile strength by 35%. Further, ZrO_2 particles act as a spacer between MWCNT and decrease the interparticle (CNT) Van der Waals forces. The field of HPNCs is still unexplored due to the lack of literature surveys done in this field. Further, understanding the distinct outcomes of MWCNT, ONPs, and hybrid MWCNT/ONP on the epoxy composite is necessary to explore the research opportunities in HPNC. Many review articles have been published to show the influence of ONPs or CNTs on the thermomechanical characteristics of epoxy nanocomposite (Goyat et al., 2021; Y. Li et al., 2019; Sharma et al., 2022).

Moreover, very little literature is available that compiles and analyses the work done in the field of property improvement of epoxy nanocomposite by hybridizing the ONPs and CNTs. Most of the review article focuses on the effect

of hybridization of fibers (glass fiber, carbon fiber, natural fibers) with oxide nanoparticles, CNTs, or graphene oxide on the properties of the epoxy nanocomposite. The epofine system is considered for the present investigation because it is the most commonly used high-performance epoxy resin system. It is very effective and lightweight, making it ideal for use in vehicles and aircraft.

CHAPTER 2
LITERATURE REVIEW

2.1 INTRODUCTION

Polymers are substances made up of big molecules with a high molar mass and consist of structural sub-units that are repeated over and over again. These materials can have a linear or branched structure, which is referred to as thermoplastic polymers, or they can have a cross-linked structure, which is referred to as thermosetting polymers. Thermoplastic polymers can be found in a condition that is either amorphous or semi-crystalline, and the ingredients that make up thermoplastic polymers can be either brittle or ductile. The thermoset polymers have an amorphous structure that arises from the three-dimensional network that is generated by crosslinking. This structure hinders the movement of polymer chains to crystallization or packing, which is why thermoset polymers have the properties they do. Polymers can be used in a wide variety of applications, including coatings, adhesives for structural support, and electrical gadgets. In earlier research, it was demonstrated that adding micro-size fillers, such as glass fiber and talc, leads in traditional microcomposites, which may display better qualities generally lacking in pure polymers. These micro composites can be made by including micro-size fillers. In recent years, the integration of low-volume fractions of nano-size fillers has been the technique that has been generally employed for diversifying and upgrading polymer composites. This is due to the fact that nano-size fillers have the ability to fill very small spaces. The utilization of polymer nanocomposites has been shown to yield significant improvements in electrical, thermal, and mechanical characteristics when compared to conventional composites or pure polymers. The extent to which the polymer chains are constrained or the polymer's toughening efficiency is enhanced is contingent upon the specific characteristics and composition of the nano-filler employed. The alterations witnessed in the characteristics of polymer nanocomposites, wherein inorganic nanoparticle fillers are incorporated, predominantly arise from the interplay and amalgamation of distinct phases.

The inclusion of the inorganic phase significantly contributes to superior thermal and mechanical properties, while the organic phase plays a crucial role in providing the necessary processing capabilities and adhesive properties (Tsai et al., 2016).

2.2 POLYMERS

Polymer molecules are composed of a significant quantity of comparable repeating units, referred to as a homopolymer, or diverse kinds of monomers, known as a copolymer. The molecular entities often exhibit linear, branching, or cross-linked topologies. In instances of extensive interconnectivity, the arrangement of these entities gives rise to a substantial three-dimensional network structure. Polymers, characterized by their linear or branching structure without cross-linking, are often referred to as thermoplastic materials. These polymers possess the ability to undergo reprocessing by exposure to heat or dissolving in an appropriate solvent. A cross-linked polymer, sometimes known as a thermosetting polymer, is characterized by a three-dimensional network structure. Unlike thermoplastics, it cannot be melted or molded without undergoing irreversible destruction of its chemical connections. There are both naturally derived polymers, such as silk, cellulose, DNA, and proteins, as well as manmade polymers, including nylon, polyethylene, and epoxy.

The prospective uses of these matrices have piqued the interest of the polymer researchers. Thermosetting polymers are the focus of this research because of their promising electrical and mechanical characteristics and a wide variety of possible industrial uses. Limited mechanical property and inherent brittles of thermosetting polymer limits its industrial application. Thermosetting polymers are developed by crosslinking polymer resin with a curing media, which is a transitional reactive chemical. This particular chemical reaction can potentially transpire at ambient temperature, although it is commonly executed under heightened temperatures. This process is commonly denoted as polymerization or cure. Instances of such materials encompass phenolic, epoxy polymers and unsaturated polyesters (Young et al., 2018).

2.3 EPOXY MATRIX

This research focuses on using epoxy as a polymer matrix, which is widely employed as a resin basis for fabricating bonding agents or operational materials. Two-component solutions are often used as epoxy adhesives or materials in structural applications. One of the components is often known as epoxy resin, while the other component is referred to as a curing agent (hardener). The conversion of epoxy resins into a three-dimensional cross-linked network occurs via the process of curing reaction with a suitable hardener. The commonly used types of epoxy resins include brominated resins, diglycidyl ether of bisphenol-A (DGEBA), epoxidized olefins, cyclo-aliphatic epoxy resins, novolac resins, Epikote and Epon (Fałtynowicz et al., 2022). The chemical structure of common epoxy resins are shown in Table 2-1. The hardeners may be classified into many major groups, including amides, amines, imidazoles, anhydrides and carboxylic acids (Pham & Marks, 2005). The features and processing characteristics that will be prioritized will determine which curing agent will be used. Curing agents, in general, may be classified as either aliphatic amines, used for curing at ambient temperature, or aromatic amines, or anhydrides, used for curing at high temperatures.

The cross-linking of DGEBA-based epoxy resin happens by opening the epoxide or oxirane ring and generating covalent bonds between an aliphatic amine and the epoxy resin molecules. The number of bonding between hydrogen and nitrogen atoms Journal Pre-proof 7 decides the reactivity and functionality of the amine (hardener). DGEBA-based epoxy resin undergoes cross-linking when an aliphatic amine opens the epoxide or oxirane ring, forming covalent connections between the epoxy resin molecules. The number of bonds between hydrogen and nitrogen atoms determines the functionality and reactivity of a hardener. The fundamental amines possess just two hydrogen atoms that can react with two epoxide groups by substituting the hydrogen atoms in the epoxy molecule.

Similarly, a secondary amine with a single hydrogen atom can form a singular bond with an epoxy molecule. In the case of a tertiary amine, the absence of

active H-atoms precludes its ability to form a bond with any epoxy molecule. However, it may serve as a catalyst to induce a ring-opening process (Mora et al., 2020). Figure 2-1 illustrates a concise reaction pathway involving the principal diamine hardener and an epoxy resin. This study concisely elucidates the curing reaction process of an epoxy resin derived from DGEBA, employing a main diamine hardener. However, it should be noted that the intricate amine groups may involve various reactions, either individually or in combination. The presented reaction scheme illustrates the process of covalently bonding a primary diamine to four epoxide groups, forming a three-dimensional cross-linked network. The gel point is only achieved when the branching extends throughout the entire system. The process of curing epoxy resin results in the formation of a densely interconnected network, which exhibits notable attributes such as elevated strength and hardness. However, it is essential to note that this network possesses restricted flexibility and toughness.

Figure 2-1: Chemical reaction of DGEBA with curing agent (a) DGEBA, (b) symbolic representation of DGEBA, (c) principle diamine (d) cured epoxy

Table 2-1: Chemical representation of typical epoxy resin

Type of epoxy	Chemical Representation
DGEBA	

Epoxidized olefin	
Cyclo-aliphatic epoxy	
Novolac	
Brominated epoxy	
Epikote	
Epon	
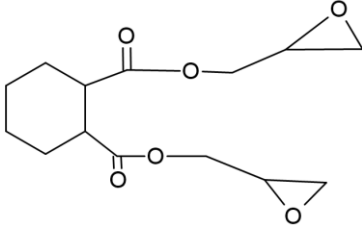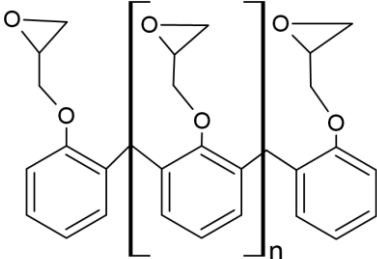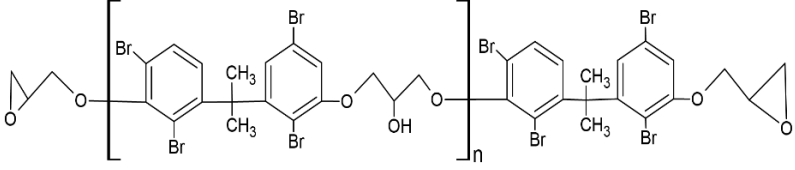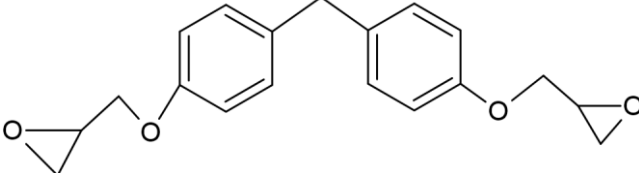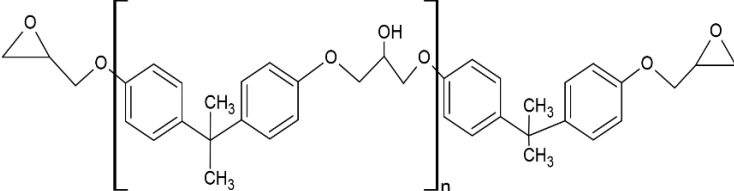
2.4 WHY ONPs AND CNTs FOR REINFORCING EPOXY?

2.4.1 OXIDE NANOPARTICLES

Metal oxides have massive utilization in many fields like materials development, metal cutting, electronics, chemical industries, and medicines (Y. Singh et al., 2014). Oxide nanoparticles contain distinctive properties because of their small size and high corner/edge density. ONPs are highly stable and rigid due to their low surface free energy. Size reduction gives rise to the domination of surface properties over bulk material properties (Corr, 2016). Researchers have identified many potential metal oxides like Al_2O_3, ZrO_2, TiO_2, Fe_2O_3, CuO, ZnO, etc.(Muñoz et al., 2015; Zabihi et al., 2012). All have different morphological geometry, such as spherical, triangular, irregular, wired, 1-D tube, etc. The properties of ONPs largely depend on their shape, size, and structure. The morphology of ONPs influences the effective interfacial area between particles and the matrix. However, the size of ONP decides the volume fraction of the interface. The mechanical properties of nanocomposite also depend on the volume fraction of the interphase. Small-sized spherical-shaped nanofillers have more volume fractions in the interfacial region than larger-sized fillers with other shapes (Liang et al., 2020; Schadler et al., 2007). This interfacial matrix material can drastically change the properties of the bulk composite. The exact property of the interfacial region is difficult to quantify, due to which inherent interaction in the interfacial region is still unrevealed. Low mobility and higher stiffness of the interfacial region are mostly explained as the reason for strengthening nanocomposite (Marouf et al., 2016).

Researchers have investigated many synthesis techniques for obtaining the ONPs with desired properties. These synthesis techniques can be classified into two groups i.e., Top-down and bottom-up (Figure 2-2). As shown in Figure 4, the top-down approach has a group of techniques in which bulk material is broken into nanosized particles. In contrast, the bottom-up approach focuses on nucleation and growth of nanoparticles from atoms. Synthesis technique, properties, structure, and application of various ONPs are shown in Table 2-2.
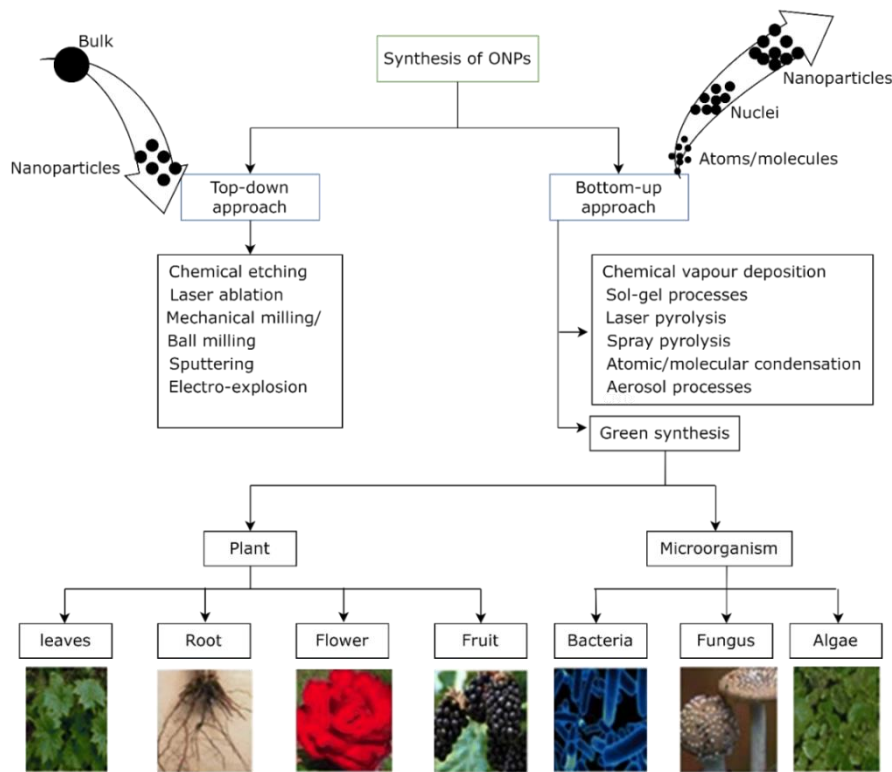
Figure 2-2: Classification of nanoparticle synthesis approaches (J. Singh et al., 2018).

Skandan et al.(Skandan et al., 1999) developed the nano SiO_2, TiO_2, and Al_2O_3 by chemical vapor condensation. They had grown the high-purity particle in a 3-50 nm size range. Chin and Yacoob (Chin & Yaacob, 2007) developed spherical iron oxide nanoparticles by micro-emulsion and Massart's procedure. They confirmed the particle size to be less than 10 nm. Fan and Lu (Fan & Lu, 2005) presented a review article focusing on the vapour transport synthesis of ZnO nanoparticles. They had shown various complex nanostructures like helix, nano types, hierarchical and nanorods, etc. The investigation of the mechanical properties of the nanoparticle is not easy because the conventional methods used for bulk material are not helpful in this case.

Bai et al. (Bai et al., 2003) found the flexural modulus by dual-mode mechanical resonance. They applied the resonating voltage across the nano-bolts and the reference electrode. Clubbing the value of resonating frequency with the classical theory of elasticity, they found the value of flexural modulus to be

nearly 52 GPa. Zirconia nanoparticles exhibit the best hardness and fracture resistance, which make them suitable for making dentures (Roy et al., 2017). Batool et al. studied the time-dependent stability and mechanical properties of zirconia nanoparticles. The produced zirconia was hard and tough and had a high dielectric constant. The conclusion was made on the variation of hardness and toughness under various manufacturing conditions. The authors concluded that the increasing power of microwaves results in the development of smaller zirconia particles (nanosize), which leads to higher density and hardness of the particles (Batool et al., 2020). Synthesis technique, properties, structure, and application of various ONPs are shown in Table 2-2.

Table 2-2: Structure, properties and application of different ONPs.

ONPs	Synthesis technique	Structure	Chemicals used	Properties	Application	Size (nm)	Ref.
αAl_2O_3	Sol-gel	Trigonal	Precursor-$AlCl_3$, $(C_3H_7O)_3Al$	High crystallinity, hardness	Biomedical	20-25	(Rogojan et al., 2011)
Al_2O_3	Glycine assisted combustion	Leaf shape, rohmbohedra	$Al(NO_3)_2$, NH_2CH_2COOH	High purity, high conductivity	Solar panel cooling	500-700	(Amalraj & Michael, 2019)
Al_2O_3	Biological reduction	Spherical, hexagonal	$Al(NO_3)_3 \cdot 9H_2O$, Prunus yedoensis leaf	Nitrate removal, high cyrstalline	Removal of contaminants	50-100	(Manikandan et al., 2019)
αAl_2O_3	Solution combustion synthesis	Rohmobohedra, spherical	$Al(NO_3)_3 \cdot 9H_2O$, $CO(NH_2)_2$	Antibacterial,	Environmental, water cleaning	20	(Prashanth et al., 2015)

SiO$_2$	Laser ablation	Cubic, Spherical	Rock garnet	Hardness, optical properties	Electronics, optoelectronics	7-75	(Rawat et al., 2018)
SiO$_2$	Sol-gel	Spherical	Tetraethylorthosilicate, Polyvinylpyrrolidone	Optical properties	Electronics	25	(Dubey et al., 2015)
C/SiO$_2$	One pot method	Amorphous	Pluronic F-127, phloroglucinol, C$_8$H$_{20}$O$_4$Si	Electrochemical	Li-ion batteries	2-5	(Nita et al., 2019)
ZnO	Microwave	Hexagonal wurtzite,	Zn(CH$_3$CO$_2$)$_2$·2H$_2$O, NaOH	Frictional resistance, thermal stability	Dye removal agent	24 - 26	(V. Kumar et al., 2016)
ZnO	Green synthesis	Hexagonal, spherical	Zinc nitrate, Euphorbia hirta	Antimicrobial	Medicines	20-25	(W. Ahmad & Kalra, 2020)
ZnO	Controlled precipitation	Wurtzite hexagonal,	Zinc nitrate, ammonium hydroxide	Antibacterial	Medicines	11-18	(ZUBAIR & AKHTAR, 2020)

		Flower like nanorod					
ZnO	Photochemical synthesis	Hexagonal, Spheroidal	$Zn(Ac)_2.2H_2O$,	-	-	13	(Joshi, 2018)
CuO	Glycine assisted combustion	Monoclinic, Polyhedral particles	$Cu(NO_3)_2$, NH_2CH_2COOH	Thermal conductivity	Coolant material	32	(Amalraj & Michael, 2019)
CuO	Green synthesis	Monoclinic, Spherical, Oval	$Cu(NO_3)_2$, Allium sativum	Antimicrobial, antioxidant	Medicine, free radical scavenging	20-40	(Velsankar et al., 2020)
CuO	Microwave and flow synthesis	Monoclinic, Cubic, Nanobolts, Spherical	$Cu(ac)_2.H_2O$, Benzyl alcohol	Thermal conductivity	Nanofluids	4.5-14	(Nikam & Dadwal, 2018)

CuO	Sputtering	Monocinic, Spherical	Copper	Large surface area	Water purification	6-13	(M. Verma et al., 2018)
ZrO_2	Microwave assisted sol-gel	Tetragonal, Monoclinic	Zirconium oxychloride	Hardness, toughness, antimicrobial	Fracture implants	30	(Batool et al., 2020)
ZrO_2	Green synthesis	Monoclinic, Tetragonal, Spherical	$ZrOCl_2 \cdot 8H_2O$, Euclea natalensis	Absorption capacity	Absorption process	5-42	(da Silva et al., 2019)
ZrO_2	Precipitation	Cubic, Spherical, Nanorods	$ZrOCl_2 \cdot 8H_2O$, NaOH, $NaNO_3$	Electrochemical stability	Fuel cell	2-20	(Sigwadi et al., 2019)
ZrO_2	Ultrasonic spray pyrolysis	Tetragonal, Cubic, Spherical	$ZrO(NO_3)_2 \cdot xH_2O$,	-	-	10	(Hwangbo & Lee, 2019)

2.4.2 CARBON NANOTUBES

Carbon nanotube (CNT) has proven its utility in various applications. It is an allotrope of carbon in which a graphite-like structure is folded in tube form, and at the end of the tube, carbon is attached in fullerene form. The CNT was discovered in 1991 by a Japanese scientist Sumio Iijima (Iijima, 1991). CNT has excellent physical properties like strength, hardness, conductivity, stiffness, melting point, thermal stability, etc. The axisymmetric structure of CNT provides these excellent physical and chemical properties. The CNTs can act as semiconductors or metals depending upon the structure of their helix. There can be three classes of CNTs based on their synthesis technique, i.e., single-wall carbon nanotubes (SWCNT) (tube thickness of one atom), double-wall carbon nanotube (DWCNT) (nested coaxial single walls), Multiwall carbon nanotube (MWCNT) (tubes in tubes structure) (see Figure 2-3) (Patil et al., 2021). The properties of the CNT also depend on lattice parameters like edge length, diameter, and chiral angle. The SWCNT can be further classified based on their rolling in a particular crystallographic direction and chirality. Madani et al. (Madani et al., 2013) have shown three forms of SWCNT (armchair, zigzag and chiral) in their review work (Figure 2-4).
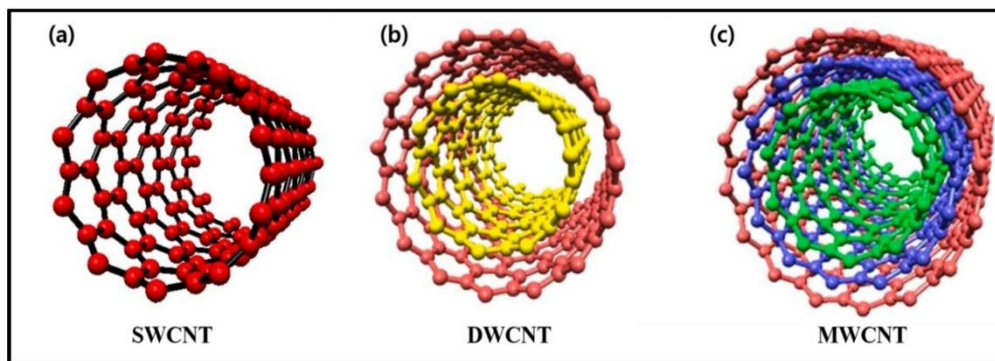
Figure 2-3: Diagrammatical representation of CNT structure a) SWCNT b) DWCNT c) MWCNT (Patil et al., 2021).
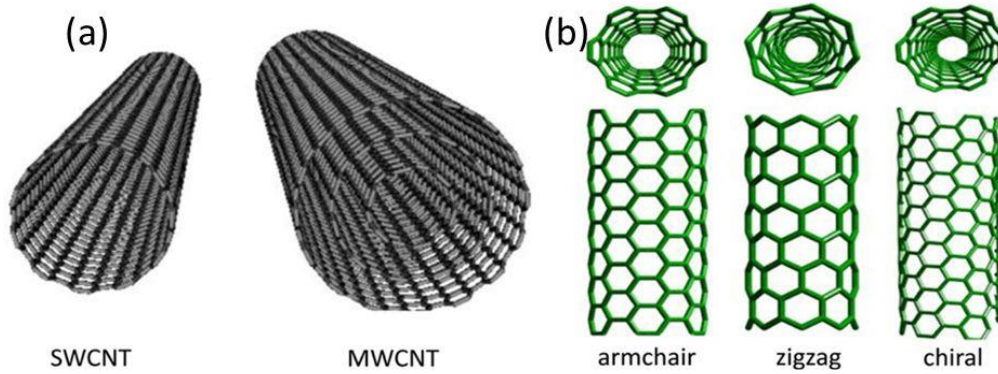
Figure 2-4: Different forms of CNT a) SWCNT and MWCNT (b) arrangement of SWCNT (Madani et al., 2013).

Treacy et al. (Treacy et al., 1996) investigated Young's modulus (E) of SWCNT by computing the amplitude of inherent vibrations using TEM. They had coupled the values found with classical mechanics to calculate the value of Young's modulus. Results show the average value to be in the range of 2-14 TPa. Yu et al. (Yu, Files, et al., 2000) developed the SWCNT by laser ablation method. They measured the tensile strength and Young's Modulus by loading the SWCNT with AFM probe. Firstly, the SWCNT paper was torn to get some small projection of SWCNT wires out of it. The projected wire was loaded by AFM, which can also read the load value. The entire scheme is shown in Figure 2-5. They had reported the value of tensile strength as 10-15 GPa and Young's modulus as 1000-1330 GPa. In another work, Yu et al. (Yu, Lourie, et al., 2000) investigated the fracture mechanism of MWCNT developed by the arc discharge method. They reported that the value of Young's modulus was 200-300 GPa and that tensile strength was 20-63 GPa. The CNTs also have excellent thermal and electrical conductivity due to the presence of the fourth valence electron in a graphitic structure.
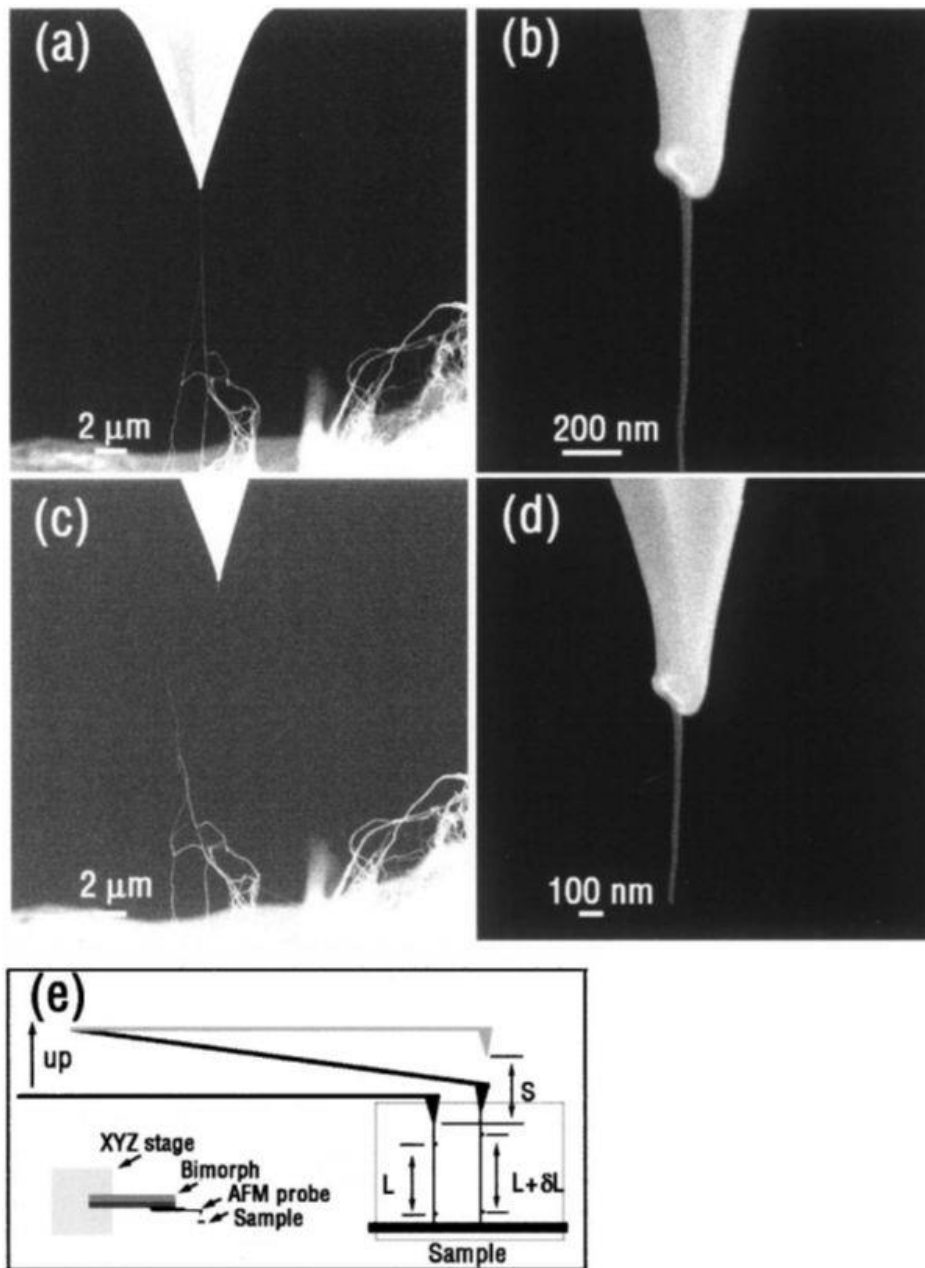
Figure 2-5: SEM image of Tensile loading experiment of SWCNT   a) loading of a particle between AFM and SWCNT paper b) View before loading c) view after braking d) close view e) schematic of experiment (Yu, Files, et al., 2000).

2.5 ONP REINFORCED EPOXY COMPOSITES

Epoxy resin is one of the most essential and extensively used polymeric resins in paints, coatings, adhesives, sealants, etc. Epoxy resins are of precise attention to structural engineers because they deliver an entire balance of mechanical and thermal characteristics combined with exciting processing flexibility. The generalized properties of epoxy resins are shown in Figure 2-6. Epoxy resin is a broad class of thermosetting polymers in which the epoxide group starts crosslinking. This high crosslinking density imparts brittleness to epoxy composites. Researchers have tried various toughening agents (Figure 2-6) to increase the toughness of the epoxy composites (Jayan et al., 2018).
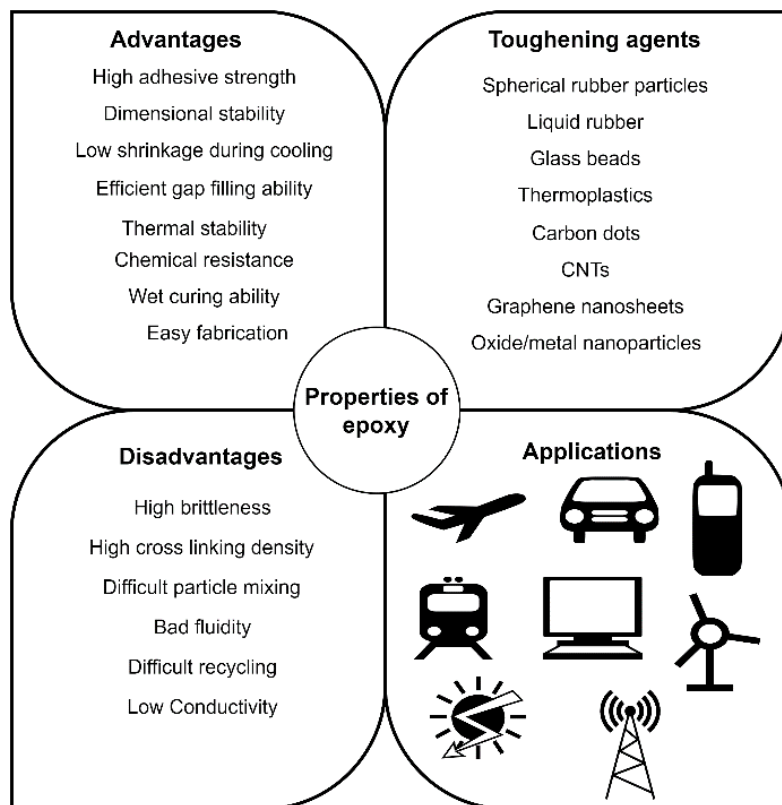
Figure 2-6: Advantages, disadvantages, toughening agents, and applications of epoxy.

ONPs reinforced epoxy composites typically comprise an epoxy matrix and homogenously distributed ONPs (Fouly & Alkalla, 2020). These ONPs can be integrated into the matrix using two different techniques. The first one is mixing

pristine ONPs into the matrix. Mixing pristine ONPs into the epoxy matrix forms an interface that governs the overall property of the epoxy. The second way is to functionalize the ONPs with active chemical groups prior to mixing them into the epoxy. Functionalized ONPs provide a stable filler-matrix interface by reducing surface energy and increasing the effective interface area (Adnan et al., 2019). Halder et al. (Halder et al., 2017) investigated the effect of surface modification of ZnO (by polyvinyl Alcohol) nanoparticles on the distribution of epoxy nanocomposite. They have reported that pristine ZnO particles had a size of 70 nm with various structures like nanorods and flakes, while the modified ZnO had uniform morphology (nanorods) and size (60 nm). Adding modifiers not only acts as a capping agent (restrict and control the particle growth) but also reduces the surface energy of the ZnO (reaction between CH-OH of modifier and –OH at the surface of ZnO). It is evident from Figure 2-7 that agglomeration is lesser in the modified ZnO than in pristine ZnO. Furthermore, the modified ZnO-reinforced epoxy composite gives better mechanical and thermal properties due to homogeneous ONP distribution.
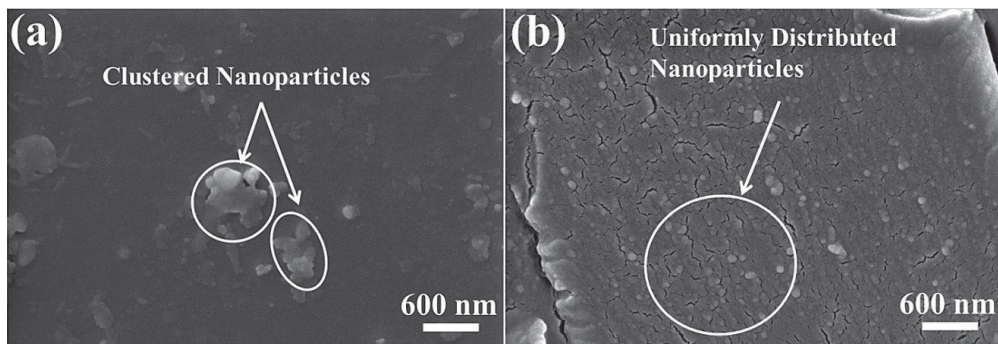
Figure 2-7: SEM micrograph of ZnO-epoxy composite a) Pristine Zirconia-epoxy b) modified ZnO-epoxy (Halder et al., 2017).

Although functionalization of ONPs is suitable for nanocomposites, it has some disadvantages like higher reaction time, high cost, and harmful chemical reactions. The mixing of non-functionalized ONPs is challenging due to the agglomeration of particles. Scientists have focused on resolving this agglomeration issue by utilizing advanced composite fabrication techniques like

ultrasonic dual mixing, bead milling, etc. [15-17]. The ONPs reduce the rate of curing reaction of epoxy because of their low value of aspect ratio (≤ 1) (Franco-Urquiza & Rentería-Rodríguez, 2021). Further, the ONPs restrict the crack propagation by deflecting the crack from the filler matrix interface (Ma et al., 2018). However, the large surface area of the ONPs increases the filler-matrix interfacial strength, but it also increases the Van der Waals forces among the ONPs. The weak Van der Waals forces become a severe concern for the ONPs due to their small size. The ONPs try to stabilize the epoxy matrix by increasing its size to the micro-level (reducing surface energy). Van der Waals forces help them to unite and become microparticles. The explained phenomena result in inadvertent particle agglomeration, which deteriorates the properties of nanocomposite (Zheng et al., 2003). Even the high viscosity of the epoxy matrix makes it challenging to get a uniform ONP distribution. So it becomes imperative to process the nanocomposites to stop the agglomeration and to achieve the maximum benefit of nanosize particles.

Interaction between polymeric chains and ONPs depends mainly on the properties of interface/interphase (region of attachment of epoxy and ONPs). The properties of the nanocomposites are outlined based on the interfacial features of the ONPs and the epoxy. There are two main types of interfacial interaction: noncovalent and covalent (see Figure 2-9). The non-covalent interaction means joining the nearest ONPs by polymer chain. Two main factors that govern the noncovalent interaction are epoxy density and filler content. The greater the filler content, the lesser the distance between fillers, resulting in improved polymer bridging of the particles (and & Winey*, 2007). Covalent interaction is nothing but a chemical reaction between ONP and filler matrix. Covalent interaction depends on the selection of ONP that can react with the active chemical group of the epoxy matrix (Rahmat & Hubert, 2011). Further, not all polymer chains need to react with the ONP. Some of the polymer chains remain unreacted and entangled end to end near the surface of ONPs. The reacted polymer chain will be anchored properly around the ONP surface (chemically reacted).
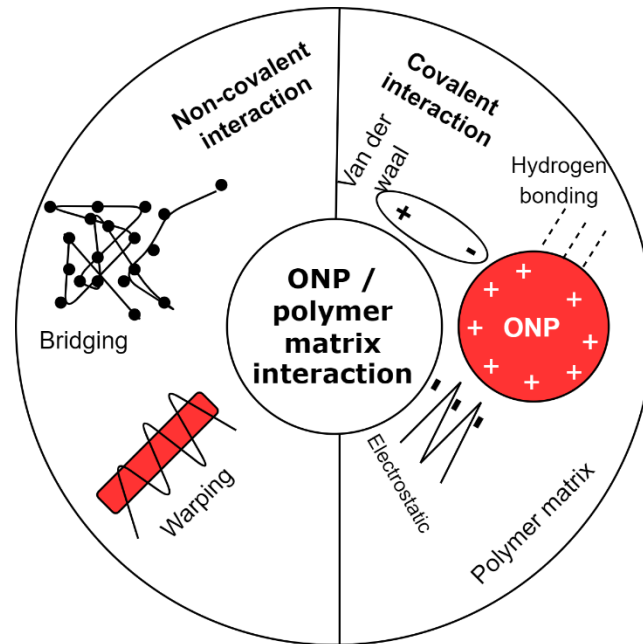
Figure 2-8: Covalent and noncovalent Interaction of epoxy-ONP in interface.

Researchers have tried a variety of techniques to get the best ONPs dispersion in an epoxy matrix. Epoxy-ONPs manufacturing techniques can be classified into two groups (Figure 2-9), i.e., in-situ and ex-situ techniques. This section aims to analyse the effect of adding ONPs on nanocomposites' mechanical and thermal properties. As discussed in the earlier section, the proper distribution of ONPs in the epoxy matrix creates a robust interface, enhancing nanocomposites' mechanical and thermal properties. The increment in the mechanical properties of ONP-epoxy nanocomposite depends on various factors like particle type, size, concentration, chemical groups at the surface, dispersion, and distribution of the ONPs (S. Wu et al., 2000). There is always an upper limit for nanoparticle addition. Crossing this limit will create a higher inter-ONP interaction.
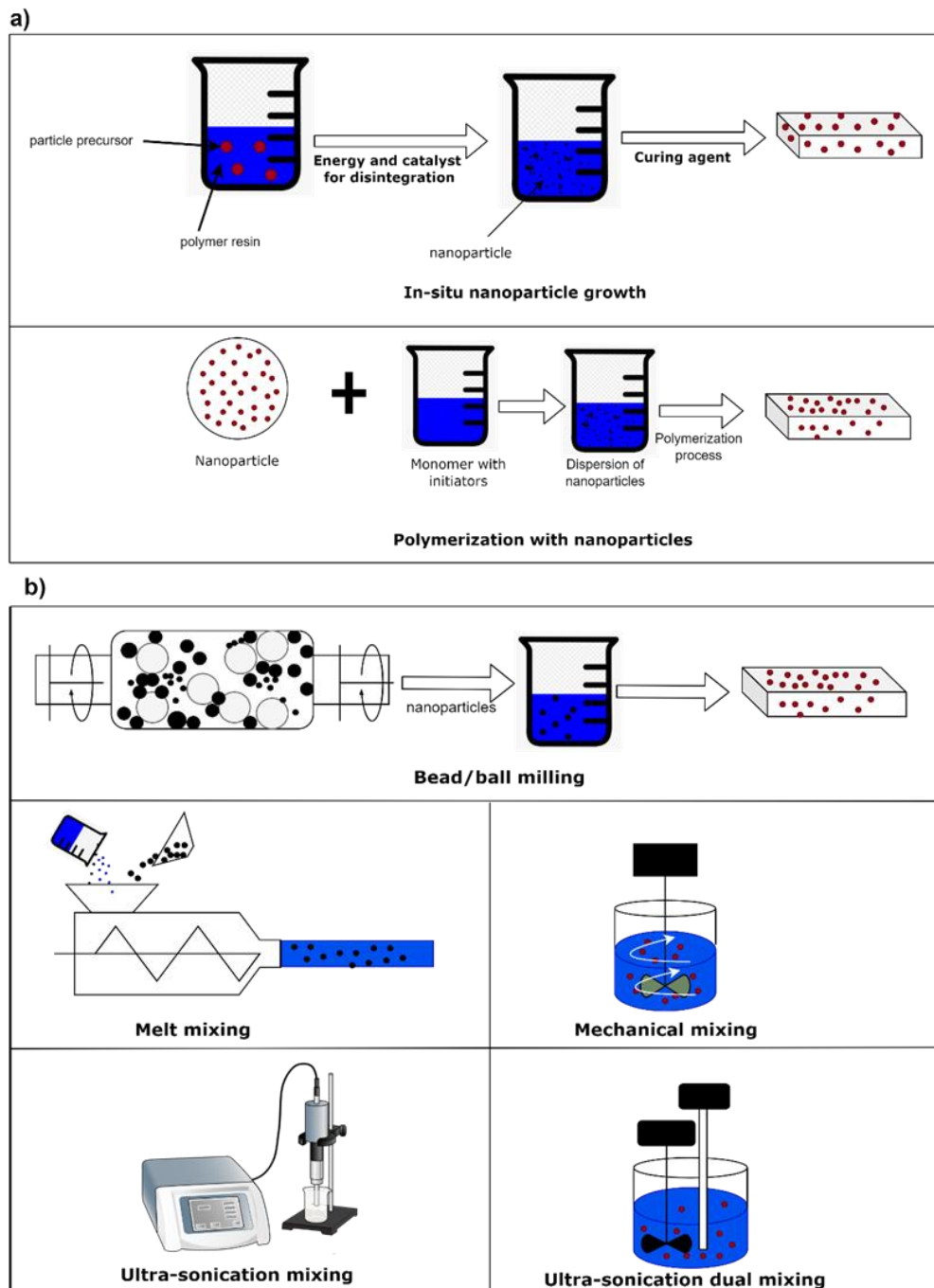
Figure 2-9: Manufacturing techniques for ONP-epoxy composites a) in-situ techniques b) ex-situ techniques.

Goyat et al. (Goyat & Ghosh, 2017) developed the TiO_2-epoxy nanocomposite by simultaneous ultra-sonication and impeller stirring and designated as ultrasonic dual mixing (UDM). The investigation was performed to reveal the

effect of TiO$_2$ nanoparticles on the mechanical and thermal properties of the developed nanocomposites. The results are summarized in

Figure 2-10. The uniformly distributed triangular lattice lake cavity (

Figure 2-10 a) was found due to the lowest energy requirements and flow mechanism of the UDM process. Cavity size and inter-cavity separation were in the range of nanometers (

Figure 2-10 c) ($\leq$ 100 nm). The nanoparticle distribution in these cavities was found to be best at 10% TiO$_2$. The increase in nanoparticle content beyond this percentage increases agglomeration and particle clustering (

Figure 2-10 b1-b3). The improved crosslinking density and restricted polymer chain mobility were crucial factors that enhanced glass transition temperature (

Figure 2-10 d). A significant improvement in tensile strength (about 52%) was achieved by adding 10% TiO$_2$ in epoxy via the reported technique. The increase in nanoparticle content beyond a threshold value results in a decline in the mechanical properties of the nanocomposite. The incorporation of ONPs provides a barrier to the movement of the crack and helps in smooth load transfer, which improves the mechanical properties of nanocomposites. Tensile toughness is a crucial indicator for estimating the strain energy absorbed by the material before fracture (Roulin-Moloney et al., 1987). The large area-to-volume ratio of ONPs decreases the stress concentration in their vicinity, making crack propagation difficult in that region. A vital interfacial region (formed by ONP- epoxy interaction) increases the nanocomposite's energy absorption capacity, leading to higher toughness (Zhao, Schadler, Duncan, et al., 2008). Figure 2-11 shows the comparison of mechanical properties (based on recently reported research works) obtained in different ONPs reinforced epoxy composite (Ma et al., 2018; M. Wu et al., 2019; Xiao et al., 2018). The comparison shows that ZrO$_2$ provides the best improvement in the mechanical properties because of better bonding with the epoxy matrix.
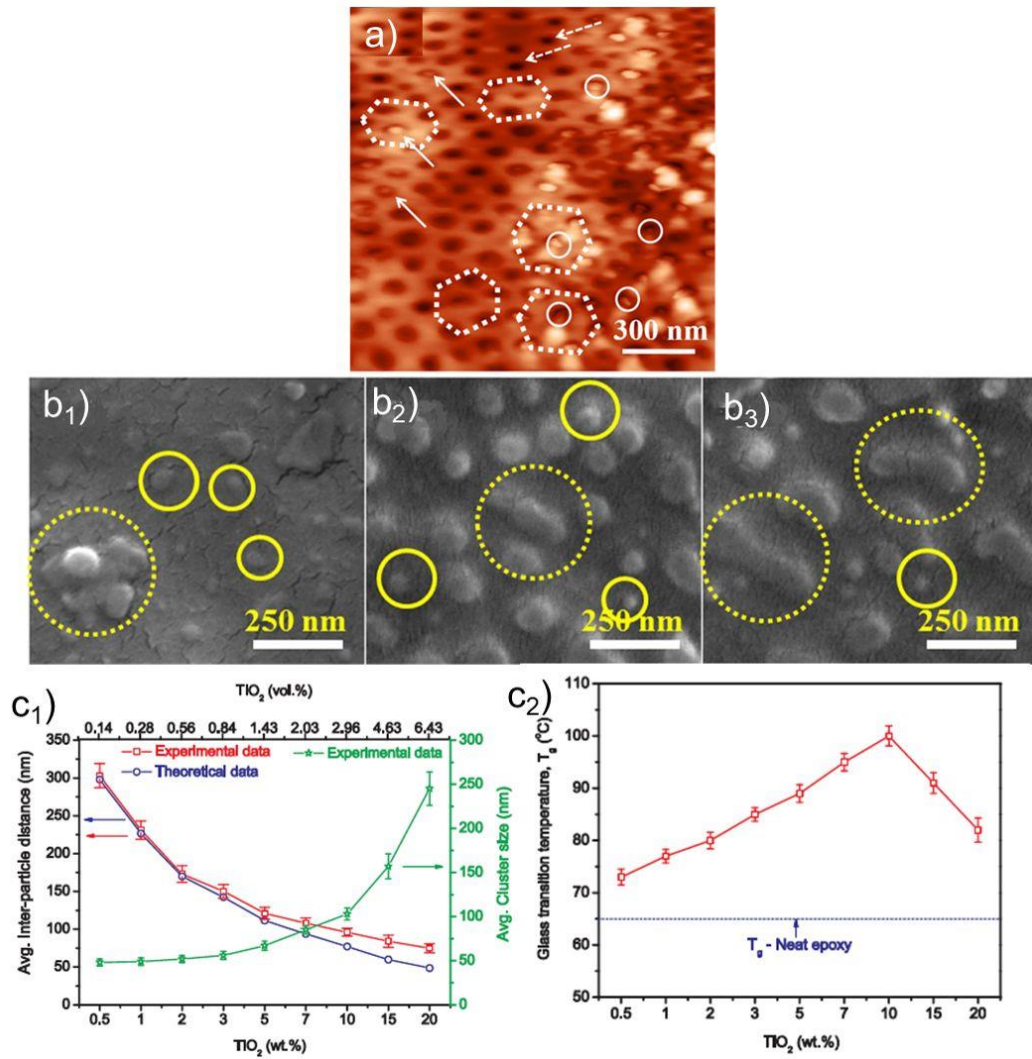
Figure 2-10: Morphological study of TiO_2-epoxy nanocomposite a) AFM image of UDM processed TiO_2-epoxy nanocomposite b1) SEM images of 5%TiO_2-epoxy, b2) SEM image of 10% TiO_2-epoxy, b3) SEM image of 20% TiO_2-epoxy composite c1) Theoretical and practical variation of cluster size with TiO_2 content c2) Variation in T_g.
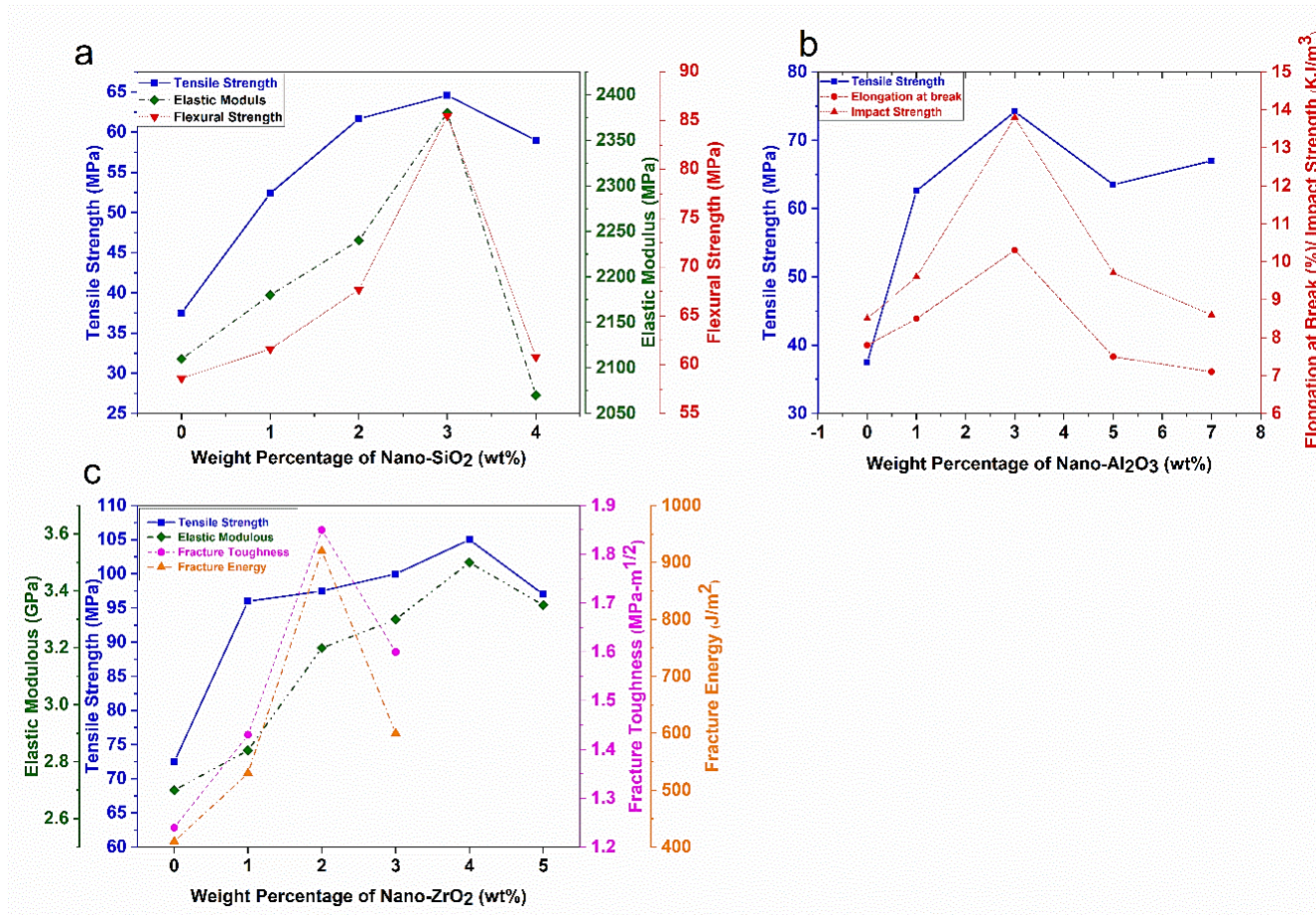
Figure 2-11: Comparison of mechanical properties of ONP-epoxy nanocomposite a) SiO_2-epoxy b) Al_2O_3-epoxy c) ZrO_2-epoxy.

SEM images reported in the mentioned works of literature reveal that the fracture surface of ZrO_2 reinforced epoxy composite is rougher than that of others, indicating better particle distribution. Further, the fracture surface shows some traces of dimple formation (ductile characteristics). The fracture surface morphology of SiO_2 (ONP) reinforced nanocomposites reveals various fracture characteristics. The reported fracture surface consists of many micro-crack, shear deformation marks, and a piece of sizeable micro-crack propagation evidence.

2.6 CNTS REINFORCED EPOXY COMPOSITES

Adding CNT into the epoxy matrix is customary because of drastic improvements in the mechanical and thermal properties of the epoxy nanocomposite. This section is dedicated to understanding the effect of adding CNT on the physical properties of the epoxy nanocomposite. Xiao et al. (Xiao et al., 2018) performed a comparative analysis of the mechanical properties of CNT reinforced and SiO_2 (ONP) reinforced nanocomposite. The authors revealed that adding MWCNT improves the tensile strength by 38% compared to pristine epoxy, while adding nano SiO_2 increases the tensile strength by 72%. This happened because of the string CNT-CNT interaction in the matrix. This interaction increases particle agglomeration and hinders the dispersion process. Further, the fracture surface revealed CNT pull out (arrow marked Figure 2-12 f) and delamination effect, which clearly indicates weak interface formation compared to ONP, reinforced composite. Figure 2-12 summarizes the above comparison. The MWCNT-reinforced composite fracture surface is comparatively smoother than the fracture of SiO_2-reinforced composite (Xiao et al., 2018). Researchers have made many attempts to utilize the exceptional properties of CNT as a filler in the epoxy matrix to enhance the tensile strength, flexural strength, glass transition temperature, wear resistance, and thermal conductivity of nanocomposite (Du et al., 2007).
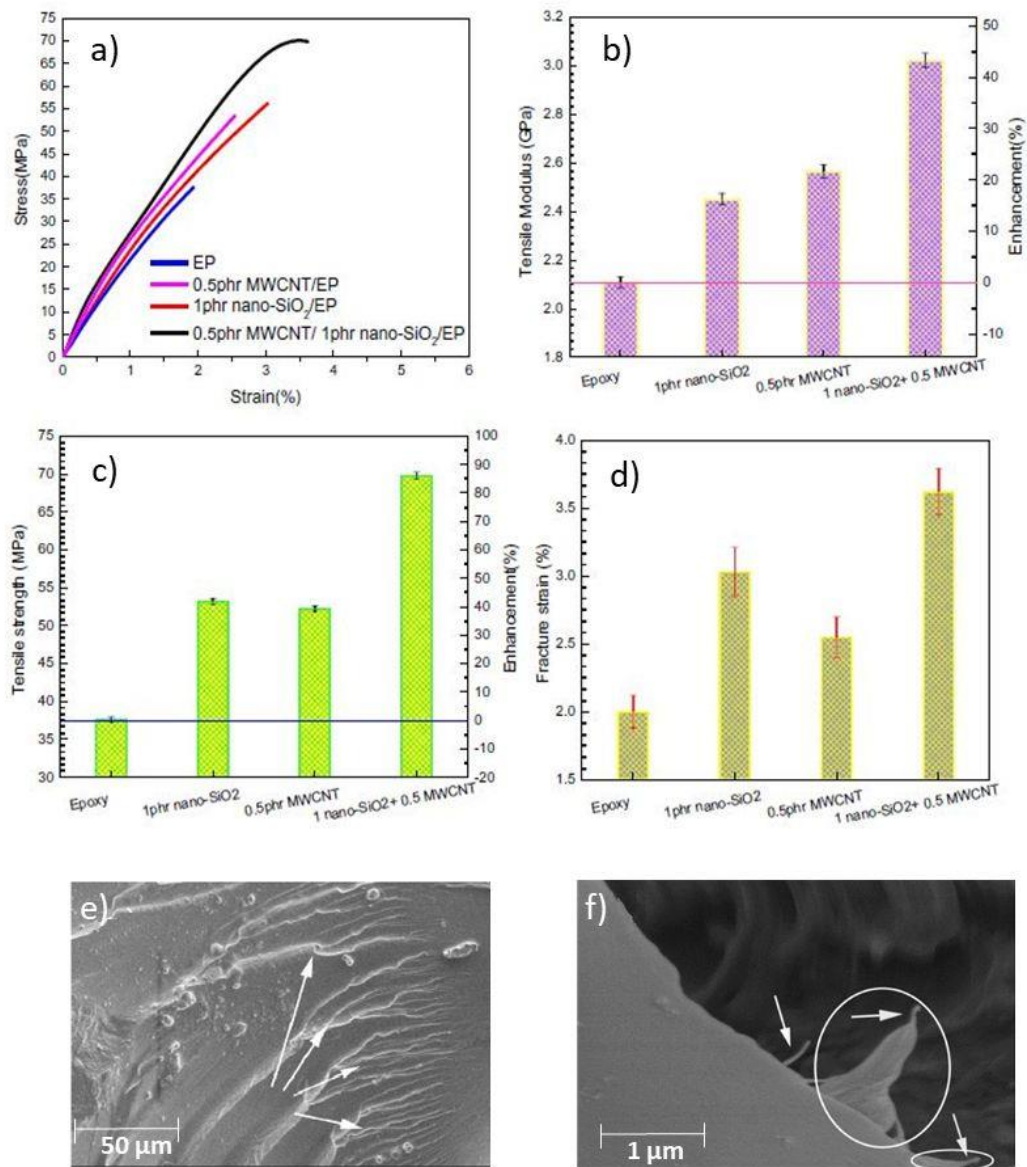
Figure 2-12: Comparison of SiO_2 (ONP) and MWCNT reinforced nanocomposite a-d) comparison of mechanical properties e) SEM micrograph of the fracture surface of MWCNT-epoxy nanocomposite f) MWCNT/ SiO_2 hybrid epoxy composite. Reproduced with permission from Ref (Xiao et al., 2018).

Though incorporating CNT in epoxy enhances its property, mixing it beyond a threshold value (1wt%) creates significant particle agglomeration due to the dominance of CNT-CNT interaction over CNT-epoxy interaction. This leads to weak epoxy-CNT interface formation and lowers mechanical and thermal

properties. There are three primary toughening mechanisms in CNT-based polymer nanocomposite: CNT pull out, interfacial deboning, and plastic deformation at CNT sites. Hyunseong Shin (Shin, 2021) compared the epoxy-CNT composite's theoretical and experimental fracture toughness. They had concluded that shear yielding is a dominant toughening mechanism in the epoxy-CNT composite. In that study, they neglected interfacial interaction. Duan et al. (Duan et al., 2021) used a molecular dynamics approach to investigate CNT-epoxy interaction at the interphase. They reported that CNT pullout interaction dominates the embedded shear interaction (at the end of CNT) in the interfacial region. For a 2 nm diameter, the solid pullout shear strength of around 132 MPa can be achieved, while the sliding shear strength (CNT shearing) will remain around 7 MPa. Further, surface defects of CNT produce mechanical linking, leading to enhancement in the fracture properties of the composite. Their proposed model is shown in Figure 2-13.
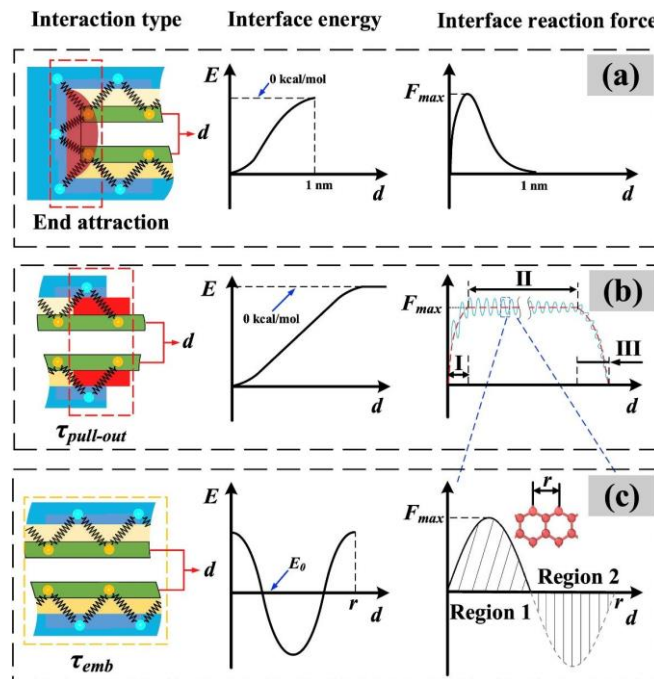
Figure 2-13: Model for CNT-epoxy interaction at the interface a) variation of interfacial energy and force with the CNT displacement at CNT ends b) variation of interfacial energy and force with CNT displacement at tip of the crack c) variation of interfacial energy (Duan et al., 2021).

Functionalization of CNT is also one of the innovative methods to get homogeneous particle distribution in the epoxy matrix (Ciofani et al., 2009). Functionalization adds covalently bonded chemicals on the surface of CNT, which enhances CNT-epoxy interaction and forms a robust interface. Further, it acts as the inter-CNT spacer, which prohibits particle agglomeration. Chet et al. (Chen et al., 2019) investigated the effect of adding thiol-functionalized CNT into the epoxy matrix. The authors reported a drastic improvement in the glass transition temperature, thermal conductivity, tensile strength, and fracture strength by incorporating functionalized CNT into the epoxy matrix.

Further, 60%, 27%, and 80% improvement in the tensile, bending, and fracture strength by incorporating functionalized CNT into the epoxy matrix was obtained, respectively. Cha et al. (Cha et al., 2017) investigated the effect of adding melamine-functionalized MWCNT on the mechanical properties of the epoxy nanocomposite. They revealed that well-dispersed CNT bridges the cracks by rupturing and pulling out (Figure 2-14). The crack-bridging ability of CNT will lead to delayed fracture.
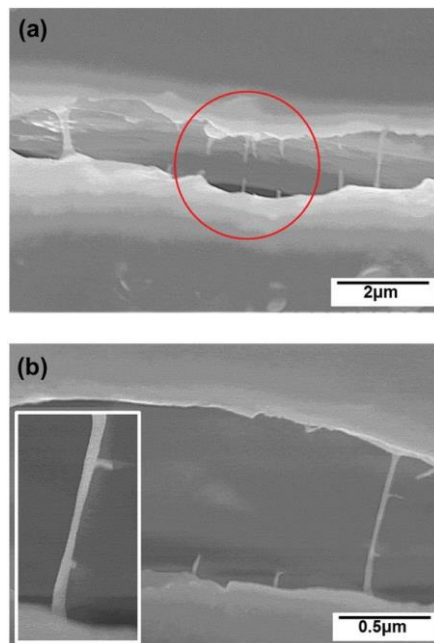
Figure 2-14: SEM of crack bridging by CNT a) CNT fracture b) CNT pull out (Cha et al., 2017).

2.7 HYBRID ONPS-CNT EPOXY COMPOSITES

Although CNT/ONP-reinforced epoxy nanocomposite shows tremendous improvement in mechanical and thermal properties, some significant challenges in both composites include low filler loading, particle agglomeration, and costlier processing (Kundalwal & Choyal, 2018). In most of the research articles, it is evident that increasing the amount of nanofiller (ONP, CNTs) beyond a threshold value decreases the mechanical and thermal properties. The high surface area of the CNT increases the intensity of attractive molecular force between CNT particles, leading to the clustering of nanoparticles (Gojny et al., 2004). A limited CNT loading into an epoxy matrix stops scientists from taking full advantage of the properties of CNT. So it has become essential to develop techniques for getting a homogeneous distribution of CNT even at higher filler content ($\geq$ 1 %). Researchers have tried a variety of innovative techniques (ultra-sonication, functionalization, ultrasonic dual mixing, hybridization, centrifugal mixing, etc.(Cha et al., 2017; Goyat et al., 2018; Goyat & Ghosh, 2017; Rathi & Kundalwal, 2020)) to disperse higher CNT concentration into the epoxy matrix. Functionalizing the CNT is the most common technique for enhancing particle distribution, but it suffers from various demerits like void creation, high cost, and ample reaction time. Ultrasonication is also one of the innovative techniques in which high-frequency sound waves propagate into epoxy during processing. The sinusoidal nature of ultrasound waves creates compression and refraction into the polymer matrix, resulting in creating millions of micron-size bubbles in the polymer matrix. After achieving a critical size, these bubbles burst, leading to a high temperature and pressure rise in the localized regions of the epoxy (A. Kumar et al., 2017). This phenomenon helps in breaking the CNT clustering in a viscous epoxy matrix. Ultrasonic waves are incorporated with the help of an ultrasonic horn or probe. Therefore, this cavitation technique is only helpful for breaking the particle clustering near the ultrasonic horn. Moreover, the technique also diminishes the quality of resin due to a temperature rise. Scientists have developed the UDM (ultrasonic dual mixing) technique to improve the shortcoming of the ultrasonication process. This technique is a unique combination of mechanical mixing and

ultrasonication process. UDM imparts a unique flow pattern into the epoxy matrix, which is quite different from the flow pattern of ultrasonication and mechanical mixing. Both ultrasonication and mechanical mixing create a non-reactive (dead zone) zone where bubbles' cavitation phenomena do not occur (S. Li et al., 2018; Nanzai et al., 2009). In UDM, mechanical mixing provides continuous flow to the resin, and ultrasonication provides the cavitation action for breaking particle aggregates (Anant et al., 2024) . Hybridization is a relatively new and innovative way of getting better CNT particle distribution by simultaneously mixing oxide nanoparticles (ONPs) and CNT into an epoxy matrix. People usually get confused between hybrid material and hybrid composite. Combining two or more fixed-size-scale materials to serve a specific function is called hybrid material. Incorporating one nanofiller in two or more types of base polymer or two or more types of fillers in one base polymer or combining both is called hybrid polymer matrix nanocomposite (HPMNC) (Ashby & Bréchet, 2003). In HPMNC, two or more chemically compatible materials are intentionally added to the polymer matrix. This creates a new class of polymer nanocomposite having unique properties than its constituents. Initially, people have tried to use the simple "rule of mixture" to quantify the properties of HPNC. The rule of mixture says that the final property of the hybrid material should be the weighted volume average of constituent property.

$$P_{cm} = \frac{1}{\sum_{x=1}^{n} V_x} \sum_{x=1}^{n} p_x V_x \qquad \text{(2-1)} \quad \text{(Ashby \& Bréchet, 2003)}$$

P_{cm}= property of final nanocomposite

V_x= Volume of xth component added into the matrix

p_x= corresponding property of xth component

Experimental results of HPNC properties contradict the mixture rule because of the complexity of hybridization. The rule of a mixture (ROM) is derived considering various assumptions, such as homogeneous constituent distribution and neglecting interfacial strength. HPMNC correctly, but it can indicate the suitability of developed HPMNC. Developed composites can be considered perfect if their experimental properties are more significant than the predicted value by ROM (Short & Summerscales, 1980). The suitability of hybrid fillers

depends on the strain developed by fillers in the matrix. We can conclude that if the hybrid filler's combined effect on the properties is more than the effect of the individual filler, then hybridization can be considered a successful process (Manjunath et al., 2021). The geometry of fillers is also one of the vital points to consider in developing a hybrid composite. Mixing two fillers of different geometry into the epoxy matrix may reduce the effective filler content. This happens due to the development of a simultaneous supporting filler network with epoxy strains. Two routes can make HPMNC; first, one is to develop the hybrid ONP and CNT structure by the chemical route and add it into the epoxy matrix (ONP-CNT hybrid-epoxy), and the second one is to develop the ONP and CNT separately and add them into the epoxy matrix (ONP-CNT-epoxy hybrid). Zakaria et al. (Zakaria, Akil, Abdul Kudus, et al., 2015) compared the MWCNT-Al_2O_3 hybrid-epoxy nanocomposite with MWCNT-Al_2O_3-epoxy HPMNC. They developed the MWCNT-Al_2O_3 hybrid structure using the CVD technique. SEM analysis reported in the above literature shows better filler dispersion in the MWCNT-Al_2O_3 hybrid-epoxy nanocomposite than in the MWCNT-Al_2O_3-epoxy system. This results in a more significant enhancement in the mechanical property of particle hybrid-epoxy composite than the particles-epoxy hybrid composite. Developing a hybrid particle structure before mixing into the epoxy creates a pre-mixed homogeneous phase hence it shows better filler dispersion into the matrix (Uddin & Sun, 2010). A similar experiment was performed by Bkhtiar et al. (Bakhtiar et al., 2016) to develop a muscovite-MWCNT hybrid-epoxy and muscovite-MWCNT-epoxy hybrid composite. Authors concluded that developing a muscovite-MWCNT hybrid structure (by CVD) before mixing it into the epoxy matrix creates a strong particle-CNT interaction due to which pull out of muscovite from the epoxy matrix takes more energy as compared to muscovite-MWCNT-epoxy HPMNC. Moreover, synthesizing hybrid ONP-MWCNT by CVD will provide strong CNT-ONP bonding, enhancing particle dispersion and inhibits the detachment of hybrid filler detachment from the epoxy matrix (Nagaraju et al., 2002). The following section will focus on the effect of hybrid fillers on the mechanical and thermal properties of the epoxy nanocomposite.

2.7.1 Al₂O₃-CNT-EPOXY HPMNC

The Al_2O_3 is a rigid, stable, and thermally conductive particle that can potentially be used as a filler in epoxy. Due to the chemical compatibility of Al_2O_3 with CNT, hybrid alumina-CNT epoxy composites show better mechanical and thermal properties. Roustazadeh et al. (Roustazadeh et al., 2020) compared the effects of Al_2O_3 and CNT on the mechanical performance of epoxy nanocomposite. Different composites (pristine epoxy PE, alumina epoxy AE, CNT epoxy CE, and alumina-CNT-epoxy ACE) were prepared using UDM. SEM analysis of the tensile fracture samples shows that the CE sample's crack-bridging ability was relatively low compared to ACE samples. They have reported a 23% improvement in the tensile strength of ACE composite compared to pristine epoxy. Zakaria et al. (Zakaria, Akil, Abdul Kudus, et al., 2015) investigated the effect of adding hybrid alumina-CNT into the epoxy matrix on the microhardness of the nanocomposite. They had developed the hybrid particle by chemical reaction. The authors revealed that chemical hybridization provides better entanglement of CNT on alumina particles than mechanical mixing of the particles into an epoxy matrix. In another work, Kudus et al.(Kudus et al., 2021) studied the thermal degradation of hybrid alumina-CNT epoxy nanocomposite. They concluded that alumina acts as a carrier for the CNT, which provides better particle distribution and interfacial properties for the composite. The degradation temperature of around 450^0C is reported in the literature. Saravanan et al. (Saravanan et al., 2018) have noted that making hybrid alumina-CNT by CVD process before mixing provides better results than mixing them directly into the epoxy matrix. This happens because alumina particles stick to the surface of CNT and reduce the inter-particle forces (Van der Walls), which prohibits particle segregation.

In another work, Zakaria et al. (Zakaria et al., 2016) have studied the effect of hybrid alumina-CNT on the compressive strength of the epoxy nanocomposites. Figure 2-15 (a-b) shows that Hybrid alumina CNT prepared by CVD makes a chemically bonded network structure, while mechanical mixing of alumina and CNT shows physically separated particles. Authors have reported 117% and

148% improvement in the compressive strength and modulus, respectively. Adding alumina provides the protrusion that facilitates the CNT to be attached to the backbone of the epoxy network. Further, such an arrangement helps in easy load transfer and stiff matrix structure. Figure 2-15 (c-d) shows some interesting facts about the fracture surface of the hybrid alumina-CNT-epoxy composite. A well-distributed nanofillers are pretty evident on the fracture surface, which confirms the ability of hybrid fillers distribution. Further, many white dots clearly indicate CNT fracture instead of pull out or shear. So we can conclude that alumina mixing provides exceptional bonding and helps in particle dispersion.
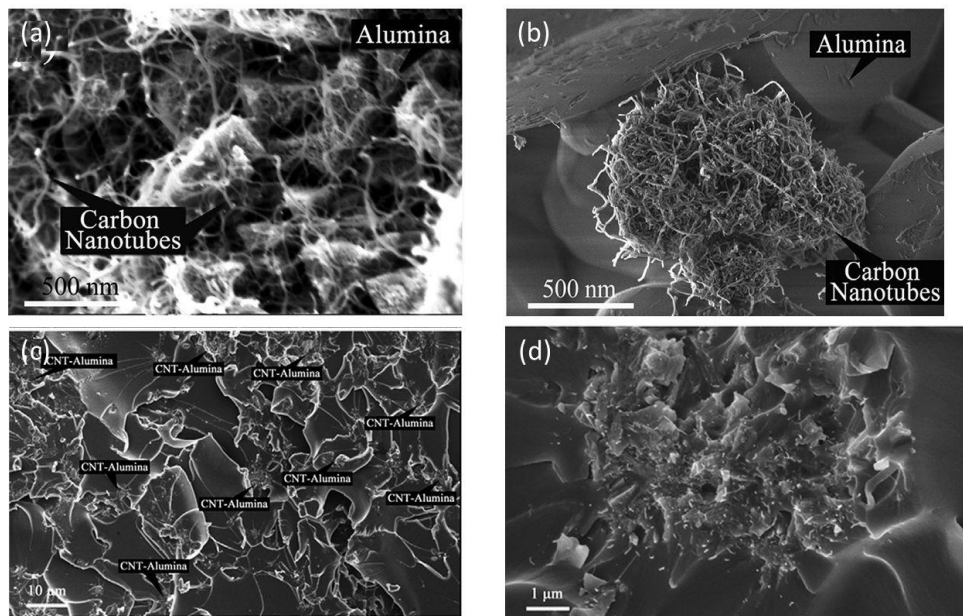
Figure 2-15: SEM images hybrid alumina-CNT epoxy composite a) hybrid CNT-alumina by CVD b) hybrid CNT-alumina by mechanical mixing c-d) fracture surface of hybrid alumina-CNT-epoxy nanocomposite (Zakaria et al., 2016).

2.7.2 ZIRCONIA-CNT-EPOXY HPMNC

Zirconia is one of the promising agents that is compatible with CNT. When added individually into the epoxy matrix, zirconia has shown the best mechanical properties. Further adding zirconia into the alumina-CNT has

shown better particle distribution and strong CNT-alumina interface formation (I. Ahmad et al., 2019). This inspires researchers to exploit the advantage of zirconia in the CNT-epoxy system. Rathi and Kundalwal (Rathi & Kundalwal, 2020) investigate the effect of hybrid zirconia-MWCNT on the mechanical properties of epoxy nanocomposites. Authors have reported that incorporating zirconia-CNT hybrid filler into the epoxy matrix (up to 1wt%) improves the fracture toughness by 32% (Figure 2-16 b). The authors also observed improvement in the elongation at fracture (Figure 2-16 a). This happens due to the rigid bonding of CNT associated with homogeneous filler distribution. Moreover, attaching zirconia to the CNT surface increases the crack pinning effect, delaying fracture. Toughening mechanism of the same is shown in Figure 2-17. Zirconia particles deflect the crack, which requires higher loading for crack propagation. Adding MWCNT produces crack bridging and pullout effect. Hybrid ZrO_2-MWCNT into epoxy matrix combines both crack deflection and crack-bridging mechanisms and enhances the dispersion of MWCNT into the epoxy matrix. These effects lead to the enhanced fracture toughness of the resulted HPMNC. Fractography of the samples revealed that at a low weight fraction of ZrO_2 (0.5%), MWCNT-epoxy interaction was very weak, which lead to a prominent CNT pull-out effect (Figure 2-18 a). Finally, the fracture surface of ZrO_2-MWCNT-epoxy (1 wt% filler loading) had typical characteristics of ductile fractures like rough surface, cleavage, and dendriform (Figure 2-18 b).
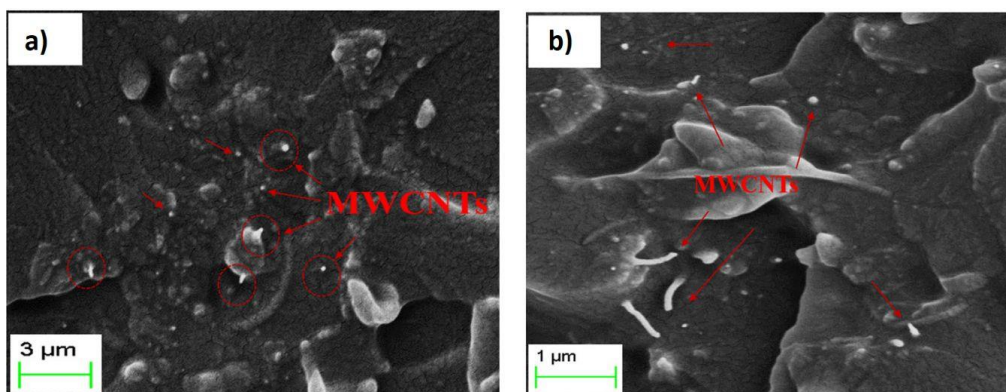
Figure 2-16: SEM micrograph of tensile fracture surface a) ZrO_2-CNT-epoxy (0.5 wt%) b) ZrO_2-CNT-epoxy (0.1 wt%) (Rathi & Kundalwal, 2020).
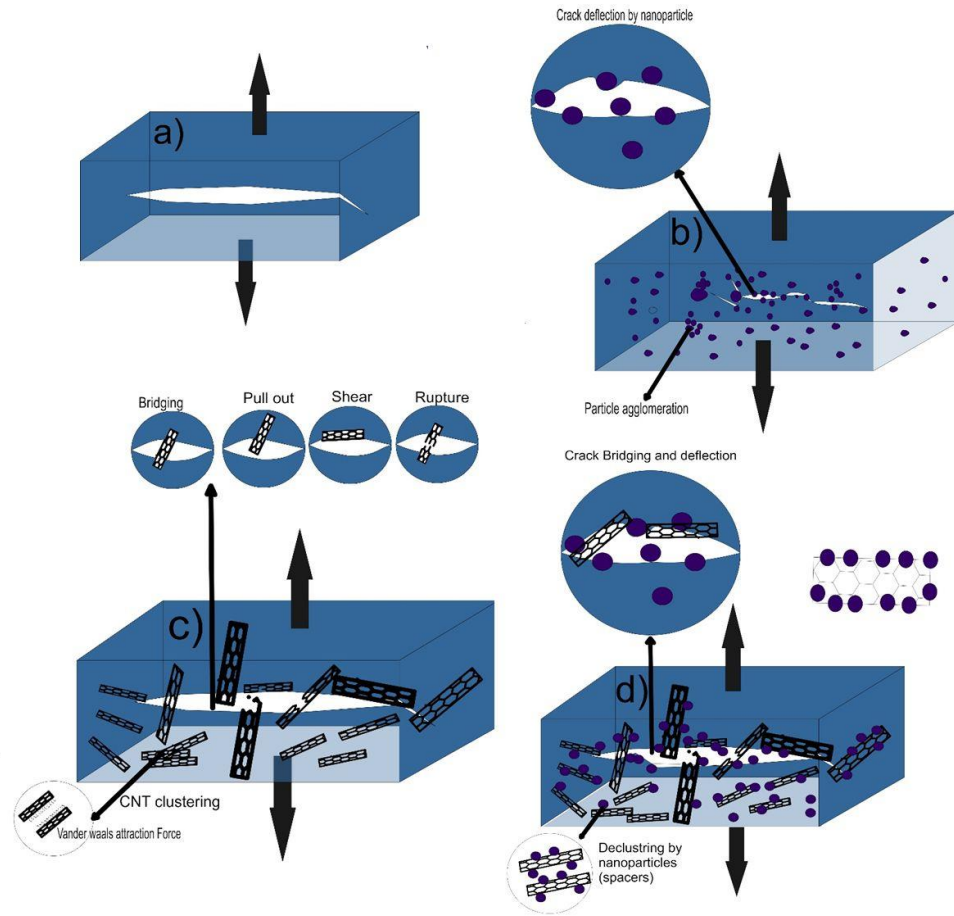
Figure 2-17: Toughening mechanism in HPMNC a) neat epoxy b) Epoxy-ZrO_2 c) Epoxy-CNT d) Epoxy-CNT-ZrO_2.
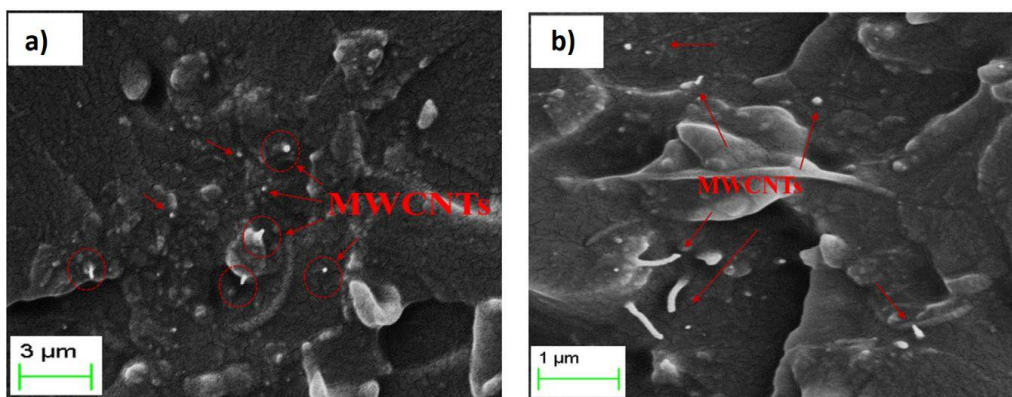
Figure 2-18: SEM images of fracture surface a) ZrO_2-CNT-epoxy (0.5 wt%) b) ZrO_2-CNT-epoxy (0.1 wt%)[24].

Though zirconia has massive potential for being considered a hybrid element in CNT-epoxy nanocomposite, literature is scarce in this field, probably due to the high cost of processing zirconia nanoparticles.

2.7.3 SiO$_2$-CNT-EPOXY HPMNC

Researchers have shown keen interest in adding silica into the CNT-epoxy system to club the properties of silica particles (hardness, crystallinity, thermal stability, stiffness) with the existing system. He et al. (He et al., 2019) investigated the effect of silica nanoparticles on the morphology and properties of CNT. Authors reported that adding silica increases the strength of MWCNT ($\cong 200\%$) and makes it thermally stable. The morphology of silica-added MWCNT resembles the human backbone in which many protrusions are formed. Moreover, the surface of CNT becomes thermally stable due to the protection of silica particles. Zhang et al. (F. Zhang et al., 2021) developed the anti-icing coating by SiO$_2$-CNT-epoxy coating over the aluminium substrate. They have reported the excellent anti-icing and mechanical durability of the coating. The incorporation of silica makes the structure more robust, inhibiting CNT's debonding from the epoxy matrix. Xiao et al. (Xiao et al., 2018) compared the mechanical properties of a hybrid silica-CNT-epoxy composite with the properties of the individual constituent nanocomposite. They have shown that the best properties can be attained with the hybrid nanocomposite (Figure 2-12).

The report revealed that hybrid silica-CNT-epoxy composite improves the tensile strength by 85% (compared to neat epoxy) while CNT-epoxy and silica epoxy composite improve it by 36% and 42%, respectively. This improvement is obviously due to the synergistic strengthening effect of silica and CNT. The SiO$_2$ addition to the CNT-epoxy system also provides chemical and oxidation resistance to the nanocomposite due to the excellent resistivity of SiO$_2$ in the harsh media (acid, temperature, alkaline) (Y. Zhang et al., 2019). Bahramnia et al. (Bahramnia et al., 2021) developed epoxy/polyurethane-MWCNT-SiO$_2$ nanocomposite by the UDM method. Functionalization of both MWCNT and SiO$_2$ nanoparticles was done before processing the composite. Authors have

shown that the hardness of the hybrid MWCNT-SiO$_2$-epoxy composite was best at 0.75% MWCNT and 2.5% SiO$_2$ (Figure 2-19). This happened due to the proper dispersion of MWCNT-SiO$_2$ in the matrix.
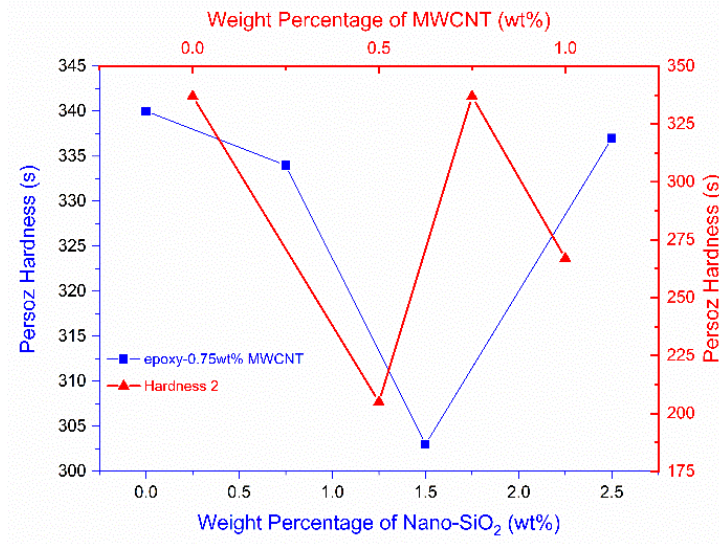
Figure 2-19: Variation of surface hardness in epoxy-MWCNT-SiO2.

Tensile test results (Figure 2-20) reported in the same paper revealed that adding 2.5 wt% of SiO$_2$ and varying wt% of MWCNT improves the elastic modulus but keeps 0.75 wt% MWCNT constant, and varying SiO$_2$ wt% gives the maximum elastic modulus at 0.75 wt% SiO$_2$. An explanation of the same exists in the filler-matrix interaction. On the one hand, MWCNT shows covalent interaction with the epoxy matrix. On the other hand, SiO$_2$ shows hydrogen bonding with the epoxy matrix (Bahramnia et al., 2020). As a covalent bond is much stronger than hydrogen, adding MWCNT reduces the adverse effects of SiO$_2$ agglomerations. The SEM images of pure epoxy, epoxy-CNT, and epoxy-CNT-SiO$_2$ samples are shown in Figure 2-21. The SEM images of hybrid particles show better particle distribution with no aggregation. This happened due to a reduction in inter-particle interaction forces. The SEM images of the samples (after wear) revealed the toughening mechanism. Crack bridging across the wear crater can be easily identified in the SEM of hybrid samples.
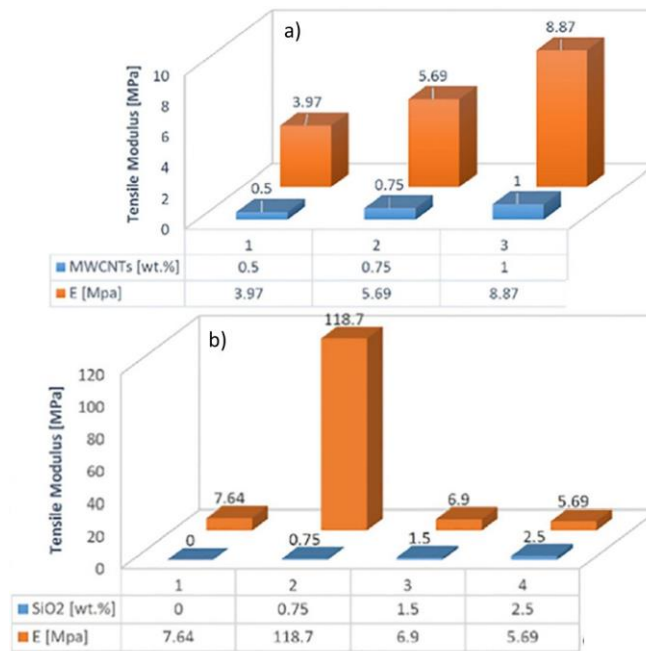
Figure 2-20: Variation of elastic modus with varying wt% of Nanoparticles a) effect of adding MWCNT at fix wt% of SiO_2 (2.5 wt%) b) effect of adding SiO_2 at fix MWCNT % (0.75 wt%) (Bahramnia et al., 2021).
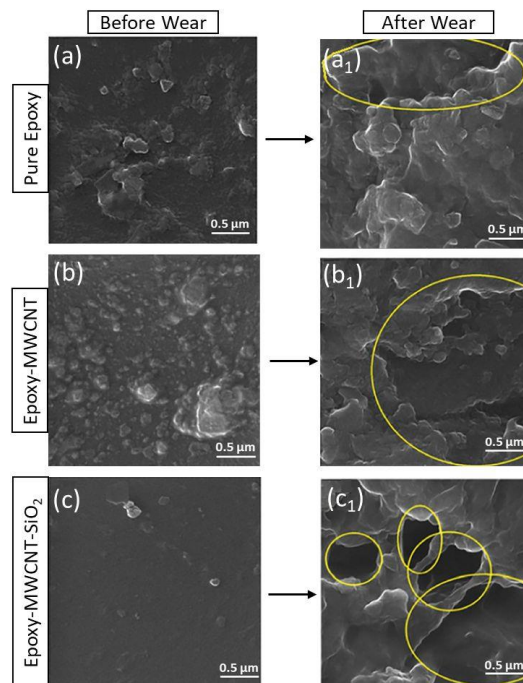
Figure 2-21: SEM micrograph of samples before and after wear a-a1) pure epoxy b-b1) epoxy-0.75 wt% MWCNT c-c1) epoxy-0.75% MWCNT-0.75% SiO_2 (Bahramnia et al., 2021).

43

The field of the CNT-SiO$_2$-epoxy hybrid system is still unexplored, with limited information about the fiber/particle and matrix interface. Intensive work is required to understand the stress transfer, crack propagation, and interfacial region.

2.7.4 TiO$_2$-CNT-EPOXY HPMNC

TiO$_2$ is stiff, optically refractive, corrosion-resistant, and ultraviolet absorbent. The unique properties of TiO$_2$ nanoparticles have brought the attention of researchers to consider it as a nanofiller in the epoxy-CNT system. The synergy of TiO$_2$ and CNT properties makes the epoxy CNT more robust and thermally stable. Kumar et al. (A. Kumar et al., 2018) attached the TiO$_2$ nanoparticles on the surface of CNT and developed the hybrid TiO$_2$-MWCNT-epoxy nanocomposite by ultrasonication. Mixing TiO$_2$ with MWCNT creates an intrinsic interaction that leads to a novel hybrid structure (Figure 2-22 a).
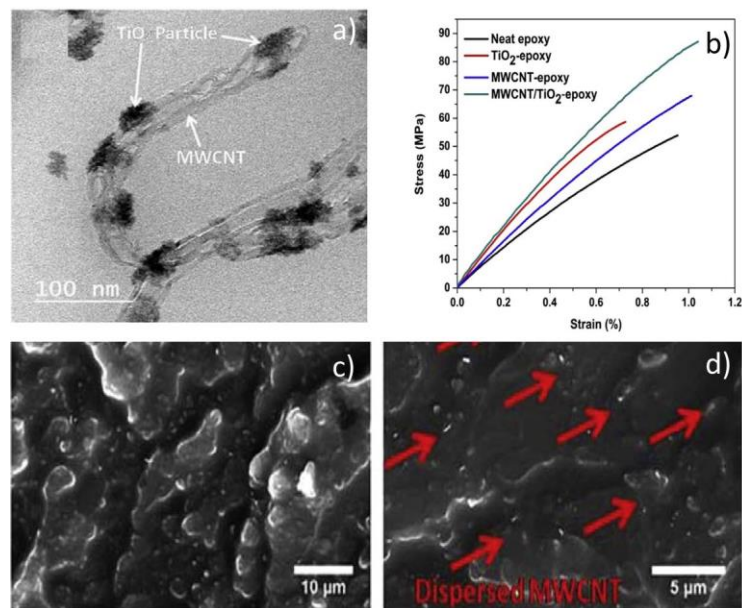
Figure 2-22: TEM, Tensile test, SEM of MWCNT-TiO$_2$ a) TEM Image of novel TiO$_2$-MWCNT structure b) Tensile test results of different samples of nanocomposites c) SEM images fracture surface of TiO$_2$-MWCNT-epoxy nanocomposite d) SEM image of TiO$_2$-MWCNT-epoxy nanocomposite (A. Kumar et al., 2018).

Further, the hexagonal structure of carbon in CNT has a strong tendency to attract TiO_2 nanoparticles (Yang & Wang, 2006). The hybrid MWCNT-TiO_2 structure stops the agglomeration of nanoparticles and creates a stiff interface in the epoxy matrix. Researchers claimed an improvement of 61% in the tensile strength (Figure 2-22 b) of hybrid nanocomposite compared to neat epoxy. Figure 2-22 c shows the SEM images of a tensile fractured surface of TiO_2-MWCNT-epoxy HPMNC. High surface roughness and good particle distribution can be seen in the SEM micrograph. Further, the TiO_2 nanoparticle has a strong affinity for the hexagonal planes of MWCNT. The fracture occurred at the middle of the sample, which is typical evidence of filler-matrix solid interaction. Askari et al. (Askari et al., 2017) performed the structural analysis of hybrid structures formed by TiO_2 and CNT nanoparticles. They have revealed that mixing TiO_2 beyond a certain percentage (> 3%) leads to the formation of TiO_2 agglomerates on the surface of CNT. The functionalization of TiO_2 nanoparticles can resolve the mentioned problem. Yuen et al. (Yuen et al., 2008) developed the Hybrid TiO_2-CNT-epoxy composite by functionalizing the hybrid fillers before processing. They have reported that adding functionalized TiO_2 into the MWCNT-epoxy system doubles the tensile strength, young's modulus, bending strength, and flexural modulus (compared to neat epoxy). Though the strength, hardness, and optical properties can be improved by hybrid TiO_2-CNT-epoxy composite, it reduces the electrical conductivity (good for insulating material). The development of TiO_2-CNT hybrid structure is better than chemical modification of the CNT because it only involves electrostatic interaction between the particles and does not degrade the atomic planes of carbon atoms in CNT. Nanoscale dispersion and rigid filler-matrix interface formation in the CNT-TiO_2-epoxy composite hinder the epoxy chain movement and ease the load transfer between the matrix and hybrid filler. Nitesh et al. (Nitesh et al., 2022) studied the fracture surface morphology in TiO_2-MWCNT-epoxy HPMNC. The authors mentioned three main regions (mirror zone, mist zone, hackle zone) at the fracture surface of neat epoxy with the crack initiation point at the corner of the surface. These entire zones were found to be flat with a river-like pattern. This is a typical feature of brittle fracture in the epoxy

(Bhatia et al., 2021). The author concluded that adding hybrid TiO_2-MWCNT into epoxy delays the crack-by-crack twisting phenomena. The fracture surface of hybrid TiO_2-MWCNT-epoxy composite (Figure 2-23) depicts two essential features, i.e., crack initiation points comes into the center with propagation in all direction (circular mist zone) and evidence of helicoid cracks (a typical quality of crack twisting).
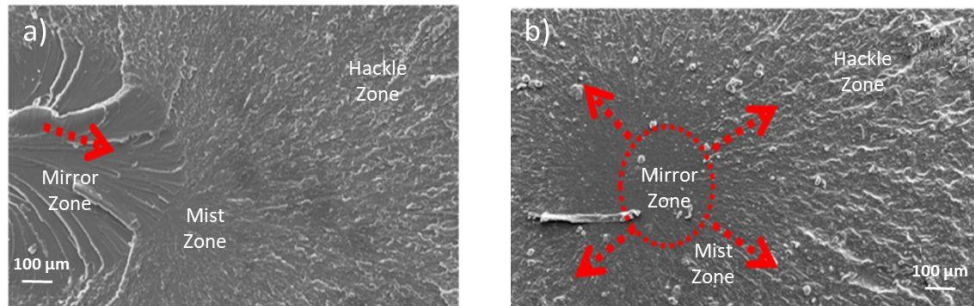
Figure 2-23: SEM of the tensile fracture surface of epoxy and HPMNC a) pristine epoxy b) TiO_2-MWCNT-epoxy nanocomposite (Nitesh et al., 2022).

Although several attempts have been made to develop TiO_2-CNT-epoxy HPMNC, researchers still need attention to address issues like high particle loading (> 1 wt%), stress transfer mechanism, optimized processing parameters, optimum particle content, etc.

Finally, the detailed comparison of various mechanical properties for the different hybrid nanocomposites is shown in Table 2-3. A closer look at the table shows some interesting comparative analyses. Ultra sonication and mechanical stirring are the most common techniques for developing epoxy-based HPMNC. Fewer efforts have been made to utilize the UDM technique for exploring the advantage of combining ultrasonication and mechanical mixing. Incorporating Al_2O_3 or TiO_2 into the epoxy-CNT system enhances the tensile strength to the largest extent. Increasing the amount of Al_2O_3 in the epoxy-CNT system increases the tensile strength and tensile modulus. The TiO_2-CNT-epoxy system provides 330% and 610% more tensile modulus than Al_2O_3-CNT-epoxy and ZrO_2-CNT-epoxy systems. There are very few studies demonstrating the synergistic effect of adding SiO_2 and CNT on the mechanical properties of the epoxy composite.

A comparison of CNT-ONP-epoxy HPMNC with the nanocomposite made by mixing individual particles (CNT-epoxy, ONP-epoxy) is shown in Table 2-4. Percentage improvement in the properties for each type of composite (as compared to neat epoxy) is shown in the small bracket beside the property value. It is worth noting here that plenty of research and review work is already published to show the influence of individual nanofillers (ONP/CNT) on the mechanical properties of epoxy nanocomposite. Still, literature is scarce in the field of hybrid nanocomposites. Significantly, few authors have compared all three types of nanocomposites, i.e., ONP-epoxy, CNT-epoxy, and ONP-CNT-epoxy nanocomposite. Hence, the same can be considered a grey area to be worked in the future. It is evident from the table that TiO_2 and SiO_2 are the two most influencing property enhancers. This may be because of the high hardness and stability of these ONPs. Another reason for this is their reactivity with epoxy.

Table 2-3: Summary of research work done on the ONP-CNT-epoxy nanocomposite (TS/CS = tensile/compressive strength, TM= tensile modules, FS= flexural strength, FM= flexural modulus, HV= Vickers hardness, Ej= energy absorbed at fracture, K_{IC}= mode I fracture toughness in Mpa.m0.5)

Type of ONP	Size (nm)	CNT type	Size d (nm)	Functionalizing agent	Processing technique	Mechanical Properties						Ref
						TS/CS$ MPa	*TM/CM! MPa*	*FS MPa*	*FM MPa*	*HV*	*KIC/JIC,COF,Ej*	
Al_2O_3	-	MW CNT	10-15	Nickel nitrate hexahydrate	Ultrasonication	-	-	-	-	17 (hv)	-	(Zakaria, Akil, Abdul Kudus, et al., 2015)
Al_2O_3	-	MW CNT	25	-	Stirring, Ultrasonication	-	-	-	-	-	-	(Kudus et al., 2021)
Al_2O_3	60	MW CNT	40	-	UDM	42.92	1911.4	-	-	-	-	(Roustazadeh et al., 2020)
Al_2O_3	-	MW CNT	10-20	Nickel nitrate	Ultrasonication	90	2300	-	-	-	Ej= 202 J	(Saravanan et al., 2018)

				hexahydrate								
Al_2O_3	50	MW CNT	10-30	Nickel nitrate hexahydrate	Ultrasonication	72.97[$]	2570 [!]	-	-	-	-	(Zakaria et al., 2016)
Al_2O_3	30	MW CNT	10-20	Nickel nitrate hexahydrate	Ultrasonication	-	-	132.6	5000	-	-	(Zakaria, Akil, Kudus, et al., 2015)
Al_2O_3	-	MW CNT	10-30	Nickel nitrate hexahydrate	Ultrasonication	-	-	-	-	-	$K_{IC}= 2$	(Zakaria et al., 2017)
Al_2O_3	-	MW CNT	20nm	Nickel nitrate hexahydrate	Ultrasonication	-	-	-	-	-	COF= 0.25 and SWR = .01	(Saravanan et al., 2019)

											$mm^3/$ Nm	
ZrO_2	25	MW CNT	25	-	UDM	-	-	-	-	-	K_{IC}= 1.7	(Rathi & Kundalwal, 2020)
ZrO_2	50	Carb on fiber	5500	Aminopro pyl triethoxysi lane (APTS)	Dip coating	-	-	-	-	-	$\tau_{interface}$= 90 Mpa, Ej= 200 J/m^2	(Q. Wu et al., 2018)
ZrO_2		GO	1.2 thick	Aminopro pyl triethoxysi lane	Ultrasonication	80	1300	-	-	-	COF= 0.8, SWR .005 $mm^3/$ Nm	(Che et al., 2018)

SiO$_2$	15	MW CNT	15-25	-	UDM	71.04	3087.38	95.0	-	-	-	(Xiao et al., 2018)
SiO$_2$	30	MW CNT	30	Glycidyloxypropyl tirmethox	Ultrasonication	-	-	-	-	-	-	(F. Zhang et al., 2021)
TiO$_2$	30	MW CNT	30	-	UDM	87.11	15190	-	-	1.7	-	(A. Kumar et al., 2018)
TiO$_2$	-	MW CNT	30	-	Ultrasonication	-	-	-	-	-	-	(Askari et al., 2017)
TiO$_2$		MW CNT	10-50	Aminopropyl trimethoxy silane	Mechanical stirring	36.53	2080	116.54	3410	-	-	(Yuen et al., 2008)
TiO$_2$	30	MW CNT	30	-	Ultrasonication	88	9900	-	-	-	-	(Nitesh et al., 2022)

51

Table 2-4: comparative study of mechanical properties of CNT-epoxy, ONP-epoxy, CNT-ONP-epoxy system (TS/CS = tensile/compressive strength, TM= tensile modules, FS= flexural strength, FM= flexural modulus, HV= Hardness, Ej= energy absorbed at fracture, KIC= mode I fracture toughness in Mpa.m0.5)

	TS/CS$ MPa	TM/CM! MPa	FS MPa	FM MPa	HV	TS/CS$ MPa	TM/CM! MPa	FS MPa	FM MPa	HV	TS/CS$ MPa	TM/CM! MPa	FS MPa	FM MPa	HV	
Al_2O_3	40.1 (+14.2 %)	2360 (+10.2 %)	-	-	-	30.5 (-18%)	2209.2 (+3.1 %)	-	-	-	42.92 (+22.3 %)	1911.4 (-10.8%)	-	-	-	(Roustaz adeh et al., 2020)
Al_2O_3	61.04 (+15.1 %)	2190 (+5.3%)	-	-	-	67.64 (+27.6 %)	2470 (18.7 %)	-	-	-	-	-	-	-	-	(Uyaner & Akdemir, 2021)
ZrO_2	60.21 (+45.4 %)	-	-	-	-	-	-	-	-	-	69.5 (+67.9 %)	-	-	-	-	(Rathi & Kundalw al, 2022)
SiO_2	52.22 (+38.8 %)	2565.72 (+21.7 %)	82.7 (+39.7)	-	-	64.75 (+72.1 %)	2656.98 (+26 %)	85.9 (+45.1 %)	-	-	71.04 (+88.8 %)	3087.38 (+46.4 %)	95.0 (+60.5 %)	-	-	(Xiao et al., 2018)

TiO$_2$	67.23 (+24.2%)	12760 (+53.9)	-	-	1.12 (+113%)	58.62 (+8.2%)	10870 (+31.1%	-	-	0.69 (+30%)	87.12 (+60.7%)	15190 (+83.2%)			1.74 (+228%)	(A. Kumar et al., 2018)
TiO$_2$	27.85 (+39.2%)	1470 (+5%)	81.04 (+34.3%	2510 (+34.2%)	-	-	-	-	-	-	36.53 (+115.9%)	2080 (+48.6%)	116.54 (+93%)	3410 (+82.4%)	-	(Yuen et al., 2008)

2.8 GAPS IN THE DEVELOPMENT OF HYBRID POLYMER NANOCOMPOSITES

The development of nanomaterials starts with the selection of appropriate nanofillers. There should be a balance between the cost and the gains by incorporating nanofillers. Due to cost and gain issues, researchers often find it difficult to investigate plenty of combinations (nanofillers, weight ratios). The eventual aim of epoxy nanocomposites is to induce the excellent fundamental characteristics of the nanofillers to the matrix material. However, more effort is still needed to incorporate this objective at the industrial level. Evolving polymer nanocomposite manufacturing techniques that can deliver quality products at an industrial scale is still one of the most significant challenges. Most of the manufacturing techniques have dispersion issues due to the strong tendency of the nanofillers to agglomerate. Further, if we try to break the agglomerates by mechanical forces, there can be a chance of premature failure. Another important issue in the development of the polymer nanocomposite is degassing. Entrapment of atmospheric gases during the processing of the MPNC may lead to the development of internal cracks in the product.

Characteristics and morphology of the nanofillers play an important role in achieving the final properties of the nanocomposites. For example, single-wall carbon nanotubes are comparatively defect-free than multiwall carbon nanotubes (Han & Jaffe, 1998). Functionalization of CNT for better particle distribution also suffers from various issues like harmful chemicals, duration, cost, etc. (S. Kumar et al., 2018). Moreover, achieving a strong filler-matrix bonding is challenging for the industrial-scale development of nanocomposites. The final mechanical and thermal property of the HPMNC largely depends on interface interaction, filler-filler interaction, and immobilization of polymer molecules. This requires vital characterization techniques to reveal the real-time molecular behavior while adding the nanofillers to the polymer matrix. Moreover, optimum filler content for the best

mechanical and thermal properties is always debatable. It is pretty evident from the literature that increasing the filler content beyond a threshold value will degrade mechanical properties. This typically happens due to a change in the nanofiller size because of particle agglomeration (Zare, 2016).

Adding hybrid particles into the epoxy matrix can give better particle distribution due to the lowering of interparticle forces, but this technique also deals with various challenges. The selection of chemically compatible particles is one of the significant issues. For example, suppose the oxide particles do not involve the covalent interaction with the CNT. It will act as a separate filler, resulting in more agglomeration and poor CNT-polymer bonding. Processing techniques for hybrid polymer composite still need to be improved for industrial applications. Some of the issues are selecting optimized process parameters, degassing arrangement, deagglomeration arrangement, cost-effectiveness, etc. Though the ONP-CNT hybrid structure has emerged as a potential reinforcement for lightweight epoxy composites, their fabrication and performance are still meagre. Researchers have identified the following main reasons for the limited performance of HPMNC:

(1) The opposite nature of CNT and ONP (hydrophobic and hydrophilic) limits their interaction with each other as well as with epoxy matrix,

(2) Only a small amount of ONP (1 to 10 wt%) and CNT (0.1 to 1 wt%) have been incorporated to produce the HPMNC,

(3) Inadequate bonding at filler-matrix interface since many researchers have shown fiber pull out and particle debonding at the fracture surface of HPMNC.

(4) Scarcity of proper fabrication routes to develop HPMNC with the best properties.

The scientific community is continuously working to resolve the mentioned issues. For example, scientists tried to create a hybrid ONP-CNT structure with chemically compatible functional groups (with epoxy) before mixing it into the matrix (Rathi & Kundalwal, 2022). Researchers have also tried to reveal the conditions for stable and uniform particle dispersion. Naskae et al. (Naskar et al., 2016) mentioned that

stable dispersion could be achieved when the radius of gyration of polymer matrix molecules is higher than that of nanofiller.

HPMNCs have many advantages over other PMNCs, such as better filler matrix interaction, lower cost of manufacturing as compared to functionalization method, environment-friendly approach for property enhancement, a combination of properties that can be achieved by mixing more than one nanofillers, better filler dispersion due to lower inter-filler attraction force and better mechanical and thermal properties. Apart from many advantages, HPMNCs suffer from a few limitations, such as a lack of clearly defined fabrication techniques for large scale production, more time-consuming approaches for the development of HPMNCs, Scarcity of knowledge for selecting the particle type, size, shape, and weight fraction for optimum properties, limited literature availability for understanding the structure-property relations in HPMNCs.

2.9 OBJECTIVES

The main objectives of current research work are as following:

1. Development of hybrid polymer matrix nanocomposite using epoxy, CNT and oxide particles using ulrasonication dual mixing
2. Optimization of concentration of Nano fillers and there distribution with respect to the mechanical properties of the resulting nanocomposite using DOE.
3. Mechanical Testing and Characterization of nanocomposite by XRD, FTIR, SEM, TGA and DSC etc.

CHAPTER 3

RESEARCH METHODOLOGY

3.1 OVERVIEW

Methodology used in current research work is shown in Figure 3-1. In current study MWCNT with mean diameter of 20 nm and SiO_2 nanoparticles with mean diameter of 15 nm (spherical shape) were utilised as nanofillers. The MWCNTs and SiO_2 nanoparticles were purchased from Reinste Nano Venture ltd. Delhi, India. The epoxy polymer was used as a matrix procured from Fine, and the finish was organic Pvt. Limited (India). The epoxy comprises Epofine-557 (medium viscosity laminating grade multifunctional liquid epoxy resin) and Finehard-5200 aromatic amine hardener. The epoxy used in the current study is a typical material used in bulk, especially in the automobile and aerospace sector (K. Kumar et al., 2021). Typical physical properties of the epoxy system reported by the manufacturer are shown in Table 3-1. Common solvents like acetone and methyl ethyl ketone (MEK) were procured from Sigma Aldrich, India.

Table 3-1: Typical properties of epoxy system.

Material	Viscosity at $25°C$ (mPa-S)	Density at $25°C$ (g/cm^3)	Flash Point ($°C$)	Storage Life (years)
Epofine-557	25000-40000	1.15-1.12	>200	3
Finehard-5200	140-200	0.99-1.02	>120	1
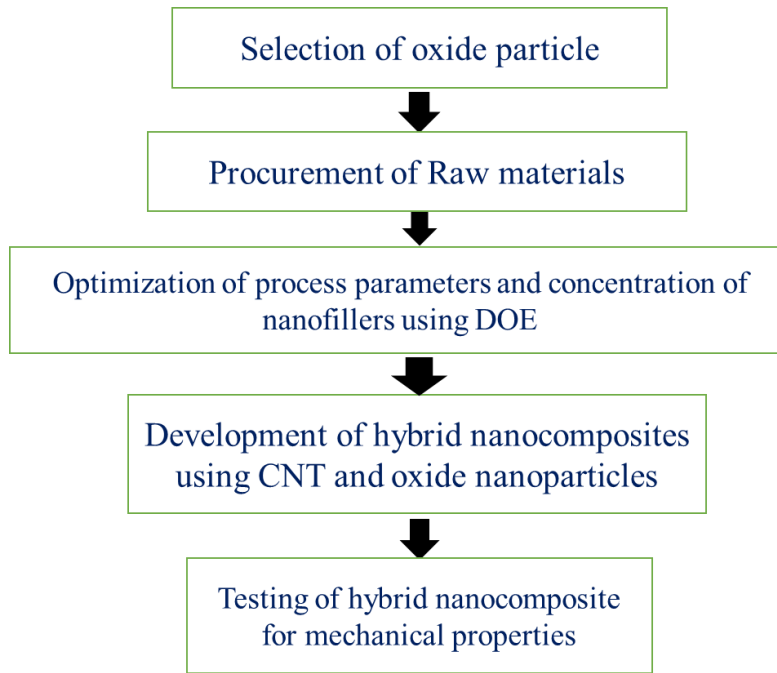
Figure 3-1: Schematic of the research process.

3.2 PREPARATION OF HYBRID NANOCOMPOSITE

Dispersing nanoparticles in a viscous epoxy resin via sonication necessitates an energy level high enough to break up nanoparticle clusters. At the same time, it needs to be quick enough so that the pristine epoxy does not lose its molecular structure. Ultrasonic horns dipped into epoxy resin generate localised heat during UDM, which can compromise base material qualities. A number of factors, including pulseon time (t_{on}), sonication time (t_s), pulse-off time (t_{off}), material volume, sonication amplitude (a) and stirring speed (N_s), contribute to the localised heat generation during UDM. Therefore, MEK solvent was mixed into the epoxy, which worked as a coolant and diminished the base epoxy's viscosity. To regulate the temperature increase in the ultrasonic probe region, an automatic temperature control probe and an ice water bath were used to keep the resin/MEK combination at a constant 30 ^{0}C throughout the process. The hybrid epoxy nanocomposite samples were prepared following the optimized UDM process variables like t_s = 60 min, t_{on} = 10 min, a = 80%, and N_s = 500 rpm (Goyat & Ghosh, 2017).

Hybrid nanocomposite samples were prepared by varying the concentration of MWCNTs (0.1 – 1 wt.%), SiO_2 nanoparticles (1 – 10 wt.%) and curing cycle (1 – 5) as per Taguchi L5 orthogonal array. The range has been decided as per the extensive literature review. All the literature reports clearly mention that if we increase CNT content by more than 1% and Silica doping greater than 10%, properties will decline due to non-controllable agglomeration at such doping level. These three parameters were varied up to 5 levels, as shown in Table 3-2. Compared to a full-factorial experiment, which would require $5^3 = 125$ runs to evaluate three parameters at five levels, Taguchi's factorial experiment only requires 25 experiments. Signal to noise ratio (S/N) values was calculated by analysing the impact of three control variables on the tensile strength and fracture toughness (K_{IC}) of hybrid nanocomposite using the "larger-the-better" formula (Eq. 2) to conclude the optimal arrangement of control parameters.

$$\frac{s}{n} = -10log\frac{1}{n}\sum_{i=1}^{n}\frac{1}{y_i^2} \quad n = 25 \tag{3-1}$$

Here, n = number of runs, y_i = ultimate tensile strength / fracture toughness (K_{IC}) (in the ith experiment (MPa).

Table 3-2: Variables or parameters and their levels used for the optimization.

level	MWCNT (wt%)	SiO$_2$ (wt%)	Curing cycle
1	0.1	1	120℃ / 2 h + 160℃ / 6 h (C1)
2	0.3	3	100℃ / 4 h + 120℃ / 2 h + 160℃ / 6 h (C2)
3	0.5	5	100℃ / 4 h + 120℃ / 2 h + 140℃ / 2 h + 180℃ / 2 h (C3)
4	0.7	7	140℃ / 4 h + 160℃ / 4 h + 180℃ / 2 h (C4)
5	1	10	160℃ / 2 h + 180℃ / 4 h + 200℃ / 4 h (C5)

A measured quantity of MEK (3 times the volume of epoxy) was introduced into the pristine epoxy to decrease its viscosity. The resulting mixture was subsequently blended with SiO_2 and MWCNTs nanopowder at varying concentrations (as per

Table 3), utilizing mechanical stirring by magnetic stirrer at 500 rpm for 30 min. Thereafter, the solution was UDM processed with optimized parameters. For UDM processing ultrasonicator (Sonics & Materials Inc., vibracell VCX -750 Figure 3-2 a) and magnetic stirrer (Remilab pvt. Ltd, REMI-2MLH, 0-1200 rpm) was used. Subsequently, the MEK was extracted from the mixture by keeping the solution on a magnetic stirrer at 50 ℃ for 4 h. The MEK removal was confirmed by comparing the initial and final weights of the epoxy system (before and after adding the MEK). Then, a hardener was added in the ratio of 100:26 and hand stirring was applied for 20 min. The trapped air in the mixture during mixing hardener was removed using a high vacuum pump at 50 ℃ for 30 min. The mixture was introduced into iron moulds coated with Teflon tapes. Moulds were kept in the muffle furnace (Nobertherm make Figure 3-2 b) for curing at different curing cycles. Samples were cleaned and dried properly after curing. The step-by-step process of manufacturing hybrid epoxy nanocomposites is shown in Figure 3-3. Neat epoxy samples were also prepared at different curing cycles for the comparison of results.

Figure 3-2: Images of Instruments used in setup a) Ultrasonicator (Sonics & Materials Inc., vibracell VCX -750) b) Programable muffle furnace Nobertherm, 30-3000 ℃
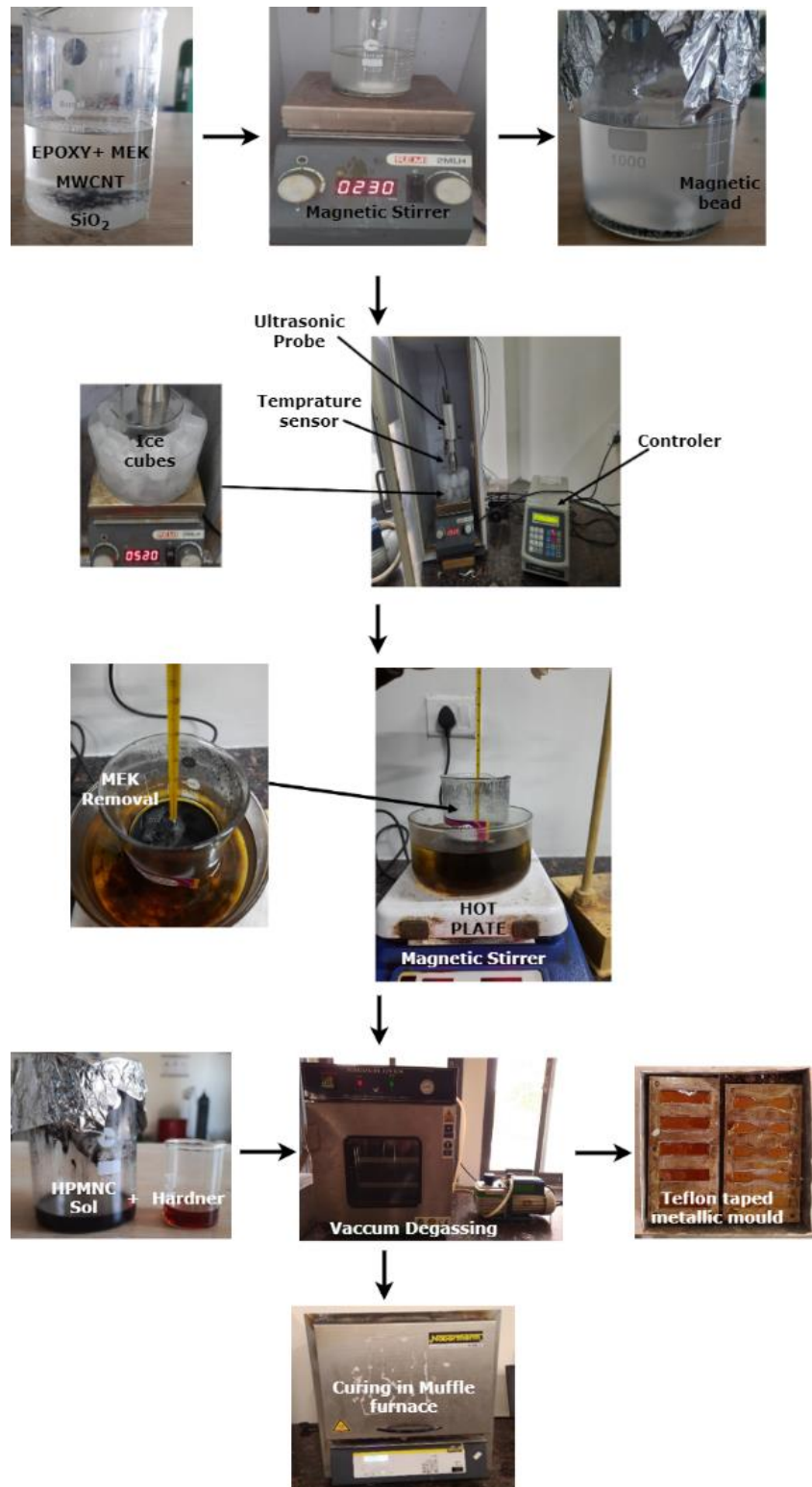
Figure 3-3: Fabrication process for preparation of HENCs.

3.3 MECHANICAL TESTING

3.3.1 TENSILE TESTING

The stress-strain curves were recorded as per ASTM D-638(V) using Computerized Tinius Olsen 50ST Figure 3-4 a. A strain rate of 1 mm/min until fracture was selected. The stress-strain curves were utilized to determine various mechanical characteristics such as tensile strength, elastic modulus (Young's modulus) and percentage of strain-to-break. The determination of the elastic modulus involves the computation of the ratio between the tensile stress and axial strain within the linear elastic region. Figure 3-4 b displays the dimensions of tensile specimens as per the ASTM standard. At least 5 specimens were examined for each composition, and the average values with standard deviations were reported.
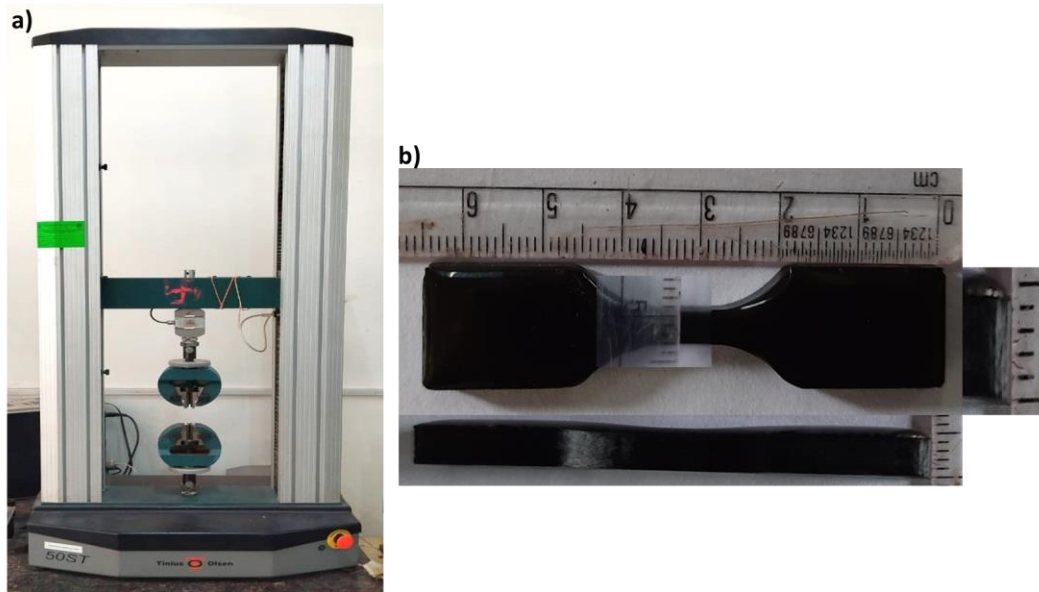
Figure 3-4: Tensile test setup a) UTM, Tenius Olsen, 50ST b) Dimensions of Moulded tensile test specimen.

3.3.2 SINGLE EDGE NOTCH BEND (SENB) TEST

The fracture toughness assessment was conducted following the guidelines of the American Society for Testing and Materials (ASTM-D5045-99) standard

(Standard, 1996). Rectangular 3-P SENB specimens with dimensions conforming to the ASTM standard were fabricated for HPMNC, as depicted in Figure 3-5. Using a 3-P SENB test, the Mode I fracture toughness (K_{Ic}) of an HPMNC specimen of given dimension, having a pre-crack length of 6.25 mm was calculated. The casted specimen was ground and finished as per dimensions given in Figure 3-5. The 6 mm crack length was produced by using precision jewellery cutter. Sharp razor blades was pushed in the crack and moved with a gentle pressure to produce the end of the crack. The test was performed at normal temperature by UTM with a crosshead moving at a constant speed of 10 mm/min. The experimental test equipment used by SENB is shown in Figure 3-6 for mode I fracture specimens. Please take into account that the average K_{IC} values were derived from at least five separate experiments. The relationship below was utilised to get the critical stress intensity factor (K_Q) for mode I:
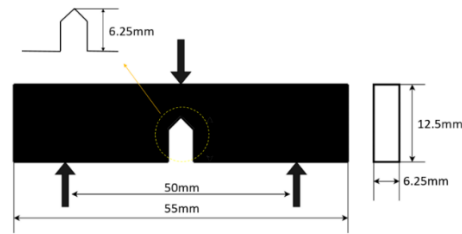
Figure 3-5: Diagrammatical representation of SENB test specimen.
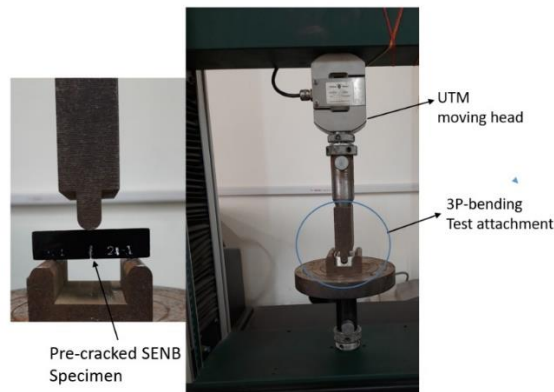
Figure 3-6: 3P SENB testing setup.

$$K_{IC} = \frac{F}{t\sqrt{D}} f(x) \tag{3-2}$$

Here,

K_{IC} = Mode 1 fracture Toughness in MPa-m$^{1/2}$.

F = Applied load at Fracture in KN.

t = Thickness of Specimen in cm.

D = Depth of the Specimen in cm.

$f(x)$ = geometrical multiplication factor it can be determined by Eq. 4.

$$f(x) = 6\omega^{1/2} \frac{[1.99 - \omega(1-\omega)(2.15 - 3.93\omega + 2.7\omega^2)]}{(1+2\omega)(1-\omega)^{3/2}} \tag{3-3}$$

Here,

$$\omega = \frac{z}{D}$$

z = Crack length in cm

3.3.3 VICKERS HARDNESS TEST

The specimens' hardness was tested using a micro-hardness tester (Future-tech FM800, Figure 3-7 a) in accordance with ASTM E 384. Sandpaper (Grit size 200, 400, 600, 1200, 2000) was used to polish the samples followed by cloth polish with diamond paste, to provide a smooth finish so that impressions could be made easily. For this evaluation, a 136^0-square-based Vicker's diamond pyramid indenter was employed. Each sample had an average of ten measurements taken at various locations (10 readings on each specimen). To get the indentation, a force of 100 g was applied for 15 seconds. Vicker's Hardness (HV), provides the definition and the magnitude of the hardness, which is calculated using Eq. 3-4 (Figure 3-7 b).
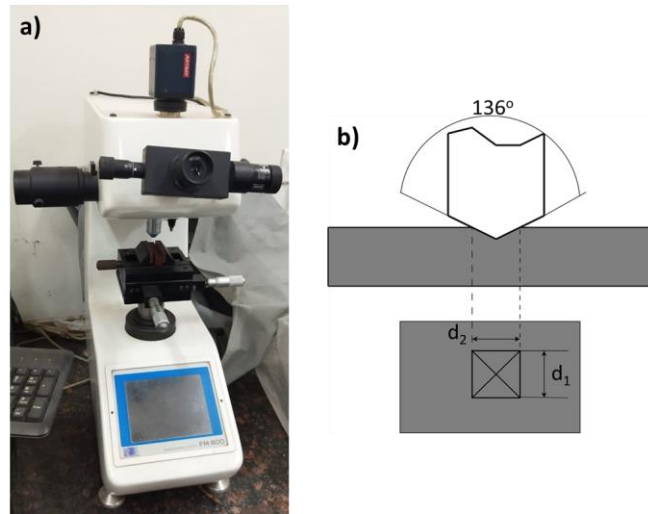
Figure 3-7: Vickers hardness test a) hardness tester, Future-tech corp, FM800 b) diagrammatical representation of Vickers test.

$$HV = \frac{2P \sin 136/2}{d^2} = 1.854 \frac{P}{d^2} \qquad\qquad (3\text{-}4)$$

Here,

P = Applied force in grams.

d = Average indentation diagonal dimension in mm, $d = \frac{d_1 + d_2}{2}$.

3.4 THERMAL TESTING

3.4.1 THERMAL GRAVIMETRIC ANALYSIS

The thermo-gravimetric analysis (TGA) is performed on the manufactured HPMNC samples using a NEXTA STA 200, Hitachi High-Tech Science Corporation, Japan make instrument (Figure 3-8 a) in a nitrogen atmosphere to prevent oxidation effects. At this stage, the nanocomposite samples are weighed, then transferred to a graphite crucible. They are then heated at a rate of 20 degrees Celsius per minute from 50 degrees Celsius to 700 degrees Celsius.

3.4.2 DIFFERENTIAL SCANNING CALORIMETRY

Differential scanning calorimetry (DSC 7020, Hitachi High-Tech Science Corporation, Figure 3-8 b) was performed on samples taken from the bulk nanocomposites. The substance of choice was alumina. Heating at a rate of 10 °C/min, and a temperature range of 30-300 °C while purged with nitrogen gas were used in the DSC study. The data shown here is based on the mean of three to five independent samples.
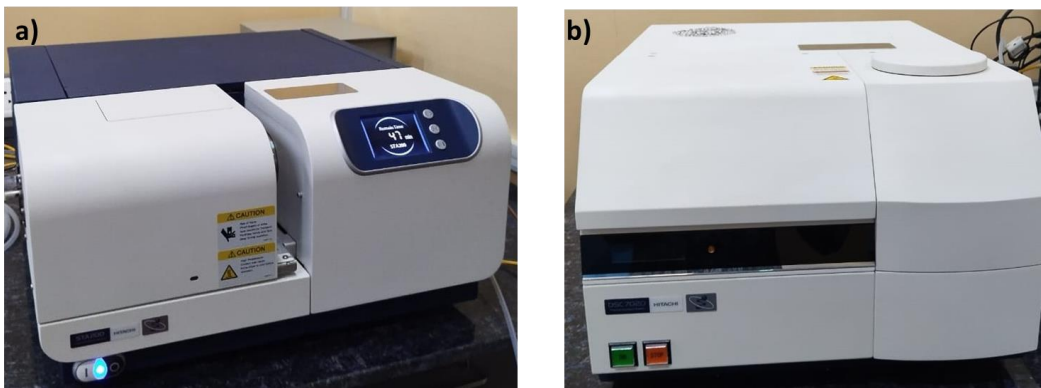
Figure 3-8: Thermal testing setup a) TGA, Hitachi High-Tech Science Corporation, Nexta-STA200 b) DSC, Hitachi High-Tech Science Corporation, DSC

3.5 OPTIMIZATION OF PARAMETERS

The present work mainly focused on finding an optimum concentration of MWCNT, SiO_2 nanoparticles and the best curing cycle that can provide maximum tensile strength and Facture toughness (K_{IC}). As mentioned earlier, Taguchi DOE optimization was performed using Minitab statistical software version 18.

3.5.1 TAGUCHI DOE

Taguchi Design of Experiments (DOE) is a methodical and highly effective approach for optimizing processes and improving product quality through controlled experimentation. Developed by Japanese engineer Genichi Taguchi, this

methodology aims to enhance the robustness and performance of products and processes while minimizing variations and reducing costs. Taguchi DOE involves a structured process that starts with identifying key factors or variables that influence the outcome of a process or product. These factors are categorized into control factors, which can be adjusted, and noise factors, which introduce variability but are not directly controllable (Davis & John, 2018). The goal is to find the optimal combination of control factor settings that yield the desired outcome while being robust to variations caused by noise factors. Central to Taguchi DOE is the concept of orthogonal arrays, which are pre-designed matrices used to efficiently test different factor combinations with a minimal number of experiments. This approach reduces the number of required trials while providing a comprehensive understanding of the factor interactions and their impact on the process or product.

Control variables and their levels incorporated in the current investigation is shown in Table 3-2. The DOE table created on MINITAB is based on three parameters, i.e., % CNT, % SiO_2 % and curing cycle. Based on the parameters discussed, 25 hybrid epoxy nanocomposite samples are prepared and tested for tensile strength and stress concentration factor. A GRA analysis has also been done to find the optimum concentration of %CNT, %SiO_2 and curing time. Later, a sample is prepared using the optimum parameters, and material characterisation is performed using XRD, FTIR, and SEM. The curing cycle impacts the properties of hybrid nan Tensile strength and Fracture toughness, which was the response variable in the current research. The mean value of five repetitive Gray relation analysis tests was filled in the DOE software, and the Taguchi optimization module was used by taking larger the better criteria.

3.5.2 GRAY RELATION ANALYSIS

Though the Taguchi technique is easy and efficient, one major drawback is that it cannot be used for multiple-objective optimization. To solve this problem, Taguchi

coupled with (GRA) can be used. GRA converts multiple responses into single responses by using grey rank analysis. The GRA method started with normalizing the initial data set. The complete process of optimization is briefed in Figure 3-9. Since the objective was to maximize the tensile strength and fracture toughness, the larger the normalization was selected (Kopparthi et al., 2021). The equation for the larger, better criteria is as follows:

$$y_i(k) = \frac{x_i^0(k) - min x_i^0(k)}{\max x_i^0(k) - min x_i^0(k)} \tag{3-5}$$

Where

$y_i(k)$= Normalized measure value

$x_i^o(k)$= Measure value of ith experiment

$maxx_i^o(k)$=Maximum of measure value of ith experiment

$minx_i^o(k)$=Minimum of measure value of ith experiment
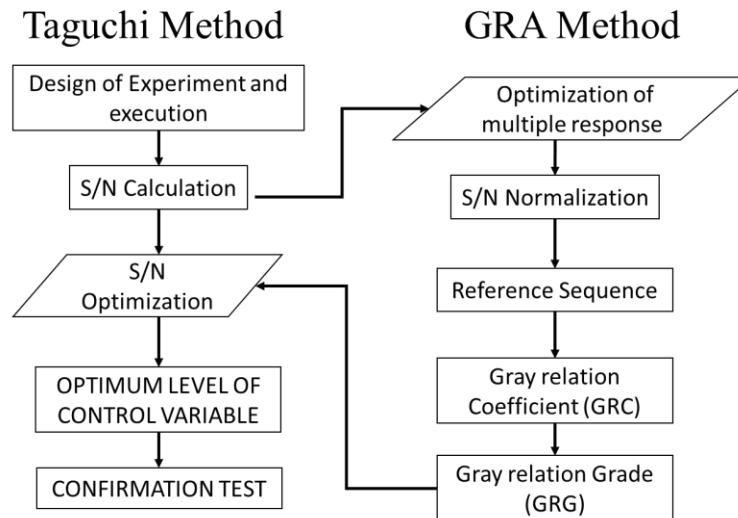
Figure 3-9: Flowchart for GRA based optimization.

After normalization, the Gray relation coefficient was measured by equation 7. Lastly, the Gray relation grade (GRG) was measured by an average of the sum of the Gray relation coefficient as per equation 8.

$$\xi_i(k) = \frac{\Delta_{min} + \zeta \Delta_{max}}{\Delta_{oi}(k) + \zeta \Delta_{max}} \qquad\qquad (3\text{-}6)$$

$$GRG = \frac{1}{n} \sum_{i=1}^{n} \xi_i(k) \qquad\qquad (3\text{-}7)$$

3.6 CHARACTERIZATION

3.6.1 X-RAY DIFFRACTION ANALYSIS

MWCNTs and SiO_2 nanoparticles were dehydrated in an oven at $100\,^{0}C$ for 2 h to remove the moisture content before their characterization. The X-ray diffraction (XRD) investigation was carried out using a Bruker D8 ADVANCE ECO Figure 3-10 with a Cu-Kα radiation source and a wavelength of 1.54 Å. The test was performed at an accelerating voltage of 40 kV with an accelerating current of 20 mA, a step size of 0.05 scanning.

Figure 3-10: XRD setup, Bruker D8 ADVANCE ECO

3.6.2 FIELD EMISSION SCANNING ELECTRON MICROSCOPY (FESEM)

Field emission scanning electron microscope (JEOL make JSM-7610 Fplus, Figure 3-11) analysis of MWCNTs and SiO_2 nanoparticles was performed at a accelerating voltage of 5 kV. Before FESEM analysis, the specimens were washed in ethanol, poured on sample mounts, and allowed to dehydrate at room temperature. The dried specimens were gold-coated using a sputtering set up to obtain high-quality images. A field-emission scanning electron microscope (FESEM) was used to evaluate the morphology of the samples and the fracture surface. The FESEM was used with an accelerating voltage of 15 kV and an operating distance of 10 mm when it was in operation. The ultra-thin layer of gold that was used to create the FESEM samples of selected HPMNC was sputtered on using a thickness of 6 nm.

Figure 3-11: FESEM setup, JEOL make JSM-7610 FPlus, 1 kV 1.0 nm, 15 kV 0.8 nm

CHAPTER 4

RESULT AND DISCUSSION

4.1 PHASE ANALYSIS AND MORPHOLOGY OF MWCNT AND SiO$_2$ NANOPARTICLES

The XRD diffraction pattern of MWCNT and SiO$_2$ nanoparticles is shown in Figure 4-1. The XRD pattern of MWCNT (Figure 4-1 a) shows clear, sharp peaks corresponding to the crystal planes of (002) and (100) at diffraction angles of 26° and 44°. The peaks correspond to a typical shape of a hexagonal graphitic structure. The diameter of MWCNT was determined using the Debye-Scherer equation (Eq. 4-1).

$$d = K \frac{\lambda}{\beta \cos \emptyset} \qquad (4\text{-}1)$$

Where,

d = Average diameter of crystallite

K = Shape constant (0.9),

λ = Radiation wavelength (1.54 Å),

β = Full width at half maxima,

$\emptyset$ = Bragg's angle of respective peaks.

Using Eq. 4-1, the crystallite size of MWCNT was found to be about 10 nm. However, the XRD pattern of SiO$_2$ (Figure 4-1 b) indicates its amorphous nature, marked by a broad hump and the absence of distinct peaks.
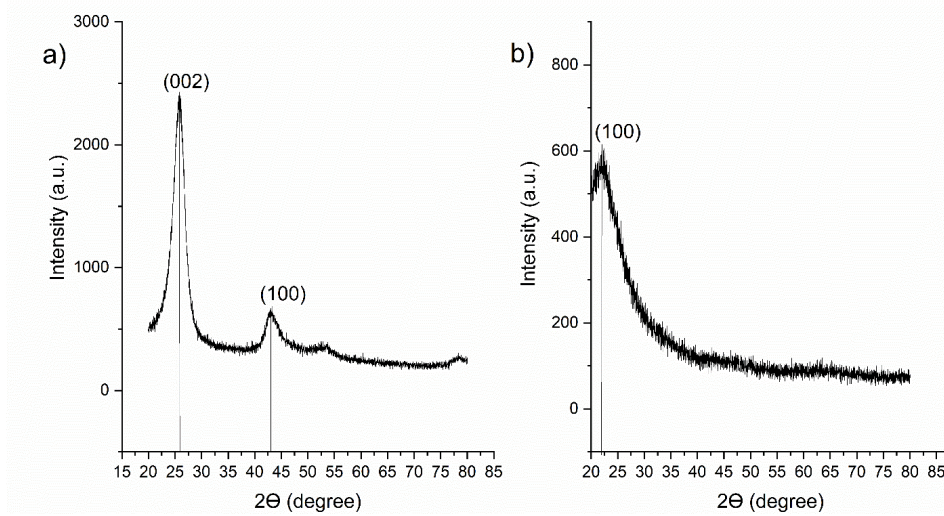
Figure 4-1: XRD pattern of (a) MWCNT and b) SiO_2 nanoparticles.

FESEM images of MWCNT and SiO_2 nanoparticles are shown in Figure 4-2. A typical structure of MWCNT having an average diameter of 15 nm is revealed in Figure 4-2 a, which is found in close agreement with the result of XRD. Spherical shape SiO_2 nanoparticles with a mean diameter of 15 nm is evident from the FESEM image (Figure 4-2 b). However, some large size clusters of nanoparticles are also revealed.
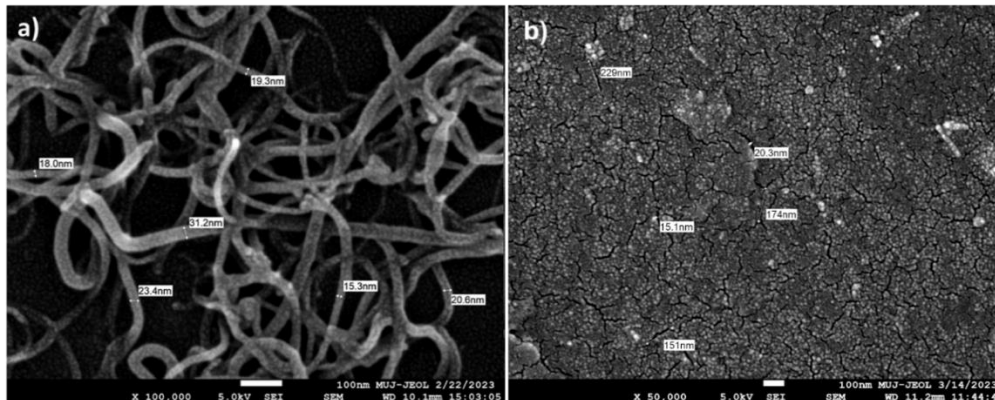
Figure 4-2: FESEM micrograph of (a) MWCNT and (b) SiO_2 nanoparticles.

4.2 OPTIMIZATION OF PARAMETERS

The present work mainly focused on finding an optimum concentration of MWCNT, SiO_2 nanoparticles and the best curing cycle that can provide maximum tensile strength and

Fracture toughness (K_{IC}). As mentioned earlier, Taguchi DOE optimization was performed using Minitab statistical software version 18.

4.2.1 OPTIMIZATION FOR TENSILE STRENGTHS

The tensile strength, associated S/N ratio and Rank are presented in Table 4-1. Table 4-2 shows the response table of the S/N ratio. The table concludes that the curing cycle is the most influencing parameter, followed by MWCNT wt%. This is because the curing cycle decides the level of cross linking in polymer composite. Incomplete cross linking produces a weak matrix which results in low tensile strength (Zaghloul et al., 2023). MWCNT is the most influential particle because of the fact that MWCNT can not only bridge the propagating crack but also produce a better filler matrix interface (Özbek & Çakır, 2022). Table 4-1shows the influence of individual parameters on the tensile strength. It shows that the best set of combinations is 1% MWCNT, 10% SiO2, and 2nd curing cycle. Further, Regression analysis of the data was performed, and a regression equation was predicted (Eq. 4-2). The effect of individual parameters on the mean tensile strength is shown in Figure 4-3. Figure concludes that increasing the content of MWCNT (0.3 wt.%) decreases the tensile strength of the HENC. This may happen due to low level of interlocking of the polymer chain with the particle. Increasing the particle content further increases the high level of polymer chain interlocking, resulting in rigid interface formation. The same effect is observed in the plot of SiO_2 particle content.

$$\sigma_{pr} = 73.31 + 7.22\,a + 0.717b - 5c \hspace{4cm} (4\text{-}2)$$

Where,

σ_{pr} = Predicted tensile strength.

a = Wt% of MWCNT.

b = Wt% of SiO2.

c = Curing cycle number (1, 2, 3…).

The predicted value of tensile strength and associated percentage error is shown in Table 4-1. HS9 and HS17 showed the most deviation from the predicted value, and the same is

the output from Taguchi as they ranked lower in DOE. The average % error is found to be -1.2%. Hence, the predicted model is in agreement with the actual result. The graphical depiction of the same is presented in Figure 4-4. Further experiments were performed to prepare hybrid epoxy nanocomposites using an optimized set of variables, and the results were found to be in close agreement with the predicted values.

Table 4-1: L5 orthogonal array showing value of tensile strength and associated S/N ration. (PTS = predicated tensile strength by regression analysis).

Sample No	wt% CNT	wt% SiO_2	Curing cycle	Mean Tensile strength (MPa)	S/N ratio	PTS (RA)	% error	Rank
HS1	0.1	1	1	69.2	36.80212	69.739	-0.779	13
HS2	0.1	3	2	78.5	37.89739	66.163	15.716	3
HS3	0.1	5	3	54	34.64788	62.587	-15.902	22
HS4	0.1	7	4	65	36.25827	59.011	9.214	17
HS5	0.1	10	5	58	35.26856	56.152	3.186	20
HS6	0.3	1	2	59	35.41704	66.173	-12.158	19
HS7	0.3	3	3	65.5	36.32483	62.597	4.432	16
HS8	0.3	5	4	70.7	36.98839	59.021	16.519	10
HS9	0.3	7	5	38	31.59567	55.445	-45.908	25
HS10	0.3	10	1	72.5	37.20676	77.636	-7.084	9
HS11	0.5	1	3	70	36.90196	62.607	10.561	12
HS12	0.5	3	4	57	35.1175	59.031	-3.563	21
HS13	0.5	5	5	59.7	35.51949	55.455	7.111	18
HS14	0.5	7	1	74.4	37.43146	76.929	-3.399	4
HS15	0.5	10	2	74	37.38463	74.07	-0.095	5
HS16	0.7	1	4	66.2	36.41716	59.041	10.814	15
HS17	0.7	3	5	43.45	32.7598	55.465	-27.652	24
HS18	0.7	5	1	73.8	37.36113	76.939	-4.253	6

HS19	0.7	7	2	73.2	37.29022	73.363	-0.223	7
HS20	0.7	10	3	69.2	36.80212	70.504	-1.884	13
HS21	1	1	5	51.7	34.26981	56.197	-8.698	23
HS22	1	3	1	73	37.26646	77.671	-6.399	8
HS23	1	5	2	79.2	37.9745	74.095	6.446	1
HS24	1	7	3	70.2	36.92674	70.519	-0.454	11
HS25	1	10	4	78.6	37.90845	67.66	13.919	2

Table 4-2: S/N ratio response table.

Level	1	2	3	4	5	Delta	Rank
wt% CNT	36.17	35.51	36.47	36.13	36.87	1.36	2
wt% SiO$_2$	35.96	35.87	36.5	35.9	36.91	1.04	3
Curing cycle	37.21	37.19	36.32	36.54	33.88	3.33	1
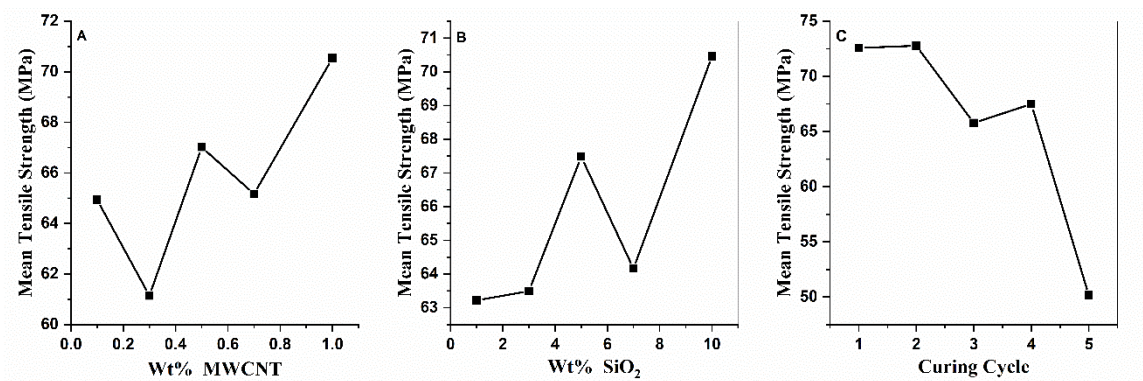
Figure 4-3: Effects of variables on tensile strength of HENCs
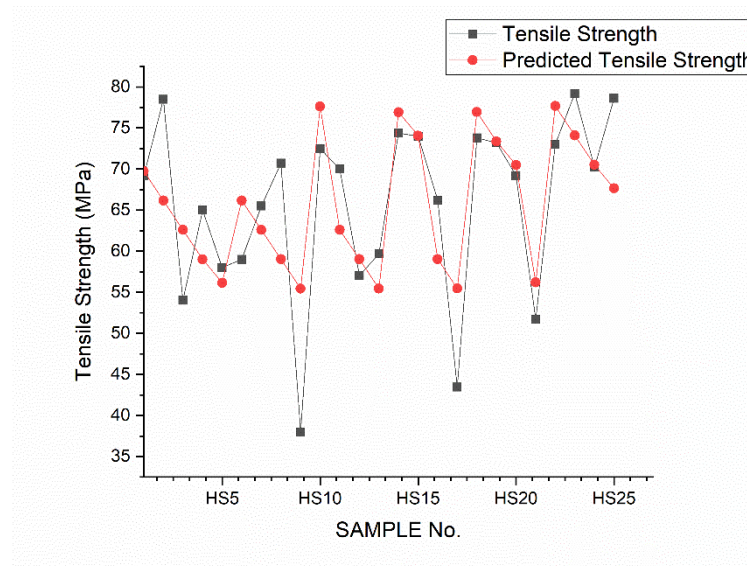
Figure 4-4: Tensile strength of the actual HENCs specimen v/s predicted values.

4.2.2 OPTIMIZATION FOR FRACTURE TOUGHNESS (K_{IC})

The average fracture toughness (K_{IC}) and associated S/N ratio and Rank are presented in Table 4-3. Response table S/N ratio of mean K_{IC} is shown in Table 4-4. It is evident from the results that out of all samples HS7 is the best combination which had given maximum K_{IC}. Load vs deflection curve of the same shows a typical nature of brittle fracture and linear elastic behaviour. The linearity of the force-extension curves and compliance with ASTM D5045-99 requirements are also recognized. Table 4-4 concludes that wt% of SiO2 is the most influencing parameter, followed by curing cycle and wt% MWCNT for maximizing fracture toughness. This happens because CNT helps in crack bridging during fracture, while SiO_2 nanoparticles help in crack deflection (V. Verma et al., 2020). In the SENB test, bending stress is critical to crack opening. CNT is relatively weak in bending; hence, the aligned CNT will rupture during crack propagation. On the other hand, SiO_2 nanoparticles are spherical in shape and can deflect the crack propagation direction (Çakır, 2023). Figure 4-5 describes the influence of control variables on the K_{IC}. 0.3 wt% per cent MWCNT, ten wt% percent SiO_2, and the fifth curing cycle were found to be the optimal conditions for maximum K_{IC}. A confirmation test was executed to obtain the value of K_{IC} for HENC prepared at obtained optimized condition. The result of the same was in close agreement with the modelled value.

76

Table 4-3: Fracture toughness and S/N ratio of the HENC.

Sample No	Wt% CNT	Wt% SiO$_2$	Curing cycle	K_{IC} (Mpa-m$^{1/2}$)	S/N Ratio	Rank
HS1	0.1	1	1	1.47	3.34635	19
HS2	0.1	3	2	1.2	1.58362	25
HS3	0.1	5	3	1.72	4.71057	14
HS4	0.1	7	4	2.04	6.1926	7
HS5	0.1	10	5	1.96	5.84512	9
HS6	0.3	1	2	1.56	3.86249	17
HS7	**0.3**	**3**	**3**	**2.51**	**7.99347**	**1**
HS8	0.3	5	4	1.42	3.04577	21
HS9	0.3	7	5	1.63	4.24375	15
HS10	0.3	10	1	2.35	7.42136	3
HS11	0.5	1	3	1.37	2.73441	23
HS12	0.5	3	4	1.62	4.1903	16
HS13	0.5	5	5	1.87	5.43683	11
HS14	0.5	7	1	1.77	4.95947	13
HS15	0.5	10	2	2.46	7.8187	2
HS16	0.7	1	4	2.29	7.19671	5
HS17	0.7	3	5	2.24	7.00496	6
HS18	0.7	5	1	1.95	5.80069	10
HS19	0.7	7	2	1.43	3.10672	20
HS20	0.7	10	3	1.41	2.98438	22
HS21	1	1	5	2.01	6.06392	8
HS22	1	3	1	1.31	2.34543	24
HS23	1	5	2	2.34	7.38432	4
HS24	1	7	3	1.54	3.75041	18
HS25	1	10	4	1.84	5.29636	12

Table 4-4: Data Table for Signal-to-Noise Ratio Investigations

Level	1	2	3	4	5	Delta	Rank
Wt% CNT	4.336	5.313	5.028	5.219	4.968	0.978	3
Wt% SiO$_2$	4.641	4.624	5.276	4.451	5.873	1.423	1
Curing cycle	4.775	4.751	4.435	5.184	5.719	1.284	2
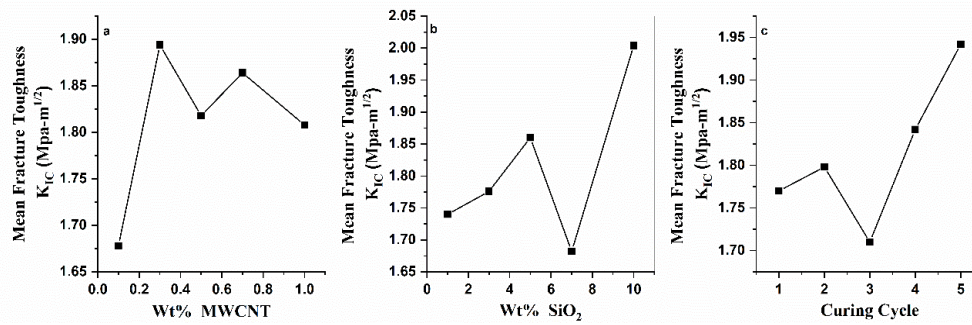
Figure 4-5: Effect of control variables on mean K_{IC}.

4.2.3 GRAY RELATION ANALYSIS-MULTI RESPONSE OPTIMIZATION

The results of the Taguchi-based Gray Relation Analysis (GRA) are shown in Table 4-5. Results revealed that HS-23 (1 wt% MWCNT, 5 wt% SiO_2, 2nd curing cycle) is the best sample out of all developed samples. The obtained GRG was used to run the Taguchi optimization again and the response of the same is mentioned in the Table 4-6. Table revealed that most influencing variable is curing cycle followed by SiO_2 wt% and MWCNT wt%. This result is with respect to tensile strength and fracture Toughness both. Effect of individual parameters is shown in the Table 4-6. It is evident from the results that optimum combination of control variable is 1 wt% MWCNT, 10% SiO_2 and 2nd curing cycle. Samples were prepared based on these control variables, and fracture toughness was in agreement with the modelled value. Numerical analysis revealed the optimum combination of control variables that can be utilized to produce the HENC that can give maximum Tensile strength and fracture toughness. The optimum variable set obtained from the GRA is the same as obtained through Taguchi optimization for tensile strength. Hence, we left with two sets of optimum variables. i.e OP 1 (1 wt% MWCNT, 10 wt% SiO_2, 2nd curing cycle) and OP2 (0.3 wt% MWCNT, 10% SiO_2, 5th curing cycle). Samples were prepared considering OP1 and OP2; the results are mentioned in Figure 4-7.

Table 4-5 Gray relation table for maximizing both tensile strength (TS) and Fracture Toughness (FT) (SNRA= signal to noise ratio, NSNR= normalized signal to noise ratio, D= differential sequence, GRC = Gray relation coefficient, GRG= Gray relation Grade)

Sample No.	Wt% CNT	Wt %SiO2	Curing	tensile strengt	SNRA 1 (TS)	SNRA 1 (FT)	NSNR (TS)	NSNR (FT)	D(TS)	D(FT)	GC (TS)	GC(FT	GI	Rank
HS1	0.1	1	1	69.2	36.80	3.35	0.82	0.28	0.18	0.73	0.73	0.41	0.57	17
HS2	0.1	3	2	78.5	37.90	1.58	0.99	0.00	0.01	1.00	0.98	0.33	0.65	9
HS3	0.1	5	3	54	34.65	4.71	0.48	0.49	0.52	0.51	0.49	0.49	0.49	24
HS4	0.1	7	4	65	36.26	6.19	0.73	0.72	0.27	0.28	0.65	0.64	0.65	10
HS5	0.1	10	5	58	35.27	5.85	0.58	0.66	0.42	0.34	0.54	0.60	0.57	16
HS6	0.3	1	2	59	35.42	3.86	0.60	0.36	0.40	0.64	0.55	0.44	0.50	22
HS7	0.3	3	3	65.5	36.32	7.99	0.74	1.00	0.26	0.00	0.66	1.00	0.83	3
HS8	0.3	5	4	70.7	36.99	3.05	0.85	0.23	0.15	0.77	0.76	0.39	0.58	14
HS9	0.3	7	5	38	31.60	4.24	0.00	0.42	1.00	0.58	0.33	0.46	0.40	25
HS10	0.3	10	1	72.5	37.21	7.42	0.88	0.91	0.12	0.09	0.81	0.85	0.83	4
HS11	0.5	1	3	70	36.90	2.73	0.83	0.18	0.17	0.82	0.75	0.38	0.56	18
HS12	0.5	3	4	57	35.12	4.19	0.55	0.41	0.45	0.59	0.53	0.46	0.49	23
HS13	0.5	5	5	59.7	35.52	5.44	0.62	0.60	0.38	0.40	0.57	0.56	0.56	20

HS14	0.5	7	1	74.4	37.43	4.96	0.91	0.53	0.09	0.47	0.85	0.51	0.68	8
HS15	0.5	10	2	74	37.38	7.82	0.91	0.97	0.09	0.03	0.84	0.95	0.90	2
HS16	0.7	1	4	66.2	36.42	7.20	0.76	0.88	0.24	0.12	0.67	0.80	0.74	6
HS17	0.7	3	5	43.45	32.76	7.00	0.18	0.85	0.82	0.15	0.38	0.76	0.57	15
HS18	0.7	5	1	73.8	37.36	5.80	0.90	0.66	0.10	0.34	0.84	0.59	0.72	7
HS19	0.7	7	2	73.2	37.29	3.11	0.89	0.24	0.11	0.76	0.82	0.40	0.61	11
HS20	0.7	10	3	69.2	36.80	2.98	0.82	0.22	0.18	0.78	0.73	0.39	0.56	19
HS21	1	1	5	51.7	34.27	6.06	0.42	0.70	0.58	0.30	0.46	0.62	0.54	21
HS22	1	3	1	73	37.27	2.35	0.89	0.12	0.11	0.88	0.82	0.36	0.59	13
HS23	**1**	**5**	**2**	**79.2**	**37.97**	**7.38**	**1.00**	**0.90**	**0.00**	**0.10**	**1.00**	**0.84**	**0.92**	**1**
HS24	1	7	3	70.2	36.93	3.75	0.84	0.34	0.16	0.66	0.75	0.43	0.59	12
HS25	1	10	4	78.6	37.91	5.30	0.99	0.58	0.01	0.42	0.98	0.54	0.76	5

Table 4-6 response table for Gray relation grade

parameters	1	2	3	4	5	Delta	rank
Wt% CNT	0.586265	0.625659	0.639353	0.638987	**0.681322**	0.095057	3
Wt%SiO2	0.581788	0.618423	0.653447	0.585522	**0.723053**	0.141266	2
Curring cycle	0.677491	**0.715351**	0.607398	0.642769	0.528577	0.186774	1
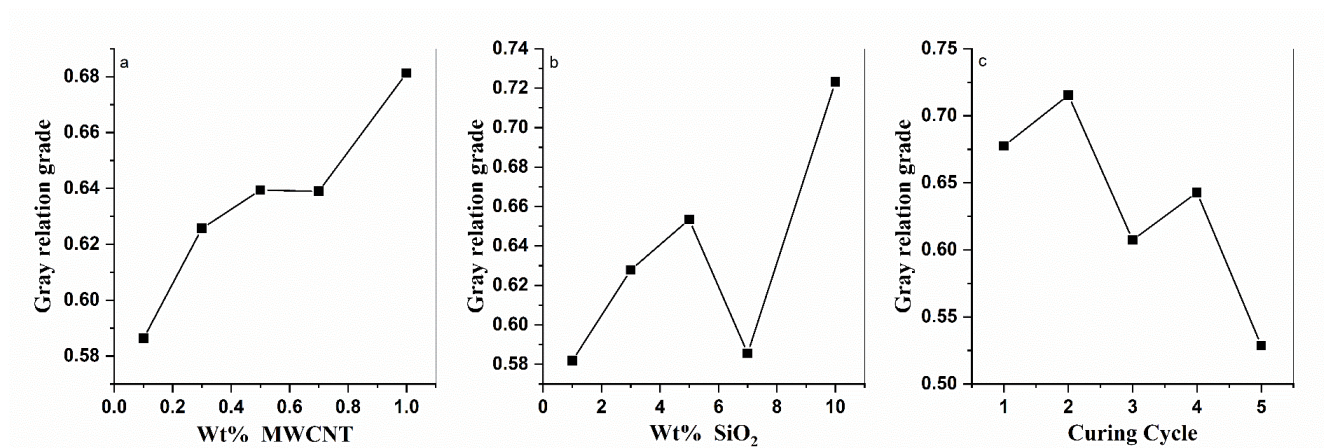
Figure 4-6: Effect of control variables on mean GRG (both tensile strength and fracture toughness).
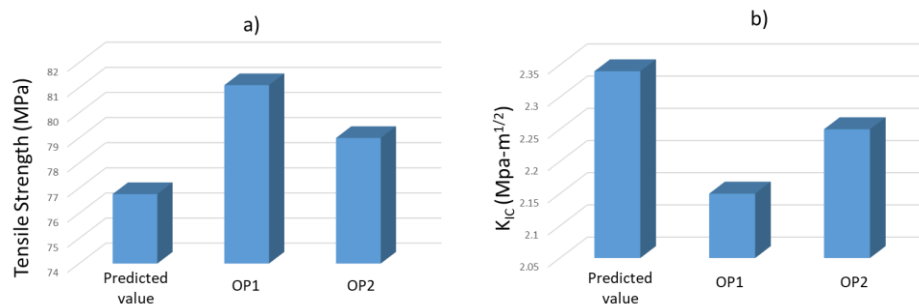
Figure 4-7: Result of response for confirmation test a) Tensile strength b) fracture toughness

4.3 MECHANICAL PROPERTIES

4.3.1 TENSILE TEST RESULTS

The tensile strength of base samples at three different curing cycles and hybrid samples is shown in Figure 4-8 a. The tensile modulus and strain for break % of hybrid samples are shown in Figure 4-8 b. The HENC HS23 demonstrated a maximum increase of approximately 13% in its tensile strength as equated to pristine epoxy composite. The superior strength exhibited by the nanocomposites in contrast to the pure epoxy can be ascribed to a robust interface between the matrix and particles. This is due to the absence of any notable defects resulting from the de-bonding of nanoparticles, which is a common occurrence with fillers of micron scale. A robust interface facilitated a consistent transmission of stress and augmented the yield strength of the nanocomposite (Das et al., 2022). HENCs showed better mechanical properties compared to single particle nanocomposite (epoxy-SiO_2, epoxy-MWCNT) reported in other literature (Bharadwaja et al., 2022; Uyaner & Akdemir, 2021). HS-23 showed the best tensile strength compared to other developed HENCs. HS15 showed the best tensile modulus due to more rigidity imparted by the curing cycle. Tensile modulus and strain to break % of the HENCs demonstrated a maximum increase (compared to neat epoxy) of 200% and

81 %, respectively. Strain to break percentage is a clear indication of a decrease in brittleness. Hence, the hybrid nanocomposites show delayed cracking at a high value of strain. This may happen because of better MWCNT and matrix interaction. Adding spherical nanoparticles along with MWCNT acts as a spacer, prohibits MWCNT clustering, and results in better mechanical properties even at higher particle loading. The elevated STB % of the HENC suggests the participation of multiple fracture and energy dissipation mechanisms in contrast to the composite filled with micro-particles. The enhanced elastic modulus of the HENC can be attributed to the existence of nanoparticles with high elastic modulus.

4.3.2 HARDNESS TEST

Vicker's hardness value of all samples is shown in Figure 4-9. HENCs showed a maximum improvement of around 17% in hardness as compared to the base sample. HENC HS24 showed maximum hardness, i.e., 20.4 HV. Improvement in the hardness is also in agreement with the tensile strength of the HENCs. The hybrid nanocomposite's mechanical properties were better than those of both neat epoxy and epoxy-nanoparticle nanocomposites. Further, better mechanical properties can be achieved at high particle loading in the case of HENCs.
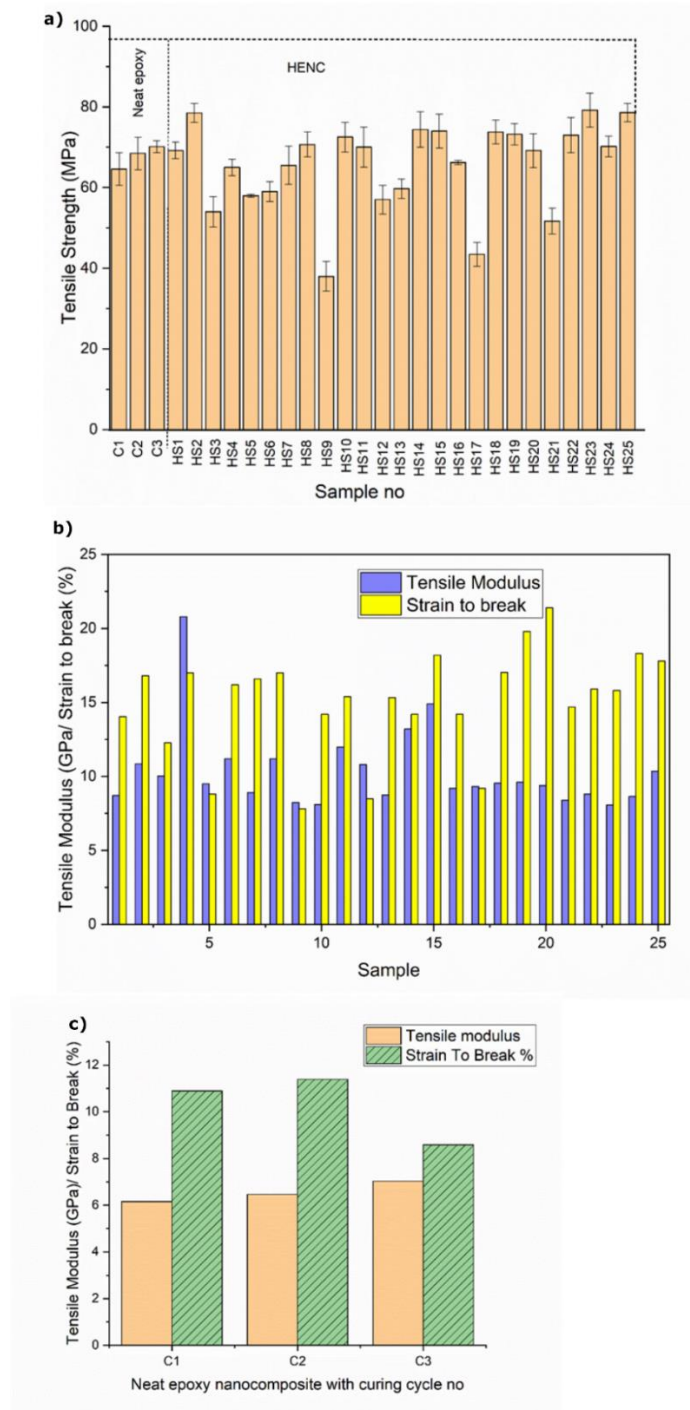
Figure 4-8: Mechanical characteristics of HENCs (a) tensile strength and (b) STB % and tensile modulus. Mechanical properties of neat epoxy (c) Strain to break % and tensile modulus.
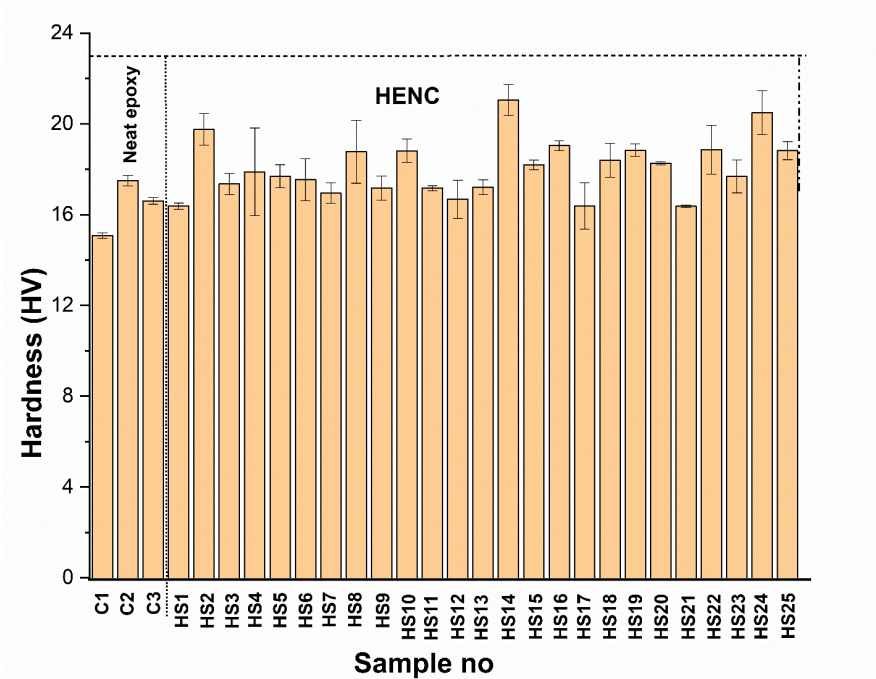
Figure 4-9: Hardness of neat epoxy and HENCs.

4.3.3 FRACTURE TOUGHNESS (K_{IC})

Figure 4-10 shows the values of fracture toughness of neat epoxy at three different curing cycle and HENCs. Maximum value of fracture toughness is obtained in the HS-7. Fracture toughness of HENC was around 65% more than the neat epoxy. Developed HENCs shows better fracture toughness than the single particle or neat epoxy reported in the earlier literature. The enhanced fracture toughness qualities and greater load-bearing capacity in the HENC samples could be explained by the uniform dispersion of the MWCNT/SiO$_2$ hybrid nanofillers and their excellent interfacial contact with the surrounding epoxy matrix. Another important fact to notice here that keeping MWCNT content constant (till 0.3 wt%) and incresing SiO$_2$ content increase the fracture toughness of the HENC. This happened becouse of crack deflection capacity of silica nanoparticles. Further incresing MWCNT Wt% beyond 0.3 % adversely affects the fracture toguhness. This may happnes due to dominance of secondary bonding force between MWCNT particles resulting in agglomeration. Agglomeration makes it so the polymer can't get in between the

85

filler particles to form a strong connection with the epoxy. As the fracture spreads, it comes into contact with the clumps of particles, which causes the particles' weak bonds to break, creating gaps and ultimately causing the particles to separate from the matrix (Muralidhara et al., 2020). It is also established that, under stress, the crack propagates in all directions parallel to the original crack, a finding corroborated by previous experimental research. Thus, two important high-energy dissipation processes—plastic deformation and crack bowing—improve the fracture toughness of HENC samples with 0.3% hybrid nanofillers.
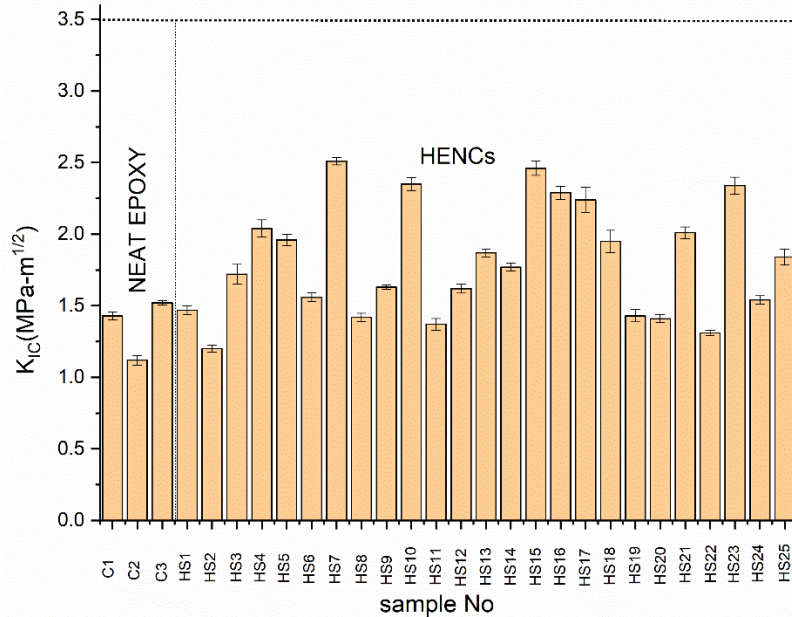
Figure 4-10: Bar graph of fracture toughness for prepared samples.

4.4 THERMAL PROPERTIES

DSC curve of neat epoxy prepared at curing cycle 1, 2 and 3 and HENC is presented in Figure 4-11. The value of obtained T_g is presented in Figure 4-12. T_g of the hybrid epoxy nanocomposite is increasing because of addition of nanoparticle. HS-9 was the best sample having greatest increment in the Tg. When contrasted with plain epoxy, the Tg values of all HENC were much higher. An appreciable

increment of about 37% in the glass transition temperature was obtained for HS-9. Glass transition temperature depends on epoxy chain mobility. Adding hybrid nanoparticles creates a robust structure, resulting in lower chain mobility. Hence HENC shows better Tg as compared to neat epoxy or single-particle reinforcement. Another important element in determining the Tg of thermosetting polymers is the density of their cross-links. The SiO_2 not only attaches to the MWCNT but also acts as the cross-linking media for epoxy resin. This results in an increment in the cross-linking density.
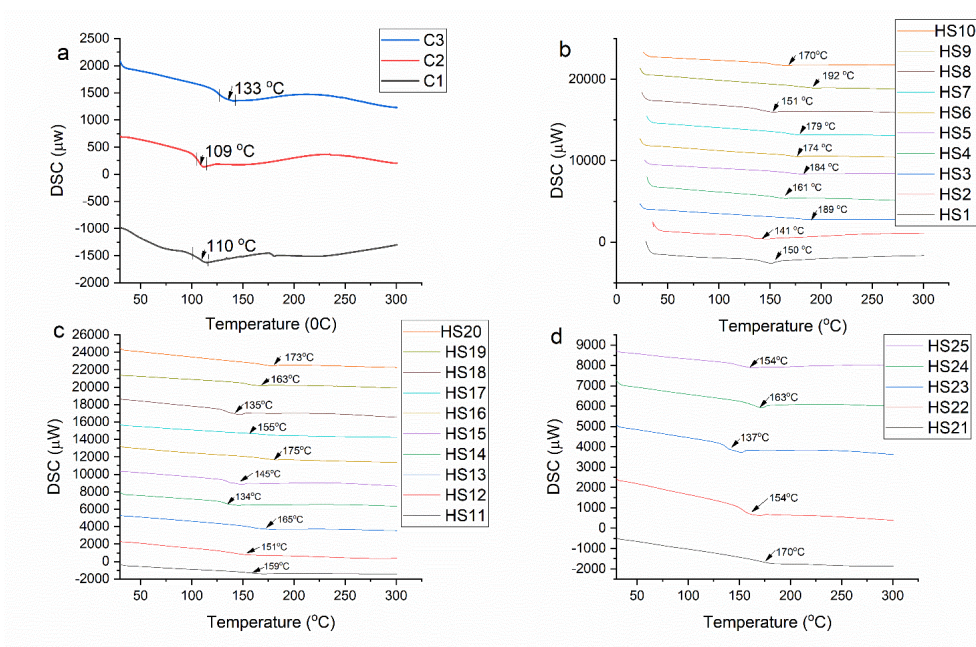
Figure 4-11: DSC curve of pristine epoxy and HENC a) neat epoxy b) HENC from HS1 to HS-10 c) HENC from HS11 to HS20 d) from HS20 to HS25
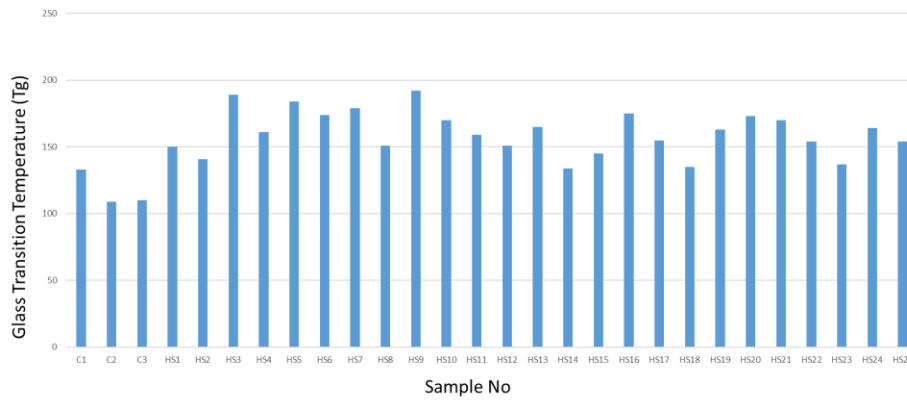
Figure 4-12: Tg of neat epoxy and HENC.

Epoxy composites containing varying amounts of nano SiO2 and multi-wall carbon nanotubes (MWCNTs) were subjected to thermos gravimetric analysis (TGA) to evaluate their thermal stability in relation to the thermal characteristics of the clean epoxy samples formed during the 1, 2, and 3rd curing cycles. Figure 4-13 illustrates the temperature dependence of the decomposition behaviour.
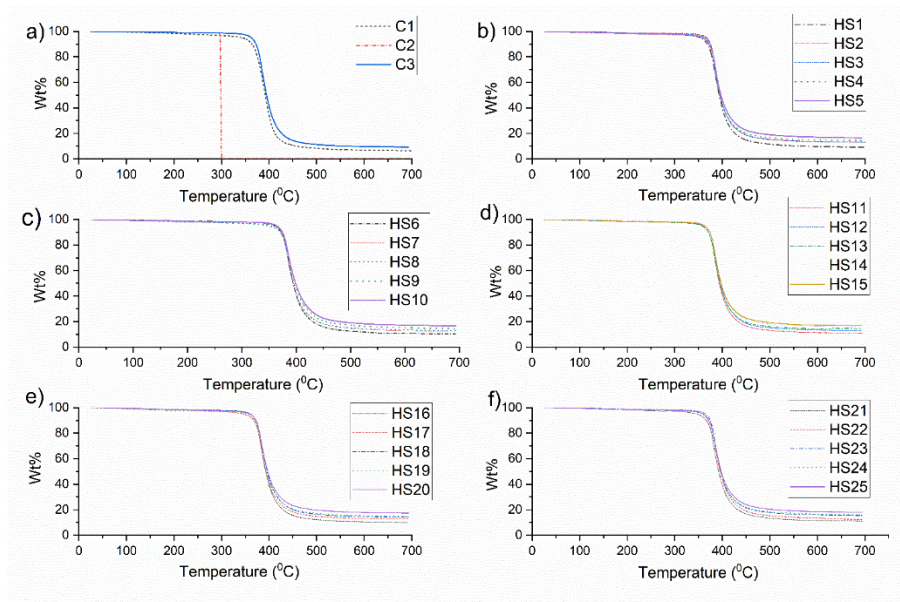
Figure 4-13: Degradation behaviour of neat and HENC a) neat epoxy b) HS1-HS5 c)HS6-HS10 d) HS11-HS12 e) HS16-HS20 f) HS21-HS25.

Nanotube incorporation resulted in improved thermal stability, as measured by the samples' percent weight loss with respect to temperature, despite the temperature 380 0C, which is indicative of the beginning of thermal deterioration, was almost the same for all of the samples. Temperature-dependent weight loss rate of the nanocomposite is shown in Figure 4-14. Maximum degradation rate appeared almost at the same temperature for all the samples but the rate of degradation was slow in the HENC compared to neat epoxy. The addition of a hybrid nanoparticle creates a dense cross-linking network with robust structure, leading to increments in the thermal stability of the HENC. A close analysis of the degradation behaviour reveals another fact: increasing SiO2 concentration (at constant MWCNT) delays thermal degradation. This may happen because of thermal stability of SiO_2 nanoparticles.
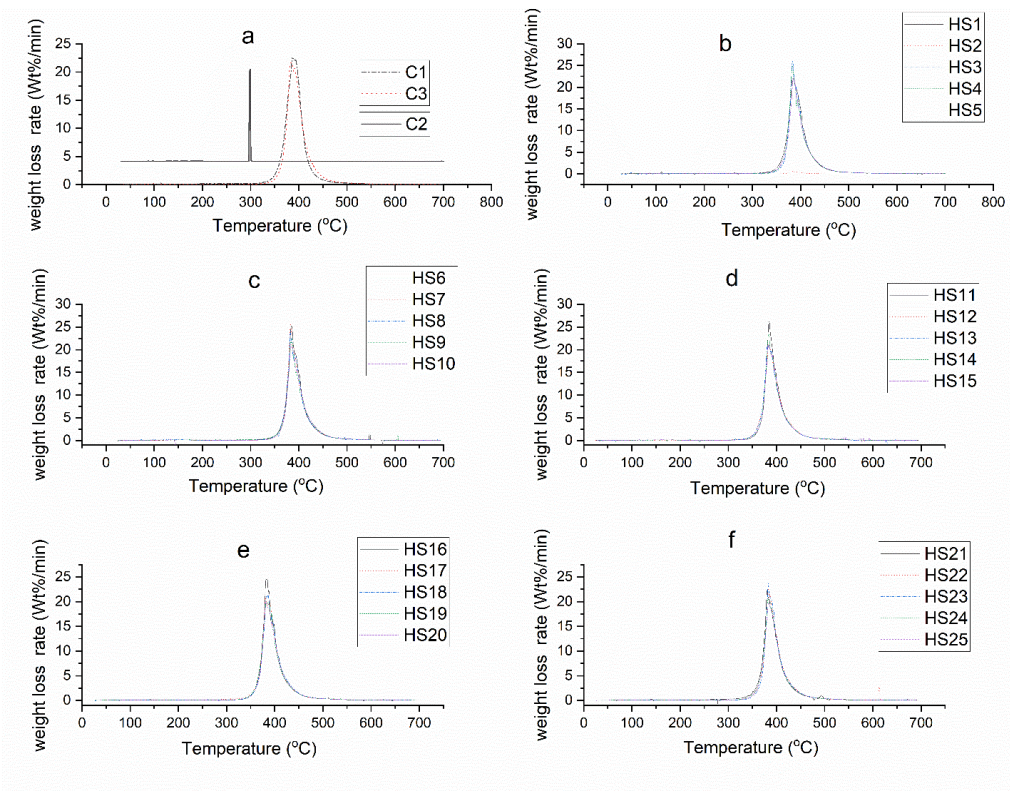
Figure 4-14: Temperature dependent Weight loss rate HENC a) neat epoxy b) HS1-HS5 c)HS6-HS10 d) HS11-HS12 e) HS16-HS20 f) HS21-HS25.

4.5 FRACTURE MORPHOLOGY

4.5.1 TENSILE FRACTURE

Figure 4-15 a) demonstrates that the fracture surface areas of tidy EP are reasonably smooth and lack any distinctive microstructure. When pure EP is compared to HENC with MWCNT and SiO2 nanoparticles, the pure EP's fracture surface is much smoother and the HENC fracture surface is much rougher. Additionally, HENCs MWCNT/nano-SiO_2 seem exfoliated into uneven flakes in the EP that has been mixed SiO_2, as seen in Figure 4-15 (b-f). These flakes are spread uniformly throughout the polymer, with some restacking occurring at random. Three distinct fracture zones, labelled (i) mirror, (ii) mist, and (iii) hackle, are visible on the tensile fractured surface of neat epoxy (Figure 4-16). A crack starts at a small defect in a thermosetting polymer and spreads in a direction normal to the tensile axis during tensile fracture. The 'mirror' zone (labelled by A) when the crack expands rapidly after initially expanding very slowly, producing a highly smooth fracture surface. A somewhat rougher and extremely thin area, the 'mist' zone (labelled by B), surrounds this fracture zone. Around the 'mist' zone is a highly rough and dense area called the Hackle zone (labelled by C). When the crack's velocity reaches its maximum, a bifurcation, or Hackel zone, occurs to release the extra energy. Another important fact to discuss here that crack propagates linearly in neat epoxy while there is bifurcation in the crack propagation direction for HENCs.
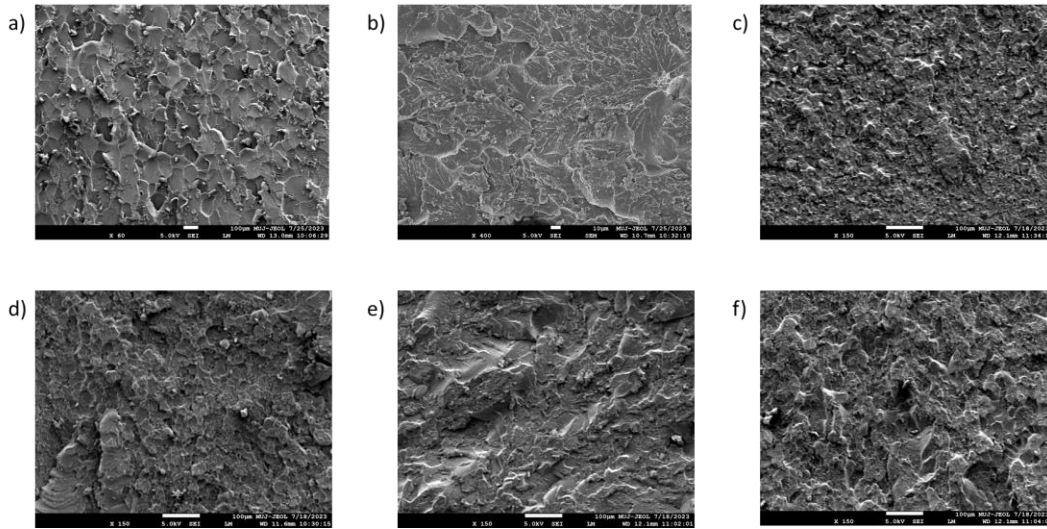
Figure 4-15: SEM micrograph of tensile fracture surface; a) neat epoxy b) HS13 c) HS14 d) HS23 e) HS24 f) HS25
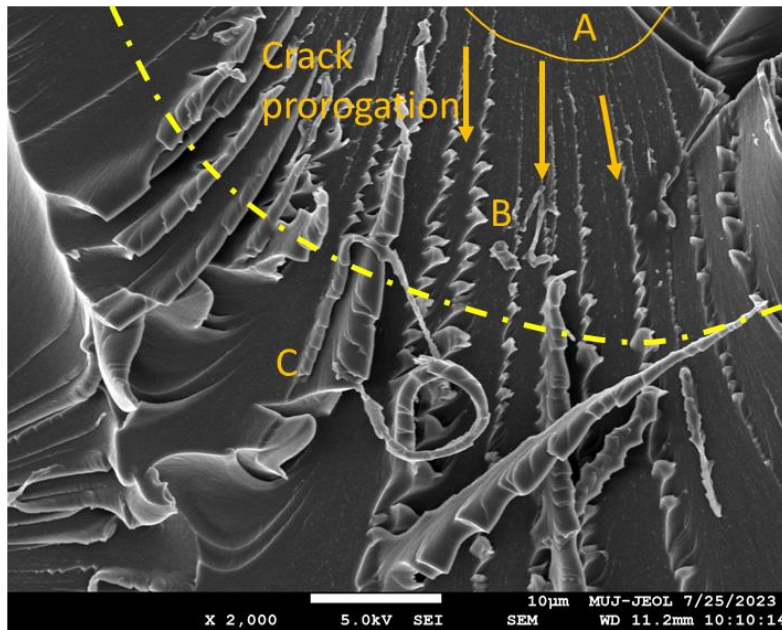
Figure 4-16: Fracture Surface morphology of neat epoxy

Well dispersed CNT and Nano-SiO$_2$ is evident in the SEM images of HS-23 as compared to other HENCs. Comparison of fracture surface morphology of HS-13 and HS23 is given in the *Figure 4-17* . The toughening mechanism known as particle pull-out, denoted as 'A', is a consequence of the extraction of nanoparticles

from the epoxy base. This extraction process leads to the formation of almost hemispherical voids or nano-scale cavities on the surface of fracture. This phenomenon has been documented in previous research (Johnsen et al., 2005). The mechanism denoted as 'A' was responsible for the observed increase in resistance to fracture propagation. The mechanism in question is well recognized in the scientific community for its applicability to both weak and strong interactions between matrices and nanoparticles. The crack exhibits a significantly reduced propagation rate inside the "mirror" region, ultimately forming a fracture surface characterized by debonding. The fracture of a robust matrix-particle interface has a greater capacity for energy absorption than a weaker interface, leading to enhanced material toughness. The toughening process of plastic void development, referred to as 'B', occurs due to the expansion of a void near the nanofiller on the exterior of the fracture. MWCNT pull out is labelled by 'c'; this phenomenon occurs at a higher value of loading when the nanoparticle at the surface of MWCNT is pulled out and crack growth is higher. It is evident from Figure 4-17 a_1 and b_1 that particle pull out effect is more in HS23 than HS13. In HS13 (Figure 4-17 a_1) fibre pull out effect is less evident as compared to HS23. This because of increase content of MWCNT. Further, dispersion of nano-SiO_2 is more homogeneous in HS23. MWCNT pull-out effect clearly indicates localised plastic deformation due to high energy absorption by the crack. MWCNT and nano-SiO_2 particle clustering can be identified at the fracture surface of HS-13. The mentioned toughening mechanism leads to better mechanical properties of HS23 than HS13. Another vary important toughening mechanism that is evident at the fracture surface of HS23 is 'D' called as crack bridging by MWCNT (Figure 4-17 b_2).
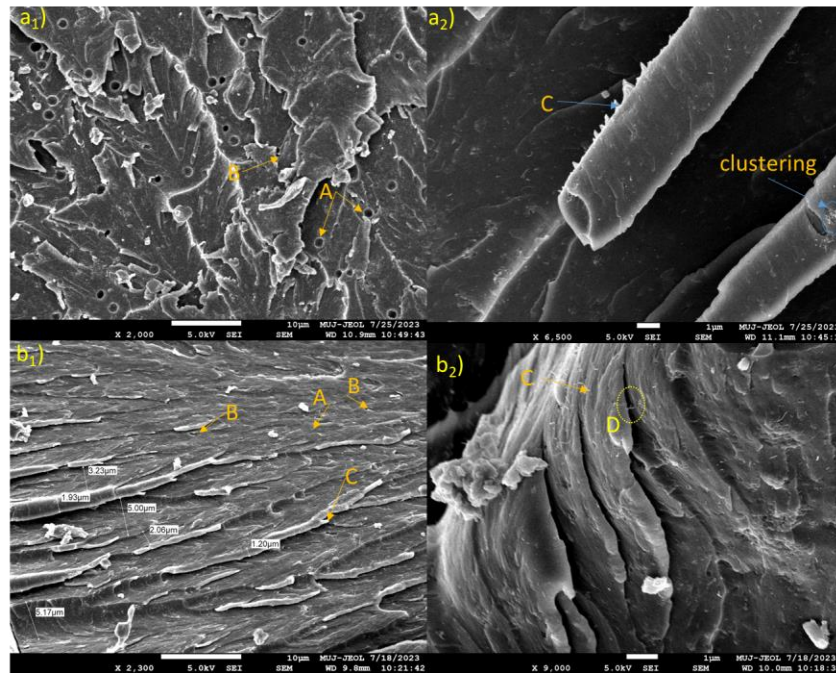
Figure 4-17: Comparison of fracture surface of tensile samples a_1) HS13 low magnification a_2) HS13 high magnification b_1) HS23 low magnification b_2) HS23 high magnification

4.5.2 SENB FRACTURE

Figure 4-18 shows the fracture surface images obtained by FESEM analysis of selected hybrid samples. Figure 4-17 a) shows that the pristine epoxy's fracture surface was smooth and without distinctive features. In contrast, the fracture surfaces of the HENC exhibited a significantly rough texture. Roughness increases on cracked surfaces suggest that (a) nanofiller imparted more barrier to the crack's propagation and (b) crack defection led to longer cracks. Improved composite fracture toughness is the result of reduced crack extension caused by crack defection and crack bridging, which squander more energy near the crack front (Zhao, Schadler, Hillborg, et al., 2008). Matrix spalling, river marks and Crack bifurcation is plainly seen on the surface of the crack of HENC same is marks by circle and arrow in Figure 4-19 and Figure 4-20. When advancing crack strikes the spherical nanoparticles, the crack tip is either advanced through the middle of the

93

particle (weak bonding) or it will be repelled and deflected by the particle (Raos & Zappone, 2021). The energy spent in the event of a crack drawn to the pole is greater. Consequently, the crack is propagating through the matrix, however void formation and subsequent void growth are not always guaranteed.

In contrast, cracks drawn towards the particle's centre consume less energy and travel above the particle surface. This results in minute crack tilting and twisting. Generally, MWCNT shows more crack twisting and tilting than spherical nanoparticles (Mousavi et al., 2022). Further, this tilting and twisting of crack depends on various factors like length, orientation and dimension of MWCNT. In SENB fracture crack moves with a faster speed as compared to tensile fracture, WMCNT is more capable in absorbing the energy of fast moving crack. The same is visible on facture surface HS-7 (Figure 4-19). Crack blunting can also be seen on the fracture surface. A slower rate of crack propagation into the material and less energy at the fracture front are the results of increased energy consumption and a blunted crack tip. The material's fracture toughness is improved due to the increased energy demand at the crack tip and the delay in the crack propagation rate.
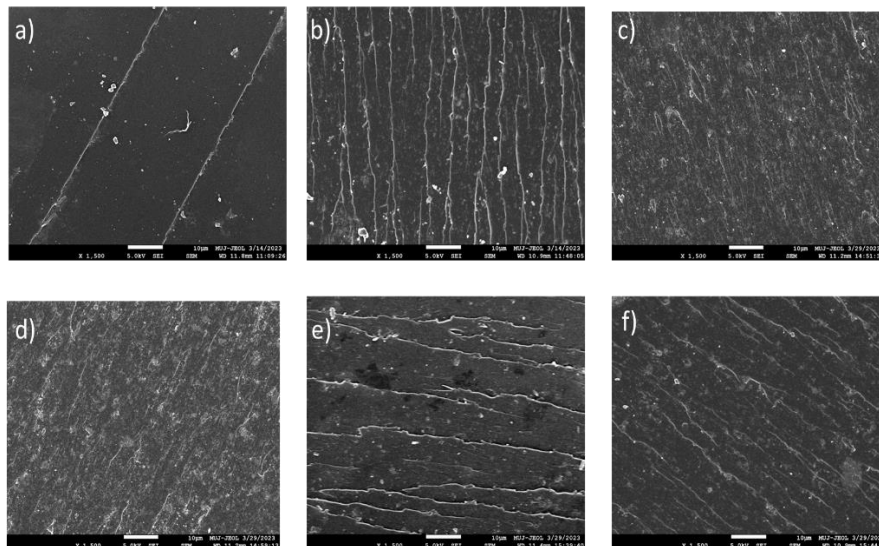
Figure 4-18: FESEM micrograph of SENB fracture of a) pristine epoxy b) HS-7 c) HS-10 d) HS-15 e) HS-16 f) HS-17.

Crack pinning, crack twisting, extended shear zone, matrix spalling, crack bifurcation, and fibre pull-out are the main toughening mechanisms that are visible on the fracture surface (Figure 4-19 c). Due to the good synergistic effect of hybrid filler, the combination of fracture feature can be seen on the surface of the composite. Moreover, good dispersion of nanofiller can be seen on the fracture of the HENC. Whereas CNT agglomeration can be seen on the fracture surface for HS-16 and HS-17 (Figure 4-20). As MWCNT and SiO_2 content increases beyond 3 wt% particle agglomeration dominates over strengthening results in reduction of fracture toughness. Agglomeration creates addition crack initiation sites and increases the effective inter-particle distance. This helps in crack propagation as majority of time crack will propagate in epoxy matrix without any effective barrier.
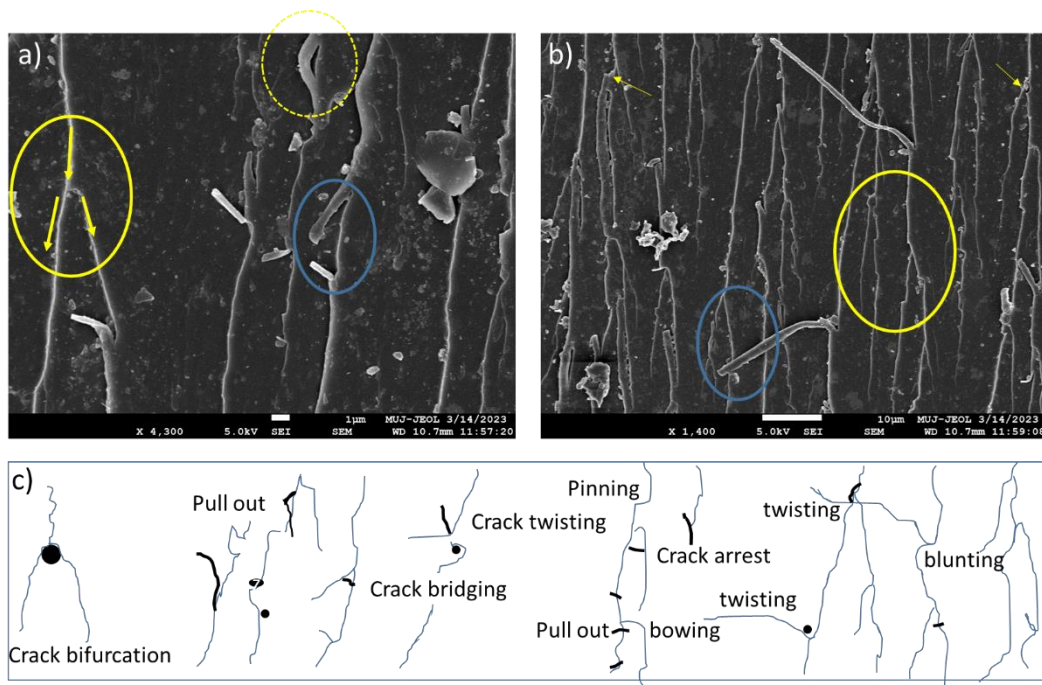
Figure 4-19: FESEM images of HS-7 at a) 4300X b) 1400X c) Toughening mechanism.
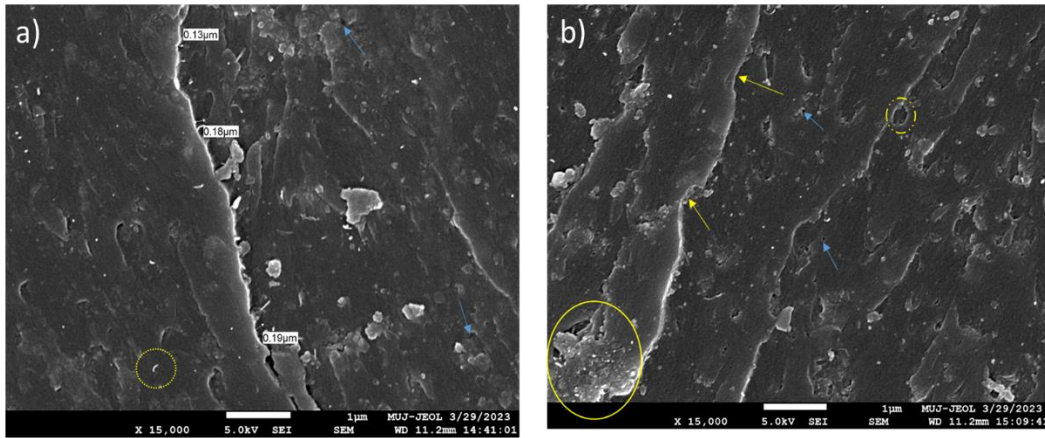
Figure 4-20: FESEM images at 15000X for a) HS-16 b) HS-17.

CHAPTER 5
CONCLUSION AND FUTURE OUTLOOK

5.1 CONCLUSIONS

Taguchi design of experiments successfully optimized the concentration of MWCNT and SiO_2 nanoparticles in epoxy and the epoxy curing cycle with respect to the tensile strength of the resulting hybrid epoxy nanocomposites (HENCs). The optimal concentration of 1% MWCNT and 10% SiO_2 and curing cycle-2 revealed a noteworthy improvement in the mechanical properties of the HENCs. Tensile strength, tensile modulus, strain to break %, and hardness and fracture toughness of HENCs were improved by 13%, 200%, 18%, 17%, and 65% respectively. HENCs showed better thermal properties than neat epoxy. Glass transition temperature of HENC was improved by around 37% compared to neat epoxy. The HENCs showed better mechanical and thermal properties compared to MWCNT/epoxy nanocomposites and SiO_2/epoxy nanocomposites because of the combined effect of both nanofillers. This happened because SiO_2 nanoparticles lowered the MWCNT-MWCNT interaction, reducing their agglomeration in the epoxy matrix. The homogeneously dispersed MWCNTs and SiO_2 nanoparticles and their threshold limit may be responsible for improved mechanical properties of HENCs. The following conclusion can be drawn after this research work.

1. The best HENC for maximum tensile strength is HS23.
2. The best HENC for maximum fracture toughness is HS7
3. The best HENC for maximum tensile strength as well as fracture toughness is HS23.
4. The optimum parameter for maximizing tensile strength is 1 wt.% MWCNT, 10% SiO_2 and curing cycle 2.
5. The optimum parameter for maximum fracture toughness is 0.3 wt% MWCNT, 10% SiO_2 and curing cycle 5.

6. The optimum parameter for maximum tensile strength as well as fracture toughness is 1 wt.% MWCNT, 10% SiO_2 and curing cycle 2.

7. HENCs show better thermal stability and T_g as compare to neat epoxy and single particle reinforced nanocomposite

8. HENCs show better mechanical properties as compare to neat epoxy and single particle reinforced nanocomposite.

9. Crack deflection, crack bridging, crack pinning, particle pull out, fibre bowing and fibre pull out are the main toughening mechanism for the HENCs.

10. SiO_2 nanoparticle imparts crack deflection and thermal stability to the matrix

11. MWCNT imparts crack bridging and fracture toughness to the matrix.

5.2 FUTURE OUTLOOK

The hybrid nanocomposite is a new and attractive field with a vast research scope. Very little work has been reported so far to investigate the effect of ZrO_2-CNT, TiO_2-CNT on the tensile strength, flexural strength, and wear properties of the epoxy hybrid nanocomposite. Moreover, proper investigation of the interfacial bonding mechanism is still required. HENCs can become one of the future high-performance materials for industries. The utmost challenge in this field is to incorporate higher filler loading without agglomeration. This can only be achieved by the research on improving processing techniques to get the optimum set of output from the HPNC. Utilizing statistical optimization techniques like RSM, Gray relation analysis, and ANN to optimize manufacturing parameters can also be exciting research areas. Research work checked the particle effect till 1 wt% MWCNT and SiO_2. The research community can explore more for adding higher nanoparticle loading. Further wear, flame retardant and corrosion resistance of the HENCs can also be investigated for finding the set of optimum control variables.

References

Adnan, M. M., Tveten, E. G., Glaum, J., Ese, M.-H. G., Hvidsten, S., Glomm, W., & Einarsrud, M.-A. (2019). Epoxy-Based Nanocomposites for High-Voltage Insulation: A Review. *Advanced Electronic Materials*, *5*(2), 1800505. https://doi.org/10.1002/AELM.201800505

Ahmad, I., Islam, M., Parvez, S., AlHabis, N., Umar, A., Munir, K. S., Wang, N., & Zhu, Y. (2019). Reinforcing capability of multiwall carbon nanotubes in alumina ceramic hybrid nanocomposites containing zirconium oxide nanoparticles. *International Journal of Refractory Metals and Hard Materials*, *84*(July), 105018. https://doi.org/10.1016/j.ijrmhm.2019.105018

Ahmad, W., & Kalra, D. (2020). Green synthesis, characterization and anti microbial activities of ZnO nanoparticles using Euphorbia hirta leaf extract. *Journal of King Saud University - Science*, *32*(4), 2358–2364. https://doi.org/10.1016/j.jksus.2020.03.014

Amalraj, S., & Michael, P. A. (2019). Synthesis and characterization of Al2O3 and CuO nanoparticles into nanofluids for solar panel applications. *Results in Physics*, *15*, 102797. https://doi.org/10.1016/J.RINP.2019.102797

Anant, R., Tiwari, A., Sundaramurthy, S., Vijay, V., & Singh, G. (2024). Synthesis Approaches, Designs, and Processing Methods of Two-Dimensional Nanomaterials. *Two-Dimensional Nanomaterials-Based Polymer Nanocomposites: Processing, Properties and Applications*, 47–81.

and, M. M., & Winey*, K. I. (2007). Improved Load Transfer in Nanotube/Polymer Composites with Increased Polymer Molecular Weight†. *Journal of Physical Chemistry C*, *111*(48), 17923–17927. https://doi.org/10.1021/JP0715530

Ashby, M. F., & Bréchet, Y. J. M. (2003). Designing hybrid materials. *Acta Materialia*, *51*(19), 5801–5821. https://doi.org/10.1016/S1359-6454(03)00441-5

Askari, M. B., Tavakoli Banizi, Z., Seifi, M., Bagheri Dehaghi, S., & Veisi, P. (2017). Synthesis of TiO2 nanoparticles and decorated multi-wall carbon nanotube (MWCNT) with anatase TiO2 nanoparticles and study of optical properties and structural characterization of TiO2/MWCNT nanocomposite. *Optik*, *149*, 447–454. https://doi.org/10.1016/j.ijleo.2017.09.078

Bahramnia, H., Mohammadian Semnani, H., Habibolahzadeh, A., & Abdoos, H. (2020). Epoxy/polyurethane nanocomposite coatings for anti-erosion/wear applications: A review. *Journal of Composite Materials*, *54*(22), 3189–3203. https://doi.org/10.1177/0021998320908299

Bahramnia, H., Semnani, H. M., Habibolahzadeh, A., & Abdoos, H. (2021). Epoxy/polyurethane hybrid nanocomposite coatings reinforced with MWCNTs and SiO2 nanoparticles: Processing, mechanical properties and wear behavior. *Surface and Coatings Technology*, *415*(January), 127121. https://doi.org/10.1016/j.surfcoat.2021.127121

Bai, X. D., Gao, P. X., Wang, Z. L., & Wang, E. G. (2003). Dual-mode mechanical resonance of individual ZnO nanobelts. *Applied Physics Letters*, *82*(26), 4806. https://doi.org/10.1063/1.1587878

Baig, Z., Mamat, O., & Mustapha, M. (2018). Recent Progress on the Dispersion and the Strengthening Effect of Carbon Nanotubes and Graphene-Reinforced Metal Nanocomposites: A Review. *Critical Reviews in Solid State and Materials Sciences*, *43*(1), 1–46. https://doi.org/10.1080/10408436.2016.1243089

Bakhtiar, N. S. A. A., Akil, H. M., Zakaria, M. R., Kudus, M. H. A., & Othman, M. B. H. (2016). New generation of hybrid filler for producing epoxy nanocomposites with improved mechanical properties. *Materials and Design*, *91*, 46–52. https://doi.org/10.1016/j.matdes.2015.11.081

Batool, T., Bukhari, B. S., Riaz, S., Batoo, K. M., Raslan, E. H., Hadi, M., &

Naseem, S. (2020). Microwave assisted sol-gel synthesis of bioactive zirconia nanoparticles – Correlation of strength and structure. *Journal of the Mechanical Behavior of Biomedical Materials*, *112*(March), 104012. https://doi.org/10.1016/j.jmbbm.2020.104012

Bazrgari, D., Moztarzadeh, F., Sabbagh-Alvani, A. A., Rasoulianboroujeni, M., Tahriri, M., & Tayebi, L. (2018). Mechanical properties and tribological performance of epoxy/Al2O3 nanocomposite. *Ceramics International*, *44*(1), 1220–1224. https://doi.org/10.1016/j.ceramint.2017.10.068

Bharadwaja, K., rao, S. srinivasa, & Baburao, T. (2022). Epoxy/SIO2 nanocomposite mechanical properties and tribological performance. *Materials Today: Proceedings*, *62*, 1712–1716. https://doi.org/10.1016/J.MATPR.2021.12.172

Bhatia, S., Khan, S., & Angra, S. (2021). Effect of the content of silane-functionalized boron carbide on the mechanical and wear performance of B4C reinforced epoxy composites. *High Performance Polymers*, *33*(10), 1165–1180. https://doi.org/10.1177/09540083211031129

Çakır, M. V. (2023). The synergistic effect of hybrid nano-silica and GNP additives on the flexural strength and toughening mechanisms of adhesively bonded joints. *International Journal of Adhesion and Adhesives*, *122*, 103333. https://doi.org/10.1016/J.IJADHADH.2023.103333

Cha, J., Jun, G. H., Park, J. K., Kim, J. C., Ryu, H. J., & Hong, S. H. (2017). Improvement of modulus, strength and fracture toughness of CNT/Epoxy nanocomposites through the functionalization of carbon nanotubes. *Composites Part B: Engineering*, *129*, 169–179. https://doi.org/10.1016/j.compositesb.2017.07.070

Che, Y., Sun, Z., Zhan, R., Wang, S., Zhou, S., & Huang, J. (2018). Effects of graphene oxide sheets-zirconia spheres nanohybrids on mechanical, thermal

and tribological performances of epoxy composites. *Ceramics International*, *44*(15), 18067–18077. https://doi.org/10.1016/j.ceramint.2018.07.010

Chen, S., Chen, L., Wang, Y., Wang, C., Miao, M., & Zhang, D. (2019). Load transfer of thiol-ended hyperbranched polymers to improve simultaneously strength and longation of CNTs/epoxy nanocomposites. *European Polymer Journal*, *120*(August), 109254. https://doi.org/10.1016/j.eurpolymj.2019.109254

Chin, A. B., & Yaacob, I. I. (2007). Synthesis and characterization of magnetic iron oxide nanoparticles via w/o microemulsion and Massart's procedure. *Journal of Materials Processing Technology*, *191*(1–3), 235–237. https://doi.org/10.1016/j.jmatprotec.2007.03.011

Ciofani, G., Raffa, V., Pensabene, V., Menciassi, A., & Dario, P. (2009). Dispersion of multi-walled carbon nanotubes in aqueous pluronic F127 solutions for biological applications. *Fullerenes Nanotubes and Carbon Nanostructures*, *17*(1), 11–25. https://doi.org/10.1080/15363830802515840

Corr, S. A. (2016). Metal oxide nanoparticles. *SPR Nanoscience*, *3*, 31–56. https://doi.org/10.1039/9781782623717-00031

da Silva, A. F. V., Fagundes, A. P., Macuvele, D. L. P., de Carvalho, E. F. U., Durazzo, M., Padoin, N., Soares, C., & Riella, H. G. (2019). Green synthesis of zirconia nanoparticles based on Euclea natalensis plant extract: Optimization of reaction conditions and evaluation of adsorptive properties. *Colloids and Surfaces A: Physicochemical and Engineering Aspects*, *583*(August). https://doi.org/10.1016/j.colsurfa.2019.123915

Das, S., Das, P., Halder, S., & Choudhury, P. (2022). Role of Nanoreinforcement onto Intra-and Interlaminar Fracture of Hybrid Laminated Composites. *Toughened Composites: Micro and Macro Systems*, 217.

Davis, R., & John, P. (2018). Application of Taguchi-based design of experiments

for industrial chemical processes. *Statistical Approaches with Emphasis on Design of Experiments Applied to Chemical Processes*, *137*.

Du, J. H., Bai, J., & Cheng, H. M. (2007). The present status and key problems of carbon nanotube based polymer composites. *Express Polymer Letters*, *1*(5), 253–273. https://doi.org/10.3144/EXPRESSPOLYMLETT.2007.39

Duan, K., Li, L., Wang, F., Liu, S., Hu, Y., & Wang, X. (2021). New insights into interface interactions of CNT-reinforced epoxy nanocomposites. *Composites Science and Technology*, *204*, 108638. https://doi.org/10.1016/J.COMPSCITECH.2020.108638

Dubey, R. S., Rajesh, Y. B. R. D., & More, M. A. (2015). Synthesis and Characterization of SiO2 Nanoparticles via Sol-gel Method for Industrial Applications. *Materials Today: Proceedings*, *2*(4–5), 3575–3579. https://doi.org/10.1016/j.matpr.2015.07.098

Fałtynowicz, H., Kułażynski, M., & Goodman, S. H. (2022). Chapter 8 - Epoxies. In H. Dodiuk (Ed.), *Handbook of Thermoset Plastics (Fourth Edition)* (Fourth Edi, pp. 175–229). William Andrew Publishing. https://doi.org/https://doi.org/10.1016/B978-0-12-821632-3.00014-2

Fan, Z., & Lu, J. G. (2005). Zinc Oxide Nanostructures: Synthesis and Properties. *Journal of Nanoscience and Nanotechnology*, *5*(10), 1561–1573. https://doi.org/10.1166/jnn.2005.182

Fouly, A., & Alkalla, M. G. (2020). Effect of low nanosized alumina loading fraction on the physicomechanical and tribological behavior of epoxy. *Tribology International*, *152*, 106550. https://doi.org/10.1016/J.TRIBOINT.2020.106550

Franco-Urquiza, E. A., & Rentería-Rodríguez, A. V. (2021). Effect of nanoparticles on the mechanical properties of kenaf fiber-reinforced bio-based epoxy resin. *Textile Research Journal*, *91*(11–12), 1313–1325.

https://doi.org/10.1177/0040517520980459

Ghosh, P. K., Halder, S., Goyat, M. S., & Karthik, G. (2013). Study on thermal and lap shear characteristics of epoxy adhesive loaded with metallic and non-metallic particles. *Journal of Adhesion*, *89*(1), 55–75. https://doi.org/10.1080/00218464.2012.739006

Gibson, R. F. (2010). A review of recent research on mechanics of multifunctional composite materials and structures. *Composite Structures*, *92*(12), 2793–2810. https://doi.org/10.1016/j.compstruct.2010.05.003

Gojny, F. H., Wichmann, M. H. G., Köpke, U., Fiedler, B., & Schulte, K. (2004). Carbon nanotube-reinforced epoxy-composites: enhanced stiffness and fracture toughness at low nanotube content. *Composites Science and Technology*, *64*(15), 2363–2371. https://doi.org/10.1016/J.COMPSCITECH.2004.04.002

Gómez-Del Río, T., Salazar, A., Pearson, R. A., & Rodríguez, J. (2016). Fracture behaviour of epoxy nanocomposites modified with triblock copolymers and carbon nanotubes. *Composites Part B: Engineering*, *87*(87), 343–349. https://doi.org/10.1016/j.compositesb.2015.08.085

Goyat, M. S., & Ghosh, P. K. (2017). Impact of ultrasonic assisted triangular lattice like arranged dispersion of nanoparticles on physical and mechanical properties of epoxy-TiO 2 nanocomposites. *Ultrasonics Sonochemistry*. https://doi.org/10.1016/j.ultsonch.2017.11.019

Goyat, M. S., Hooda, A., Gupta, T. K., Kumar, K., Halder, S., Ghosh, P. K., & Dehiya, B. S. (2021). Role of non-functionalized oxide nanoparticles on mechanical properties and toughening mechanisms of epoxy nanocomposites. *Ceramics International*, *47*(16), 22316–22344. https://doi.org/10.1016/j.ceramint.2021.05.083

Goyat, M. S., Rana, S., Halder, S., & Ghosh, P. K. (2018). Facile fabrication of

epoxy-TiO2 nanocomposites: A critical analysis of TiO2 impact on mechanical properties and toughening mechanisms. *Ultrasonics Sonochemistry*, *40*(June 2017), 861–873. https://doi.org/10.1016/j.ultsonch.2017.07.040

Goyat, M. S., Suresh, S., Bahl, S., Halder, S., & Ghosh, P. K. (2015). Thermomechanical response and toughening mechanisms of a carbon nano bead reinforced epoxy composite. *Materials Chemistry and Physics*, *166*, 144–152. https://doi.org/10.1016/j.matchemphys.2015.09.038

Halder, S., Prasad, T., Khan, N. I., Goyat, M. S., & Ram Chauhan, S. (2017). Superior mechanical properties of poly vinyl alcohol-assisted ZnO nanoparticle reinforced epoxy composites. *Materials Chemistry and Physics*, *192*, 198–209. https://doi.org/10.1016/j.matchemphys.2016.12.055

Han, J., & Jaffe, R. (1998). Energetics and geometries of carbon nanoconic tips. *The Journal of Chemical Physics*, *108*(7), 2817. https://doi.org/10.1063/1.475672

He, J., Chen, J., Shi, L., Li, Q., Lu, W., Qu, S., Qiu, W., & Zhou, G. (2019). Fabrication of thermally robust carbon nanotube (CNT)/SiO 2 composite films and their high-temperature mechanical properties. *Carbon*, *147*, 236–241. https://doi.org/10.1016/j.carbon.2019.02.088

Huang, N. J., Zang, J., Zhang, G. D., Guan, L. Z., Li, S. N., Zhao, L., & Tang, L. C. (2017). Efficient interfacial interaction for improving mechanical properties of polydimethylsiloxane nanocomposites filled with low content of graphene oxide nanoribbons. *RSC Advances*, *7*(36), 22045–22053. https://doi.org/10.1039/c7ra02439h

Hwangbo, Y., & Lee, Y. I. (2019). Facile synthesis of zirconia nanoparticles using a salt-assisted ultrasonic spray pyrolysis combined with a citrate precursor method. *Journal of Alloys and Compounds*, *771*, 821–826.

https://doi.org/10.1016/J.JALLCOM.2018.08.308

Idumah, C. I., & Obele, C. M. (2021). Understanding interfacial influence on properties of polymer nanocomposites. *Surfaces and Interfaces*, *22*, 100879. https://doi.org/10.1016/j.surfin.2020.100879

Iijima, S. (1991). Helical microtubules of graphitic carbon. *Nature*, *354*(6348), 56–58. https://doi.org/10.1038/354056a0

Jayan, J. S., Saritha, A., & Joseph, K. (2018). Innovative materials of this era for toughening the epoxy matrix: A review. *Polymer Composites*, *39*(S4), E1959–E1986. https://doi.org/10.1002/pc.24789

Johnsen, B. B., Kinloch, A. J., & Taylor, A. C. (2005). Toughness of syndiotactic polystyrene/epoxy polymer blends: Microstructure and toughening mechanisms. *Polymer[1] B. B. Johnsen, A. J. Kinloch, and A. C. Taylor, "Toughness of Syndiotactic Polystyrene/Epoxy Polymer Blends: Microstructure and Toughening Mechanisms," Polymer (Guildf)., Vol. 46, No. 18, Pp. 7352–7369, Aug. 2005, Doi: 10.1016/j.Polymer.2005.05*, *46*(18), 7352–7369. https://doi.org/10.1016/j.polymer.2005.05.151

Joshi, R. (2018). Facile photochemical synthesis of ZnO nanoparticles in aqueous solution without capping agents. *Materialia*, *2*, 104–110. https://doi.org/10.1016/j.mtla.2018.07.001

Kopparthi, P. K., Kundavarapu, V. R., Kaki, V. R., & Pathakokila, B. R. (2021). Modeling and multi response optimization of mechanical properties for E-glass/polyester composite using Taguchi-grey relational analysis. *Proceedings of the Institution of Mechanical Engineers, Part E: Journal of Process Mechanical Engineering*, *235*(2), 342–350. https://doi.org/10.1177/0954408920962592

Kudus, M. H. A., Zakaria, M. R., Omar, M. F., Hafi Othman, M. B., Md. Akil, H., Nabiałek, M., Jeż, B., & Abdullah, M. M. A. B. (2021). Nonisothermal kinetic

degradation of hybrid cnt/alumina epoxy nanocomposites. *Metals*, *11*(4), 1–16. https://doi.org/10.3390/met11040657

Kumar, A., Ghosh, P. K., Yadav, K. L., & Kumar, K. (2017). Thermo-mechanical and anti-corrosive properties of MWCNT/epoxy nanocomposite fabricated by innovative dispersion technique. *Composites Part B: Engineering*, *113*(113), 291–299. https://doi.org/10.1016/j.compositesb.2017.01.046

Kumar, A., Kumar, K., Ghosh, P. K., & Yadav, K. L. (2018). MWCNT/TiO2 hybrid nano filler toward high-performance epoxy composite. *Ultrasonics Sonochemistry*, *41*(May 2017), 37–46. https://doi.org/10.1016/j.ultsonch.2017.09.005

Kumar, A., Sharma, K., & Dixit, A. R. (2021). A review on the mechanical properties of polymer composites reinforced by carbon nanotubes and graphene. *Carbon Letters*, *31*(2), 149–165. https://doi.org/10.1007/s42823-020-00161-x

Kumar, A., & Shukla, M. (2014). Race Tracking and Related Issues in Liquid Composite Moulding Process. *Journal for Manufacturing Science and Production*, *14*(4), 209–217. https://doi.org/10.1515/jmsp-2014-0014

Kumar, K., Goyat, M. S., Solanki, A., Kumar, A., Kant, R., & Ghosh, P. K. (2021). Improved mechanical performance and unique toughening mechanisms of UDM processed epoxy-SiO2 nanocomposites. *Polymer Composites*, *42*(11), 6000–6009. https://doi.org/10.1002/PC.26280

Kumar, S., Sarita, Nehra, M., Dilbaghi, N., Tankeshwar, K., & Kim, K. H. (2018). Recent advances and remaining challenges for polymeric nanocomposites in healthcare applications. *Progress in Polymer Science*, *80*, 1–38. https://doi.org/10.1016/J.PROGPOLYMSCI.2018.03.001

Kumar, V., Gohain, M., Som, S., Kumar, V., Bezuindenhoudt, B. C. B., & Swart, H. C. (2016). Microwave assisted synthesis of ZnO nanoparticles for lighting

and dye removal application. *Physica B: Condensed Matter*, *480*, 36–41. https://doi.org/10.1016/j.physb.2015.07.020

Kundalwal, S. I., & Choyal, V. (2018). Transversely isotropic elastic properties of carbon nanotubes containing vacancy defects using MD. *Acta Mechanica*, *229*(6), 2571–2584. https://doi.org/10.1007/s00707-018-2123-5

Li, S., Ma, H., Guo, Y., Oladejo, A. O., Yang, X., Liang, Q., & Duan, Y. (2018). A new kinetic model of ultrasound-assisted pretreatment on rice protein. *Ultrasonics Sonochemistry*, *40*, 644–650. https://doi.org/10.1016/j.ultsonch.2017.07.010

Li, Y., Huang, X., Zeng, L., Li, R., Tian, H., Fu, X., Wang, Y., & Zhong, W. H. (2019). A review of the electrical and mechanical properties of carbon nanofiller-reinforced polymer composites. *Journal of Materials Science*, *54*(2), 1036–1076. https://doi.org/10.1007/s10853-018-3006-9

Liang, M., Yang, A., Zhu, Y., & Sun, S. (2020). Effects of Nanoparticles' Size and Shape on the Thermodynamic Properties of PI/SiO2 Nanocomposites. *Nano*, *15*(3), 1–17. https://doi.org/10.1142/S1793292020500411

Ma, X., Peng, C., Zhou, D., Wu, Z., Li, S., Wang, J., & Sun, N. (2018). Synthesis and mechanical properties of the epoxy resin composites filled with sol−gel derived ZrO2 nanoparticles. *Journal of Sol-Gel Science and Technology*, *88*(2), 442–453. https://doi.org/10.1007/s10971-018-4827-3

Madani, S. Y., Mandel, A., & Seifalian, A. M. (2013). A concise review of carbon nanotube's toxicology. *Nano Reviews*, *4*(1), 21521. https://doi.org/10.3402/nano.v4i0.21521

Manikandan, V., Jayanthi, P., Priyadharsan, A., Vijayaprathap, E., Anbarasan, P. M., & Velmurugan, P. (2019). Green synthesis of pH-responsive Al2O3 nanoparticles: Application to rapid removal of nitrate ions with enhanced antibacterial activity. *Journal of Photochemistry and Photobiology A:*

Chemistry, *371*(September 2018), 205–215. https://doi.org/10.1016/j.jphotochem.2018.11.009

Manjunath, R., Kumar, D., & Kumar, A. (2021). A Review on the Significance of Hybrid Particulate Reinforcements on the Mechanical and Tribological Properties of Stir-Casted Aluminum Metal Matrix Composites. *Journal of Bio- and Tribo-Corrosion 2021 7:3*, *7*(3), 1–11. https://doi.org/10.1007/S40735-021-00558-9

Marouf, B. T., Mai, Y. W., Bagheri, R., & Pearson, R. A. (2016). Toughening of epoxy nanocomposites: Nano and hybrid effects. *Polymer Reviews*, *56*(1), 70–112. https://doi.org/10.1080/15583724.2015.1086368

Moghimi Monfared, R., Ayatollahi, M. R., & Barbaz Isfahani, R. (2018). Synergistic effects of hybrid MWCNT/nanosilica on the tensile and tribological properties of woven carbon fabric epoxy composites. *Theoretical and Applied Fracture Mechanics*, *96*, 272–284. https://doi.org/10.1016/j.tafmec.2018.05.007

Mora, A. S., Tayouo, R., Boutevin, B., David, G., & Caillol, S. (2020). A perspective approach on the amine reactivity and the hydrogen bonds effect on epoxy-amine systems. *European Polymer Journal*, *123*, 109460. https://doi.org/10.1016/J.EURPOLYMJ.2019.109460

Mousavi, S. R., Estaji, S., Paydayesh, A., Arjmand, M., Jafari, S. H., Nouranian, S., & Khonakdar, H. A. (2022). A review of recent progress in improving the fracture toughness of epoxy-based composites using carbonaceous nanofillers. *Polymer Composites*, *43*(4), 1871–1886. https://doi.org/10.1002/pc.26518

Muñoz, J., Céspedes, F., & Baeza, M. (2015). Modified multiwalled carbon nanotube/epoxy amperometric nanocomposite sensors with CuO nanoparticles for electrocatalytic detection of free chlorine. *Microchemical Journal*, *122*. https://doi.org/10.1016/j.microc.2015.05.001

Muralidhara, B., Babu, S. P. K., & Suresha, B. (2020). Studies on mechanical, thermal and tribological properties of carbon fibre-reinforced boron nitride-filled epoxy composites. *High Performance Polymers*, *32*(9), 1061–1081. https://doi.org/10.1177/0954008320929396

Nagaraju, N., Fonseca, A., Konya, Z., & Nagy, J. B. (2002). Alumina and silica supported metal catalysts for the production of carbon nanotubes. *Journal of Molecular Catalysis A: Chemical*, *181*(1–2), 57–62. https://doi.org/10.1016/S1381-1169(01)00375-2

Nanzai, B., Okitsu, K., Takenaka, N., Bandow, H., Tajima, N., & Maeda, Y. (2009). Effect of reaction vessel diameter on sonochemical efficiency and cavitation dynamics. *Ultrasonics Sonochemistry*, *16*(1), 163–168. https://doi.org/10.1016/J.ULTSONCH.2008.05.016

Naskar, A. K., Keum, J. K., & Boeman, R. G. (2016). Polymer matrix nanocomposites for automotive structural components. *Nature Nanotechnology*, *11*(12), 1026–1030. https://doi.org/10.1038/nnano.2016.262

Nikam, A. V, & Dadwal, A. H. (2018). Scalable microwave-assisted continuous flow synthesis of CuO nanoparticles and their thermal conductivity applications as nanofluids. *Advanced Powder Technology*, *October*, 1–5. https://doi.org/10.1016/j.apt.2018.10.001

Nita, C., Fullenwarth, J., Monconduit, L., Le Meins, J. M., Fioux, P., Parmentier, J., & Matei Ghimbeu, C. (2019). Eco-friendly synthesis of SiO2 nanoparticles confined in hard carbon: A promising material with unexpected mechanism for Li-ion batteries. *Carbon*, *143*, 598–609. https://doi.org/10.1016/j.carbon.2018.11.069

Nitesh, Kumar, A., Saini, S., Yadav, K. L., Ghosh, P. K., & Rathi, A. (2022). Morphology and tensile performance of MWCNT/TiO2-epoxy nanocomposite. *Materials Chemistry and Physics*, *277*(October 2021),

125336. https://doi.org/10.1016/j.matchemphys.2021.125336

Özbek, Ö., & Çakır, M. V. (2022). MWCNT and nano-silica hybrids effect on mechanical and fracture characterization of single lap joints of GFRP plates. *International Journal of Adhesion and Adhesives*, *117*, 103159. https://doi.org/10.1016/J.IJADHADH.2022.103159

Patil, T. V., Patel, D. K., Dutta, S. D., Ganguly, K., Randhawa, A., & Lim, K. T. (2021). Carbon Nanotubes-Based Hydrogels for Bacterial Eradiation and Wound-Healing Applications. *Applied Sciences 2021, Vol. 11, Page 9550*, *11*(20), 9550. https://doi.org/10.3390/APP11209550

Pham, H. Q., & Marks, M. J. (2005). Epoxy Resins. In *Ullmann's Encyclopedia of Industrial Chemistry*. John Wiley & Sons, Ltd. https://doi.org/https://doi.org/10.1002/14356007.a09_547.pub2

Prashanth, P. A., Raveendra, R. S., Hari Krishna, R., Ananda, S., Bhagya, N. P., Nagabhushana, B. M., Lingaraju, K., & Raja Naika, H. (2015). Synthesis, characterizations, antibacterial and photoluminescence studies of solution combustion-derived α-Al 2 O 3 nanoparticles. *Journal of Asian Ceramic Societies*, *3*(3), 345–351. https://doi.org/10.1016/j.jascer.2015.07.001

Rahmat, M., & Hubert, P. (2011). Carbon nanotube–polymer interactions in nanocomposites: A review. *Composites Science and Technology*, *72*(1), 72–84. https://doi.org/10.1016/J.COMPSCITECH.2011.10.002

Raos, G., & Zappone, B. (2021). Polymer Adhesion: Seeking New Solutions for an Old Problem #. *Macromolecules*, *54*(23), 10617–10644. https://doi.org/10.1021/acs.macromol.1c01182

Rathi, A., & Kundalwal, S. I. (2020). Mechanical and fracture behavior of MWCNT/ZrO2/epoxy nanocomposite systems: Experimental and numerical study. *Polymer Composites*, *41*(6), 2491–2507. https://doi.org/10.1002/pc.25551

Rathi, A., & Kundalwal, S. I. (2022). Synergistic effect of ultrasonically assisted exfoliated MWCNTs by ZrO 2 nanoparticles on thermo-mechanical and anti-corrosive properties of epoxy nanocomposites. *Journal of Composite Materials*, *56*(11), 1633–1649. https://doi.org/10.1177/00219983221084770

Rawat, R., Tiwari, A., Vendamani, V. S., Pathak, A. P., Rao, S. V., & Tripathi, A. (2018). Synthesis of Si/SiO2 nanoparticles using nanosecond laser ablation of silicate-rich garnet in water. *Optical Materials*, *75*, 350–356. https://doi.org/10.1016/j.optmat.2017.10.045

Rogojan, R., Andronescu, E., Ghiţulică, C., & Ştefan Vasile, B. (2011). Synthesis and characterization of alumina nano-powder obtained by sol-gel method. *UPB Scientific Bulletin, Series B: Chemistry and Materials Science*, *73*(2), 67–76.

Roulin-Moloney, A. C., Cantwell, W. J., & Kausch, H. H. (1987). Parameters determining the strength and toughness of particulate-filled epoxy resins. *Polymer Composites*, *8*(5), 314–323. https://doi.org/10.1002/pc.750080506

Roustazadeh, D., Aghadavoudi, F., & Khandan, A. (2020). A synergic effect of CNT/Al2O3 reinforcements on multiscale epoxy-based glass fiber composite: fabrication and molecular dynamics modeling. *Molecular Simulation*, *46*(16), 1308–1319. https://doi.org/10.1080/08927022.2020.1815729

Roy, M., Pompella, A., Kubacki, J., Piosik, A., Psiuk, B., Klimontko, J., Szade, J., Roy, R. A., & Hedzelek, W. (2017). Photofunctionalization of dental zirconia oxide: Surface modification to improve bio-integration preserving crystal stability. *Colloids and Surfaces B: Biointerfaces*, *156*, 194–202. https://doi.org/10.1016/j.colsurfb.2017.05.031

Saravanan, D., Chandramohan, P., Raajeshkrishna, C. R., & Sabarinathan, C. (2018). Enhancement of mechanical properties of epoxy hybrid nanocomposites through hybridization of carbon nanotubes and alumina

nanoparticles. *Digest Journal of Nanomaterials and Biostructures*, *13*(2), 483–489.

Saravanan, D., Palanisamy, C., & Raajeshkrishna, C. R. (2019). Tribological performance of multi walled carbon nanotubes-alumina hybrid/epoxy nanocomposites under dry sliding condition. *Materials Research Express*, *6*(10). https://doi.org/10.1088/2053-1591/ab3ada

Schadler, L. S., Brinson, L. C., & Sawyer, W. G. (2007). Polymer nanocomposites: A small part of the story. *JOM 2007 59:3*, *59*(3), 53–60. https://doi.org/10.1007/S11837-007-0040-5

Sharma, H., Kumar, A., Rana, S., & Guadagno, L. (2022). An Overview on Carbon Fiber-Reinforced Epoxy Composites: Effect of Graphene Oxide Incorporation on Composites Performance. *Polymers*, *14*(8), 1548. https://doi.org/10.3390/POLYM14081548

Shin, H. (2021). Multiscale model to predict fracture toughness of CNT/epoxy nanocomposites. *Composite Structures*, *272*, 114236. https://doi.org/10.1016/J.COMPSTRUCT.2021.114236

Short, D., & Summerscales, J. (1980). Hybrids - a review. Part 2. Physical properties. *Composites*, *11*(1), 33–38. https://doi.org/10.1016/0010-4361(80)90019-1

Sigwadi, R., Mokrani, T., & Dhlamini, M. (2019). Physica B : Physics of Condensed Matter The synthesis , characterization and electrochemical study of zirconia oxide nanoparticles for fuel cell application. *Physica B: Physics of Condensed Matter*, *October*, 411842. https://doi.org/10.1016/j.physb.2019.411842

Singh, J., Dutta, T., Kim, K.-H., Rawat, M., Samddar, P., & Kumar, P. (2018). 'Green' synthesis of metals and their oxide nanoparticles: applications for environmental remediation. *Journal of Nanobiotechnology*, *16*(1), 84.

https://doi.org/10.1186/s12951-018-0408-4

Singh, Y., Singla, A., & Kumar, A. (2014). Statistical Analysis of Process Parameters in Drilling of Al/Al2O3p Metal Matrix Composites. *Journal for Manufacturing Science and Production*, *14*(3), 171–175. https://doi.org/10.1515/JMSP-2014-0012

Skandan, G., Chen, Y. J., Glumac, N., & Kear, B. H. (1999). Synthesis of oxide nanoparticles in low pressure flames. *Nanostructured Materials*, *11*(2), 149–158. https://doi.org/10.1016/S0965-9773(99)00028-8

Standard, a. (1996). Standard Test Methods for Plane-Strain Fracture Toughness and Strain Energy Release Rate of Plastic Materials. In *Annul Book of ASTM Standards* (Vol. 99, Issue Reapproved, pp. 1–9). https://doi.org/10.1520/D5045-99R07E01.2

Thostenson, E. T., Li, C., & Chou, T. W. (2005). Nanocomposites in context. *Composites Science and Technology*, *65*(3–4), 491–516. https://doi.org/10.1016/j.compscitech.2004.11.003

Treacy, M. M. J., Ebbesen, T. W., & Gibson, J. M. (1996). Exceptionally high Young's modulus observed for individual carbon nanotubes. *Nature*, *381*(6584), 678–680. https://doi.org/10.1038/381678a0

Tsai, C. L., Yen, H. J., & Liou, G. S. (2016). Highly transparent polyimide hybrids for optoelectronic applications. *Reactive and Functional Polymers*, *108*, 2–30. https://doi.org/10.1016/j.reactfunctpolym.2016.04.021

Uddin, M. F., & Sun, C. T. (2010). Improved dispersion and mechanical properties of hybrid nanocomposites. *Composites Science and Technology*, *70*(2), 223–230. https://doi.org/10.1016/j.compscitech.2009.09.017

Usuki, A., Kawasumi, M., Kojima, Y., Okada, A., Kurauchi, T., & Kamigaito, O. (1993). Swelling behavior of montmorillonite cation exchanged for ω -amino

acids by e-caprolactam. *Journal of Materials Research*, *8*(5), 1174–1178. https://doi.org/10.1557/JMR.1993.1174

Uyaner, M., & Akdemir, A. (2021). *Effects of nano reinforcing / matrix interaction on chemical , thermal and mechanical properties of epoxy nanocomposites*. https://doi.org/10.1177/00219983211037059

Velsankar, K., Aswin Kumara, R. M., Preethi, R., Muthulakshmi, V., & Sudhahar, S. (2020). Green synthesis of CuO nanoparticles via Allium sativum extract and its characterizations on antimicrobial, antioxidant, antilarvicidal activities. *Journal of Environmental Chemical Engineering*, *8*(5), 104123. https://doi.org/10.1016/j.jece.2020.104123

Verma, M., Kumar, V., & Katoch, A. (2018). Sputtering based synthesis of CuO nanoparticles and their structural, thermal and optical studies. *Materials Science in Semiconductor Processing*, *76*(October 2017), 55–60. https://doi.org/10.1016/j.mssp.2017.12.018

Verma, V., Sayyed, A. H. M., Sharma, C., & Shukla, D. K. (2020). Tensile and fracture properties of epoxy alumina composite: role of particle size and morphology. *Journal of Polymer Research*, *27*(12), 1–14. https://doi.org/10.1007/s10965-020-02359-z

Voon, C. H., Lim, B. Y., & Ho, L. N. (2018). Silicon Carbide Nanomaterials. In *Synthesis of Inorganic Nanomaterials* (pp. 213–253). Elsevier. https://doi.org/10.1016/B978-0-08-101975-7.00009-9

Wöll, C. (2020). Structure and chemical properties of oxide nanoparticles determined by surface-ligand ir spectroscopy. *ACS Catalysis*, *10*(1), 168–176. https://doi.org/10.1021/acscatal.9b04016

Wu, M., Lu, L., Yu, L., Yu, X., Naito, K., Qu, X., & Zhang, Q. (2019). Preparation and Characterization of Epoxy/Alumina Nanocomposites. *Journal of Nanoscience and Nanotechnology*, *20*(5), 2964–2970.

https://doi.org/10.1166/jnn.2020.17460

Wu, Q., Zhao, R., Liu, Q., Jiao, T., Zhu, J., & Wang, F. (2018). Simultaneous improvement of interfacial strength and toughness between carbon fiber and epoxy by introducing amino functionalized ZrO2 on fiber surface. *Materials and Design*, *149*. https://doi.org/10.1016/j.matdes.2018.03.054

Wu, S., Jorgensen, J. D., & Soucek, M. D. (2000). Synthesis of model acrylic latexes for crosslinking with cycloaliphatic diepoxides. *Polymer*, *41*(1), 81–92. https://doi.org/10.1016/S0032-3861(99)00158-5

Xiao, C., Tan, Y., Yang, X., Xu, T., Wang, L., & Qi, Z. (2018). Mechanical properties and strengthening mechanism of epoxy resin reinforced with nano-SiO2 particles and multi-walled carbon nanotubes. *Chemical Physics Letters*, *695*, 34–43. https://doi.org/10.1016/j.cplett.2018.01.060

Yakobson, B. I., & Avouris, P. (2007). Mechanical Properties of Carbon Nanotubes. In *Carbon Nanotubes* (pp. 287–327). Springer Berlin Heidelberg. https://doi.org/10.1007/3-540-39947-x_12

Yang, Y., & Wang, P. (2006). Preparation and characterizations of a new PS/TiO2 hybrid membranes by sol-gel process. *Polymer*, *47*(8). https://doi.org/10.1016/j.polymer.2006.01.019

Young, R. J., Liu, M., Kinloch, I. A., Li, S., Zhao, X., Vallés, C., & Papageorgiou, D. G. (2018). The mechanics of reinforcement of polymers by graphene nanoplatelets. *Composites Science and Technology*, *154*, 110–116. https://doi.org/10.1016/j.compscitech.2017.11.007

Yu, M.-F., Files, B. S., Arepalli, S., & Ruoff, R. S. (2000). Tensile Loading of Ropes of Single Wall Carbon Nanotubes and their Mechanical Properties. *Physical Review Letters*, *84*(24), 5552. https://doi.org/10.1103/PhysRevLett.84.5552

Yu, M.-F., Lourie, O., Dyer, M. J., Moloni, K., Kelly, T. F., & Ruoff, R. S. (2000). Strength and Breaking Mechanism of Multiwalled Carbon Nanotubes Under Tensile Load. *Science*, *287*(5453), 637–640. https://doi.org/10.1126/SCIENCE.287.5453.637

Yuan, C. X., Fan, Y. R., Tao-Zhang, Guo, H. X., Zhang, J. X., Wang, Y. L., Shan, D. L., & Lu, X. Q. (2014). A new electrochemical sensor of nitro aromatic compound based on three-dimensional porous Pt-Pd nanoparticles supported by graphene-multiwalled carbon nanotube composite. *Biosensors and Bioelectronics*, *58*. https://doi.org/10.1016/j.bios.2014.01.041

Yuen, S. M., Ma, C. C. M., Chuang, C. Y., Hsiao, Y. H., Chiang, C. L., & Yu, A. dih. (2008). Preparation, morphology, mechanical and electrical properties of TiO2 coated multiwalled carbon nanotube/epoxy composites. *Composites Part A: Applied Science and Manufacturing*, *39*(1), 119–125. https://doi.org/10.1016/j.compositesa.2007.08.021

Zabihi, O., Hooshafza, A., Moztarzadeh, F., Payravand, H., Afshar, A., & Alizadeh, R. (2012). Isothermal curing behavior and thermo-physical properties of epoxy-based thermoset nanocomposites reinforced with Fe 2O 3 nanoparticles. *Thermochimica Acta*, *527*, 190–198. https://doi.org/10.1016/j.tca.2011.10.026

Zaghloul, M. M. Y., Zaghloul, M. M. Y., & Fuseini, M. (2023). Recent progress in Epoxy Nanocomposites: Corrosion, structural, flame retardancy and applications — A comprehensive review. *Polymers for Advanced Technologies*, *March*, 1–35. https://doi.org/10.1002/pat.6144

Zakaria, M. R., Abdul Kudus, M. H., Akil, H. M., & Zamri, M. H. (2017). Improvement of fracture toughness in epoxy nanocomposites through chemical hybridization of carbon nanotubes and alumina. *Materials*, *10*(3). https://doi.org/10.3390/ma10030301

Zakaria, M. R., Akil, H. M., Abdul Kudus, M. H., & Othman, M. B. H. (2016). Compressive properties and thermal stability of hybrid carbon nanotube-alumina filled epoxy nanocomposites. *Composites Part B: Engineering*, *91*, 235–242. https://doi.org/10.1016/j.compositesb.2016.01.013

Zakaria, M. R., Akil, H. M., Abdul Kudus, M. H., & Thirmizir, M. Z. A. (2015). Synthesis and Characterization of Hybrid MWCNT-Alumina Filled Epoxy Nanocomposites. *Applied Mechanics and Materials*, *754–755*, 135–139. https://doi.org/10.4028/www.scientific.net/AMM.754-755.135

Zakaria, M. R., Akil, H. M., Kudus, M. H. A., & Kadarman, A. H. (2015). Improving flexural and dielectric properties of MWCNT/epoxy nanocomposites by introducing advanced hybrid filler system. *Composite Structures*, *132*. https://doi.org/10.1016/j.compstruct.2015.05.020

Zare, Y. (2016). Study of nanoparticles aggregation/agglomeration in polymer particulate nanocomposites by mechanical properties. *Composites Part A: Applied Science and Manufacturing*, *84*, 158–164. https://doi.org/10.1016/J.COMPOSITESA.2016.01.020

Zhang, F., Xu, D., Zhang, D., Ma, L., Wang, J., Huang, Y., Chen, M., Qian, H., & Li, X. (2021). A durable and photothermal superhydrophobic coating with entwinned CNTs-SiO2 hybrids for anti-icing applications. *Chemical Engineering Journal*, *423*. https://doi.org/10.1016/j.cej.2021.130238

Zhang, Y., Zhang, L., Xiao, Z., Wang, S., & Yu, X. (2019). Fabrication of robust and repairable superhydrophobic coatings by an immersion method. *Chemical Engineering Journal*, *369*. https://doi.org/10.1016/j.cej.2019.03.021

Zhao, S., Schadler, L. S., Duncan, R., Hillborg, H., & Auletta, T. (2008). Mechanisms leading to improved mechanical performance in nanoscale alumina filled epoxy. *Composites Science and Technology*, *68*(14), 2965–2975. https://doi.org/10.1016/j.compscitech.2008.01.009

Zhao, S., Schadler, L. S., Hillborg, H., & Auletta, T. (2008). Improvements and mechanisms of fracture and fatigue properties of well-dispersed alumina/epoxy nanocomposites. *Composites Science and Technology*, *68*(14), 2976–2982. https://doi.org/10.1016/j.compscitech.2008.07.010

Zheng, Y., Zheng, Y., & Ning, R. (2003). Effects of nanoparticles SiO2 on the performance of nanocomposites. *Materials Letters*, *57*(19), 2940–2944. https://doi.org/10.1016/S0167-577X(02)01401-5

ZUBAIR, N., & AKHTAR, K. (2020). Morphology controlled synthesis of ZnO nanoparticles for in-vitro evaluation of antibacterial activity. *Transactions of Nonferrous Metals Society of China (English Edition)*, *30*(6), 1605–1614. https://doi.org/10.1016/S1003-6326(20)65323-7

Zunjarrao, S. C., & Singh, R. P. (2006). Characterization of the fracture behavior of epoxy reinforced with nanometer and micrometer sized aluminum particles. *Composites Science and Technology*, *66*(13), 2296–2305. https://doi.org/10.1016/j.compscitech.2005.12.0

LIST OF PUBLICATIONS

Upadhyay, A. K., Goyat, M. S., & Kumar, A. (2022). A review on the effect of oxide nanoparticles, carbon nanotubes, and their hybrid structure on the toughening of epoxy nanocomposites. *Journal of Materials Science 2022 57:28*, *57*(28), 13202–13232. https://doi.org/10.1007/S10853-022-07496-Y

Upadhyay, A. K., Goyat, M. S., Kumar, A., & Nathawat, R. (2023). Taguchi design of experiments based optimization and experimental investigation of mechanical performance of hybrid epoxy nanocomposites. *Materials Protection*, *64*(4), 433–443.

UPES
UNIVERSITY OF TOMORROW

PLAGIARISM CERTIFICATE

We Dr Manjeet Singh Goyat (Internal Guide), Dr. Ajay Kumar (Co Guide/ External Guide)

certify that the Thesis titled "**Development of hybrid polymer matrix nanocomposite with**

improved mechanical and thermal properties" submitted by Scholar Mr. Avani Kumar

Upadhya having SAP ID 500051425 has been run through a Plagiarism Check Software and

the Plagiarism Percentage is reported to be 7%.

Plagiarism Report generated by the Plagiarism Software is attached.

Signature of the Internal Guide

Signature of External Guide/ Co Guide

Signature of the Scholar

121

avani

PRIMARY SOURCES

1   Submitted to University of Warwick
    Student Paper   1%

2   www.researchgate.net
    Internet Source   1%

3   M.S. Goyat, Amrita Hooda, Tejendra K. Gupta,
    Kaushal Kumar, Sudipta Halder, P.K. Ghosh,
    Brijnandan S. Dehiya. "Role of non-
    functionalized oxide nanoparticles on
    mechanical properties and toughening
    mechanisms of epoxy nanocomposites",
    Ceramics International, 2021   <1%
    Publication

4   Nalini, R., S. Nagarajan, and B. S. R. Reddy.
    "Thermoplastic polyolefin nanocomposites:
    effect of mechanical, thermal, and
    morphological properties", Journal of
    Reinforced Plastics and Composites, 2011.   <1%
    Publication

5   Vijay Verma, Ahmed Hasan Muquimuddin
    Sayyed, Chaitnaya Sharma, Dharmendra
    Kumar Shukla. "Tensile and fracture   <1%